In presenting the dissertation as a partial fulfillment of the requirements for an advanced degree from the Georgia Institute of Technology, I agree that the Library of the Institute shall make it available for inspection and circulation in accordance with its regulations governing materials of this type. I agree that permission to copy from, or to publish from, this dissertation may be granted by the professor under whose direction it was written, or, in his absence, by the Dean of the Graduate Division when such copying or publication is solely for scholarly purposes and does not involve potential financial gain. It is understood that any copying from, or publication of, this dissertation which involves potential financial gain will not be allowed without written permission.

7/25/68

BOUNDARY EFFECTS IN STRUCTURAL STABILITY: A NEW APPROACH

A THESIS

Presented to

The Faculty of the Division of Graduate Studies and Research

by

Donald Edward Struble, Jr.

In Partial Fulfillment

of the Requirements for the Degree

Doctor of Philosophy

in the School of Aerospace Engineering

Georgia Institute of Technology

January, 1970

BOUNDARY EFFECTS IN STRUCTURAL STABILITY:

A NEW APPROACH

Approved:

Chairman

Date Approved by Chairman: 4/21/72

ACKNOWLEDGMENTS

The research described herein was part of a general investigation of structural stability being carried out by the School of Aerospace Engineering at the Georgia Institute of Technology; it was sponsored by the United States Army Aviation Materiel Laboratories, under Contract No. DAA02J-68-C-0035, and by the United States Air Force Office of Scientific Research, under Grant No. 68-1476. The support of these agencies is gratefully acknowledged.

In addition, the author wishes to acknowledge his indebtedness to Professor Wilfred H. Horton, whose influence on the author's personal and professional development has been profound, and whose patience is matched only by that of the author's wife. Her sacrifices are deeply appreciated.

TABLE OF CONTENTS

TABLE OF CONTENTS (Continued)

LIST OF TABLES

LIST OF ILLUSTRATIONS

LIST OF ILLUSTRATIONS (Continued)

LIST OF ILLUSTRATIONS (Concluded)

LIST OF SYMBOLS

a	beam taper ratio
a_1	first coefficient in elastic deflection expansion
a_n	n^{th} coefficient in elastic deflection expansion
B	coefficient in expression for buckling deflected shape
$B_0(\zeta)$	function defined in equation (48a)
$B_1(\zeta)$	function defined in equation (48b)
$B_2(\zeta)$	function defined in equation (48c)
c	correction factor defined in equation (151)
c^*	correction factor defined in equation (153)
$\hat{c}$	attenuation factor defined in equation (157)
D	coefficient in expression for buckling deflected shape
E	modulus of elasticity
e_1	first coefficient in initial shape expansion
e_n	n^{th} coefficient in initial shape expansion
F	lateral end force
I	beam cross-section moment of inertia
I_0	moment of inertia at left end ($\xi = 0$) of beam
K_1	$K_1 L^3/EI$ = relative lateral spring stiffness at right end ($\xi = 1$) of beam
K_2	$K_2 L/EI$ = relative rotational spring stiffness at right end ($\xi = 1$) of beam
K_3	$K_3 L/EI$ = relative rotational spring stiffness at left end ($\xi = 0$) of beam
K_5	$K_5 L^3/EI$ = relative spring stiffness for central lateral spring

LIST OF SYMBOLS (Continued)

k_1	lateral apring stiffness at right end ($\xi = 1$) of beam
k_2	rotational spring stiffness at right end ($\xi = 1$) of beam
k_3	rotational spring stiffness at left end ($\xi = 0$) of beam
k_5	spring stiffness of central lateral spring
L	nominal beam length
L_0	distance between inflection points
ΔL	length reduction in effective length formula
M	moment due to actual beam loading
M_0	moment at left end ($\xi = 0$) of beam
M_1	moment at right end ($\xi = 0$) of beam
M_d	dummy load moment distribution
m	dummy summation index
m_b	$\pi\sqrt{R}/2$ = loading parameter
n	dummy summation index
n_b	number of half-waves in buckling
n_p	number of inflection points
P	beam axial load
P_a	buckling load of a strut with two halves like OA (Figure 28a)
P_b	buckling load of a strut with two halves like OB (Figure 28a)
P_{cr}	beam buckling load
P_1	lowest beam buckling load
P_n	buckling load corresponding to n^{th} mode
Q	lateral concentrated load

LIST OF SYMBOLS (Continued)

R	$\frac{P}{\pi^2 EI/4L^2}$ = relative axial load
R_1	reaction at right end ($\xi = 1$) of beam
R_2	quantity defined in equation (51)
R_5	reaction at intermediate lateral support
r_1	knife edge carrier radius
r_2	knife edge radius
S_0	rigid carrier length at left end ($\xi = 0$) of beam
S_1	rigid carrier length at right end ($\xi = 1$) of beam
s	quantity defined in equation (14)
T_1	sum defined in equation (108)
T_2	sum defined in equation (109)
T_3	sum defined in equation (110)
t	quantity defined in equation (15)
U^*	internal complementary work
W	total potential
W^*	total complementary potential
w	beam lateral deflection
x	beam axial coordinate
α_0	stiffness parameter defined in equation (7)
α_1	stiffness parameter defined in equation (8)
β	angle defined in Figure 24
δ	elastic lateral deflection amplitude
δ_1	deflection at right end ($\xi = 1$) of beam

LIST OF SYMBOLS (Continued)

$\tilde{\delta}$	total deflection for higher-mode cases
$\bar{\delta}$	$\frac{\delta/Q}{L^3/EI}$ = relative flexibility coefficient
ζ	upper limit of integration in equations (48)
θ	beam slope
θ_0	slope at left end ($\xi = 0$) of beam
θ_1	slope at right end ($\xi = 1$) of beam
$\bar{\theta}$	$\frac{\theta/QL}{L/EI}$ = relative slope
λ	load location
μ	slope measurement location
μ_m	extremal slope location
ν	Poisson's ratio
ξ	x/L = dimensionless beam axial coordinate
ρ	dimensionless parameter defined in equation (10)
ρ'	dimensionless parameter defined in equation (11)
ρ''	dimensionless parameter defined in equation (17)
σ	stress
φ	$L\sqrt{\frac{P_{cr}}{EI}}$ = effective length parameter

Subscripts

cr	critical value corresponding to buckling
max	maximum algebraic value
min	minimum algebraic value
m	value used in buckling load prediction

LIST OF SYMBOLS (Concluded)

Operators

d( )	denotes differentiation

SUMMARY

The relevance of boundary conditions to structural behavior has long been recognized, and much experimental work in this regard has been done. A history of attempts to achieve in the laboratory the boundary conditions prescribed by analysis is thus presented, and the various techniques are critically compared. It is shown, however, that the general thrust of these efforts has been misdirected, and that a more pertinent goal of experimental investigations must be the understanding and evaluation of boundary effects in practical structures. Accordingly, this research highlights the necessity of non-destructive test techniques and the inadequacy of current methods in buckling load, or end fixity coefficient, prediction. A new approach, also useful from an analytical point of view, is developed for columns of practical interest. The basic method uses a single concentrated non-destabilizing lateral load at a specified location and makes use of the fact that there is a relationship between boundary effects in destabilizing and non-destabilizing environments.

CHAPTER I

INTRODUCTION

Interest in the ability of structures to carry load has existed since man's earliest realization that his health and safety depended on that ability. In fashioning his own structures, man's faculties could never have matured beyond the most embryonic stages without the remarkable trait of being able to learn from past mistakes and extrapolate from prior successes. Trial and error being the only available design method, however, progress was necessarily slow. Nonetheless, the skills and knowledge acquired this way were considerable; indeed, who among us has failed to marvel at the beauty and grace still present in ancient ruins?

There comes a time, however, when trial and error is not sufficient, and, for structural design, such a time was the era of the Industrial Revolution. The introduction of iron and steel as building materials brought enormous improvements in design and construction. The increasing capability of the builders was matched stride for stride by the increasing demands of industry, resulting in designs of comparatively spare geometry and high flexibility. The result was a change in failure mode from material rupture to a condition of excessive deformation that generally rendered a structure unable to carry its full load. With this new phenomenon came a greater urgency to understand it and thus anticipate its occurrence before lives and property were lost. The stage was set for the development of the theory

of elastic stability.

Due to the ease and simplicity of obtaining a solution, and due to its wide use in architecture, the first structural member to be treated by this theory was the column. More complicated members could be dealt with by the extrapolation of column results.

Both theory and experiment indicated from the outset that the effects of boundary conditions were of primary importance. It is perhaps due to the fact that the theory preceded the experiment by a century that the boundary conditions arrived at via the calculus of variations served as the ideal toward which the experimentalist has striven in his testing. That much ingenuity has been exercised by the experimentalist in attempts to duplicate in the laboratory the boundary conditions prescribed by analysis is evident from a perusal of the literature on the subject.

The shortcoming of this approach is the fact that however clever the experimentalist, however closely he is able to approximate these ideal boundary conditions, his results are of little help to the engineer working with a structure of practical interest. Given a lack of knowledge of the boundary restraint present in the actual structure, it is pointless to insert this ignorance into analytical calculations. All the engineer can do from a theoretical point of view is to make an educated guess; analysis is thus reduced to idle speculation.

At this point the need for a practical non-destructive test should be clear. To date the only experimental technique for the determination of buckling loads has been the well-known Southwell plot approach, which depends on the occurrence of lateral displacements when destabilizing

loads are applied to the structure. In the case of the circular cylindrical shell under axial compression, however, the interpretation that should be given to the Southwell plot is not entirely clear. Furthermore, the fact that the specimen, regardless of structural form, may buckle unexpectedly implies that the term "non-destructive" should not be applied to this test.

Apparently the flaw in the Southwell method is the use of a destabilizing load; a successful non-destructive test must use a non-destabilizing load to energize the structure. It is important to note that the set of boundary conditions is often unchanged regardless of the load environment. A pertinent question can now be raised: are the boundary effects in the two cases related; if so, can this relationship be used to develop a non-destructive test, using non-destabilizing load, to predict the onset of instability? The aim of the present research is to answer that question.

CHAPTER II

END FIXITY DEVICES

Historical Summary

In the discussion of structural testing, the existence of the test machine is generally assumed. Obviously this cannot always have been the case; the development of the test machine was an extremely significant occurrence. The first such device for the determination of the strength of columns was built in 1729 by Musschenbroek (1). It is interesting to observe that he was able to propose, as a result of his investigations, an empirical formula in which the strength of a column was proportional to the square of the ratio of the cross-section dimension divided by the length. This was a correct conclusion and represented the latest thinking until Euler's (2) classic memoir of 1744. The next significant contribution occurred in 1807 when Thomas Young (3) developed a formula which associated the applied load, the Euler critical load, the initial bow, and the elastic deformation under load. This is essentially the same hyperbolic law proposed subsequently by Ayrton and Perry (4) and, later, by Southwell (5).

In 1840 a long paper describing an investigation involving many carefully-executed column tests was published by Hodgkinson (6). The purpose of the study was, in Hodgkinson's own words, "to supply the deficiencies of Euler's theory of the strength of pillars, if it should appear capable of being rendered practically useful; and, if not, to

endeavour to adapt the experiments so as to lead to useful results."

In many respects this work set the pattern for much which has followed. It must be remembered that Euler's theory was derived as an example of the power of the calculus of variations and was merely an appendix to a paper written on the latter subject. Hodgkinson subsequently set out to determine whether the mathematical development had a basis in fact, and the use of experimental work to verify analysis has persisted to this day. It is interesting to note that Hodgkinson's was the first contracted research.

It is clear from Hodgkinson's paper that he appreciated the importance of end conditions, and in his tests he attempted to achieve the limiting cases derived by the calculus of variations with homogeneous end conditions. In fact, his first series of experiments were a comparison of the strengths of columns with rounded and flat ends. With regard to round-end tests of short columns Hodgkinson noted that "It became necessary to render those which were rounded at the ends more flat there than if the ends had been hemispheres." This action was necessitated by bearing failure at the contact surfaces, a consideration that has continued to plague experimentalists. The test machine and the end shapes of the columns developed for this study are illustrated in Figures 1 and 2.

In 1879 the Watertown Arsenal (7) installed a test machine that did much to further experimental column research. It was a noteworthy pioneer, having a capacity of one million pounds compression and being the forerunner of the modern hydraulic test machine. It was in connection with work being done in this machine that the end fixity device pictured

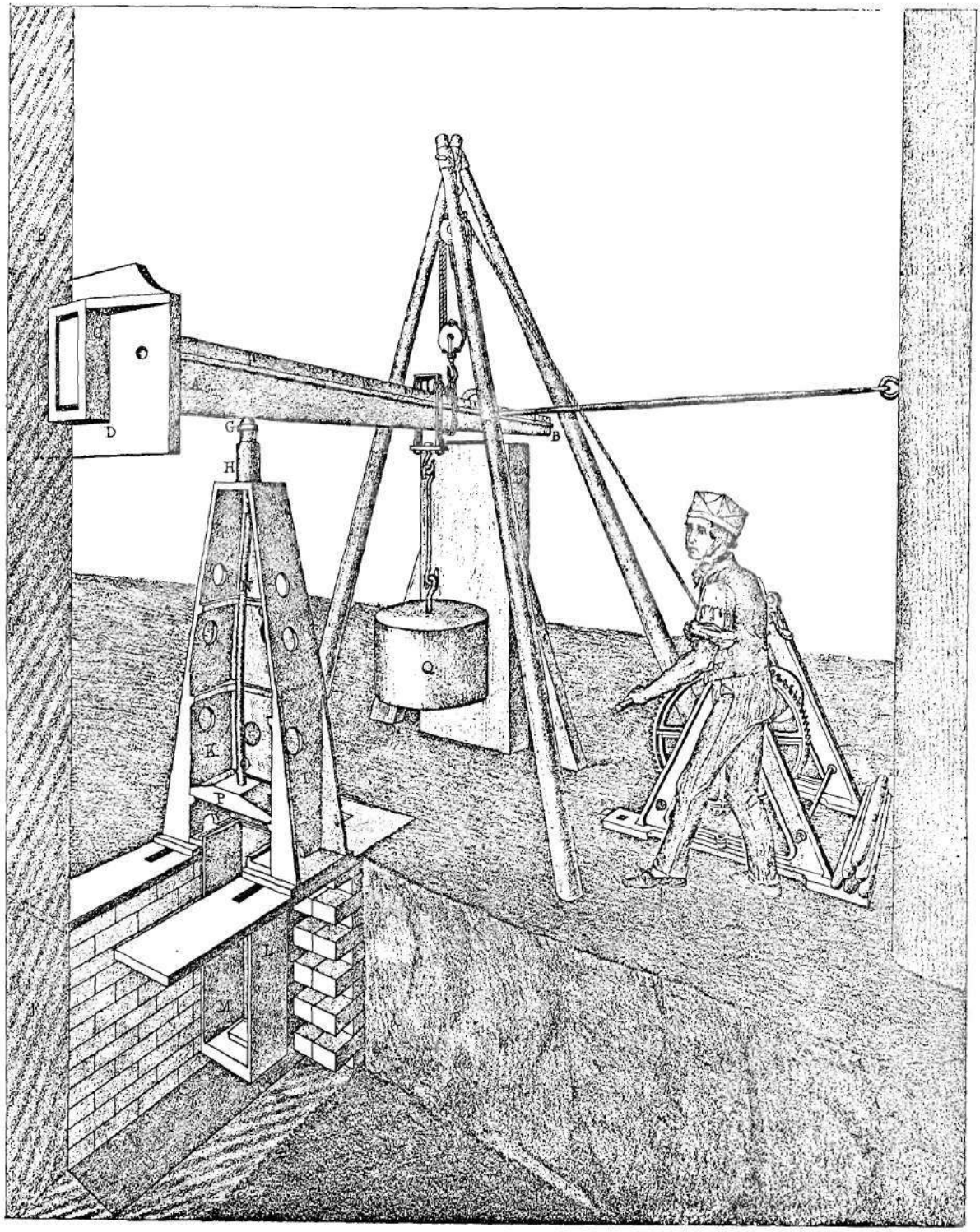

Figure 1. Hodgkinson's Test Machine

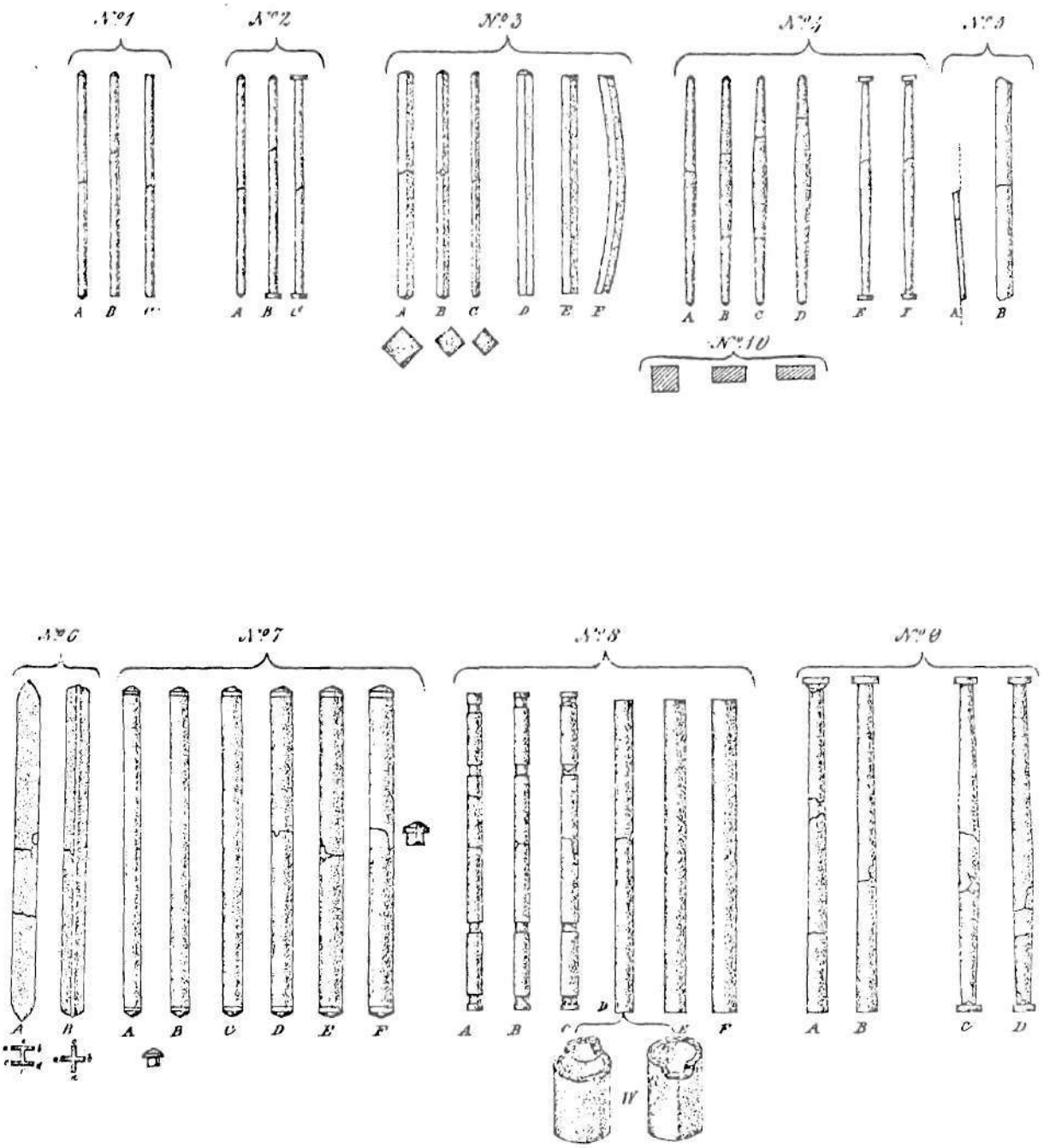

Figure 2. Hodgkinson's Specimens, Illustrating End Shapes

in Figure 3 was developed. It is apparent that it was this device which led to the description of columns as "pinned" when it was desired to convey the idea of zero rotational restraint and infinite lateral restraint at the ends. Unfortunately, the pinned fixture conveys the idea but does not deliver the performance. When the diameter of the pin is large enough to prevent bearing failure, friction can cause the rotational restraint to be effectively infinite unless great care is exercised in lubrication, surface finish, and fit. Generally, tests with this type of device are not repeatable.

Around 1884 Christie (8), in an attempt to build a device based on the same general principle but having three degrees of freedom, developed a fixture with a spherical seat, as shown in Figure 4. However, the shortcomings of the pin device are also present in the spherical seat.

In 1887 Bauschinger (9) reported on a series of reliable tests he had carried out using a device having a conical seat, the first use of such a configuration. In 1890 Tetmajer (10) used a similar device, illustrated in Figure 5. In theory the device has three degrees of freedom and ensures central load application, but in practice a bearing failure occurs at the tip of the cone, resulting in considerable friction.

Around the turn of the century Lilly (11,12) performed roundend and eccentrically-loaded column tests; to achieve the latter condition he devised a knife-edge fixture as shown in Figure 6. A knife-edge device was also used by von Karman (13) in his well-known 1910 work on the plastic buckling of columns.

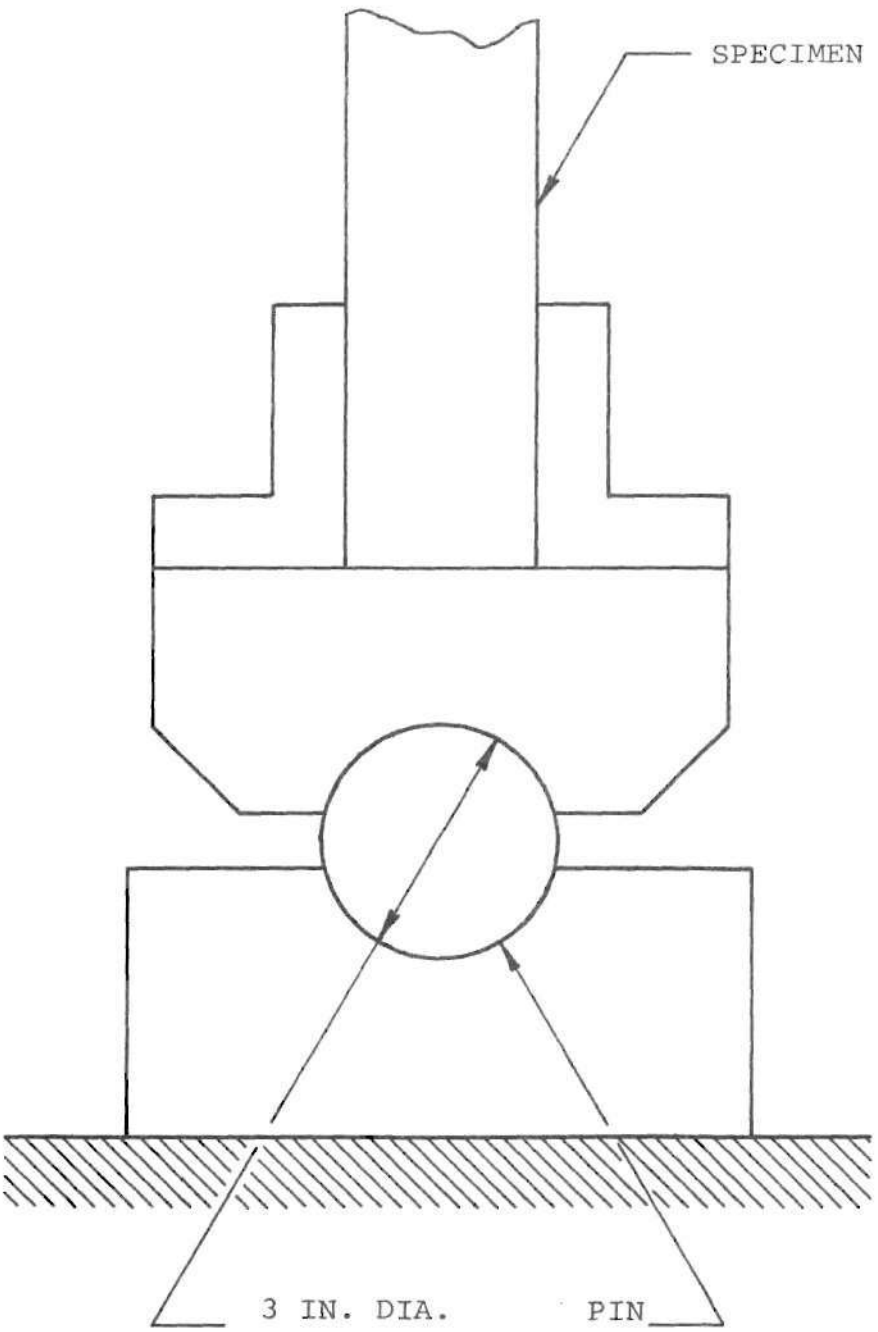

Figure 3. Watertown Arsenal End Fixture

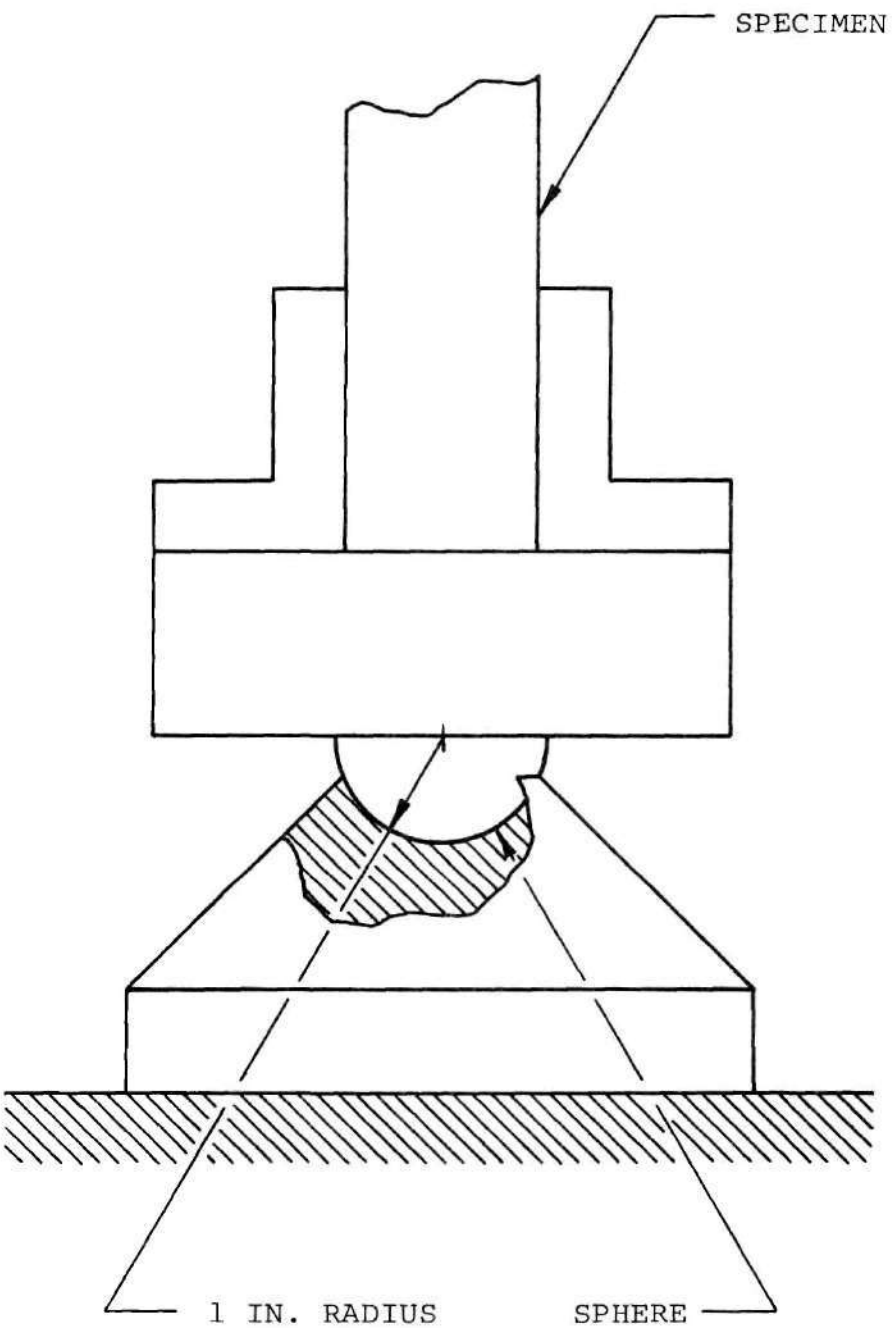

Figure 4. Christie's End Fitting

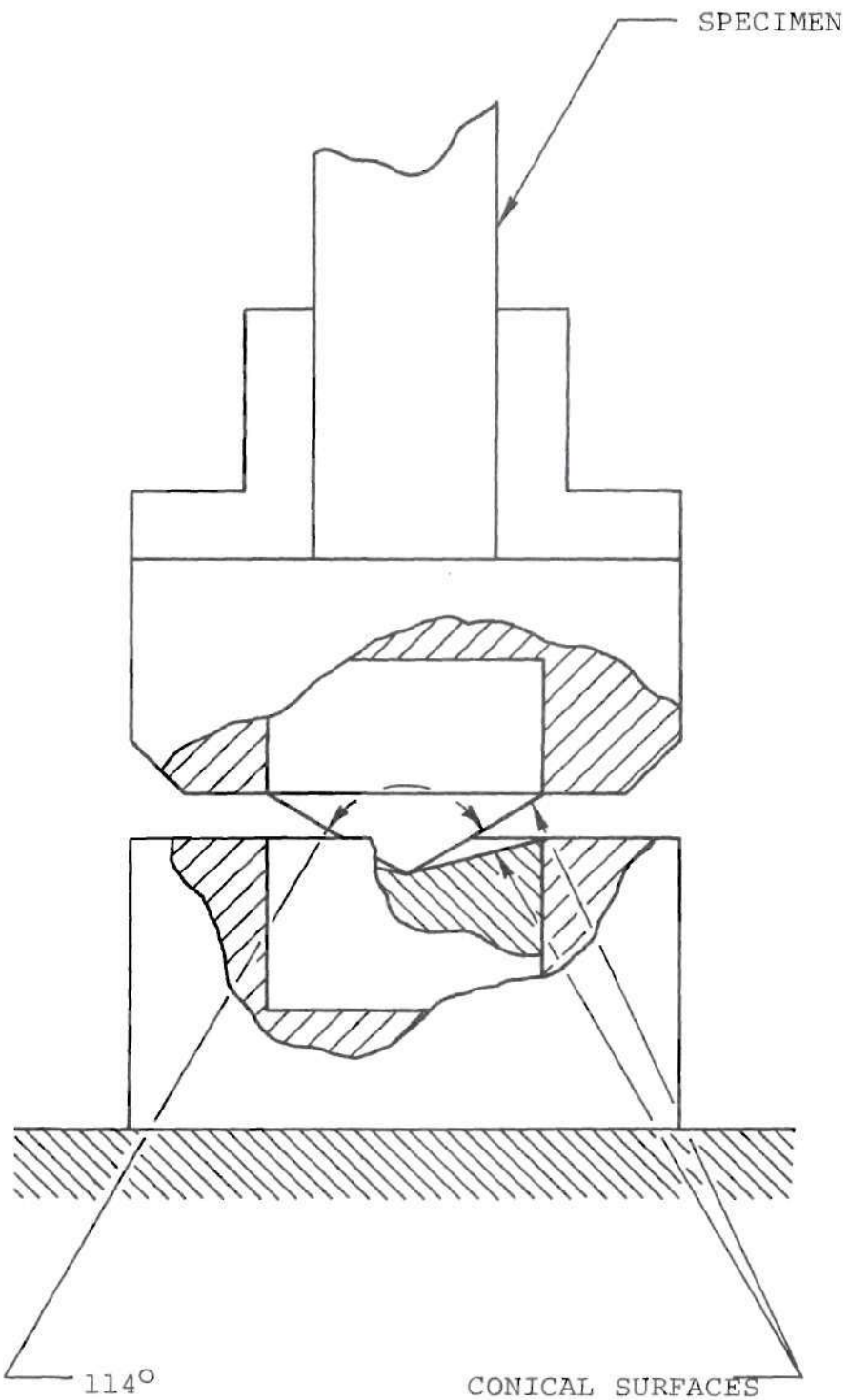

Figure 5. Tetmajer's Conical Seat

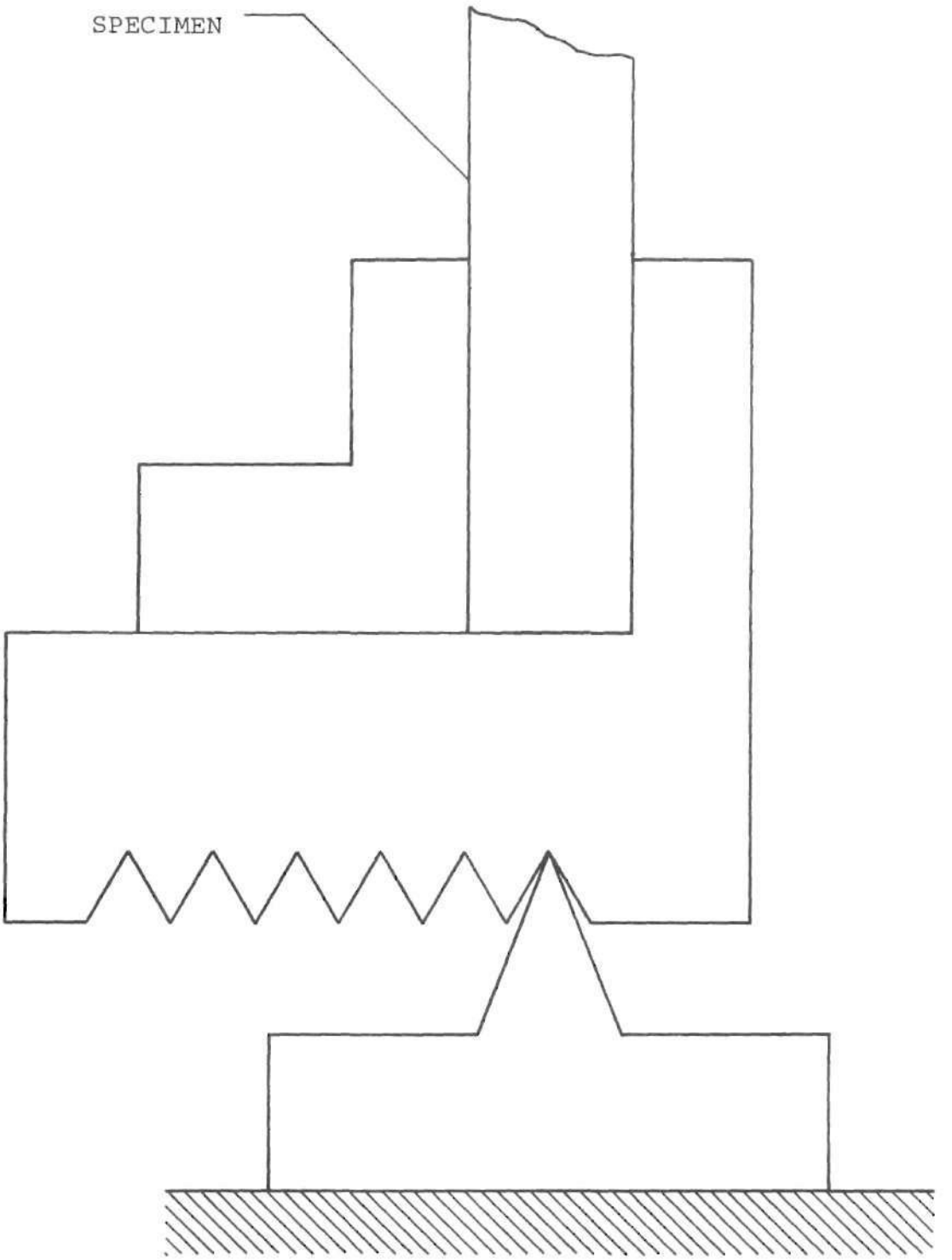

Figure 6. Lilly's Knife Edge Fixture

The knife-edge fixture is probably the best of all those mentioned so far. It does share with the Watertown Arsenal pin device the shortcoming of having only one degree of freedom, but many column cross-sections are such that no torsion occurs; furthermore, the knife edge can be positioned such that the hinge operates in the plane in which buckling is desired or anticipated. In the perpendicular direction, the rotational restraint is nearly infinite.

It might be assumed that the case of infinite rotational restraint would be easily achieved, but this is not the case. Generally the approach has been to make the ends of the specimen either flat or flanged, as did Hodgkinson. See Figures 7 and 8. In practice, trouble can be encountered owing to the difficulty of straightening the columns and of getting the end surfaces to be very flat, parallel, and normal to the axis of the column. This is particularly true of large specimens. Thus it is that all specimens start their experimental lives in a state similar to some degree to the condition portrayed in Figure 9. It is clear that small deviations in geometry can lead to large deviations in loading. To compound the situation, even if the specimen could be perfectly prepared, any lateral motion or rocking of the test machine platens would again lead to a situation equivalent to that in Figure 9.

In practice, the case of zero rotational restraint, the "pin-end" condition, has received by far the most attention. It is clear that, if bearing failure is avoided, the problem of producing a satisfactory fixture is largely one of minimizing friction. Toward this end many improvements have been introduced.

One of the improvements on the Watertown Arsenal device was

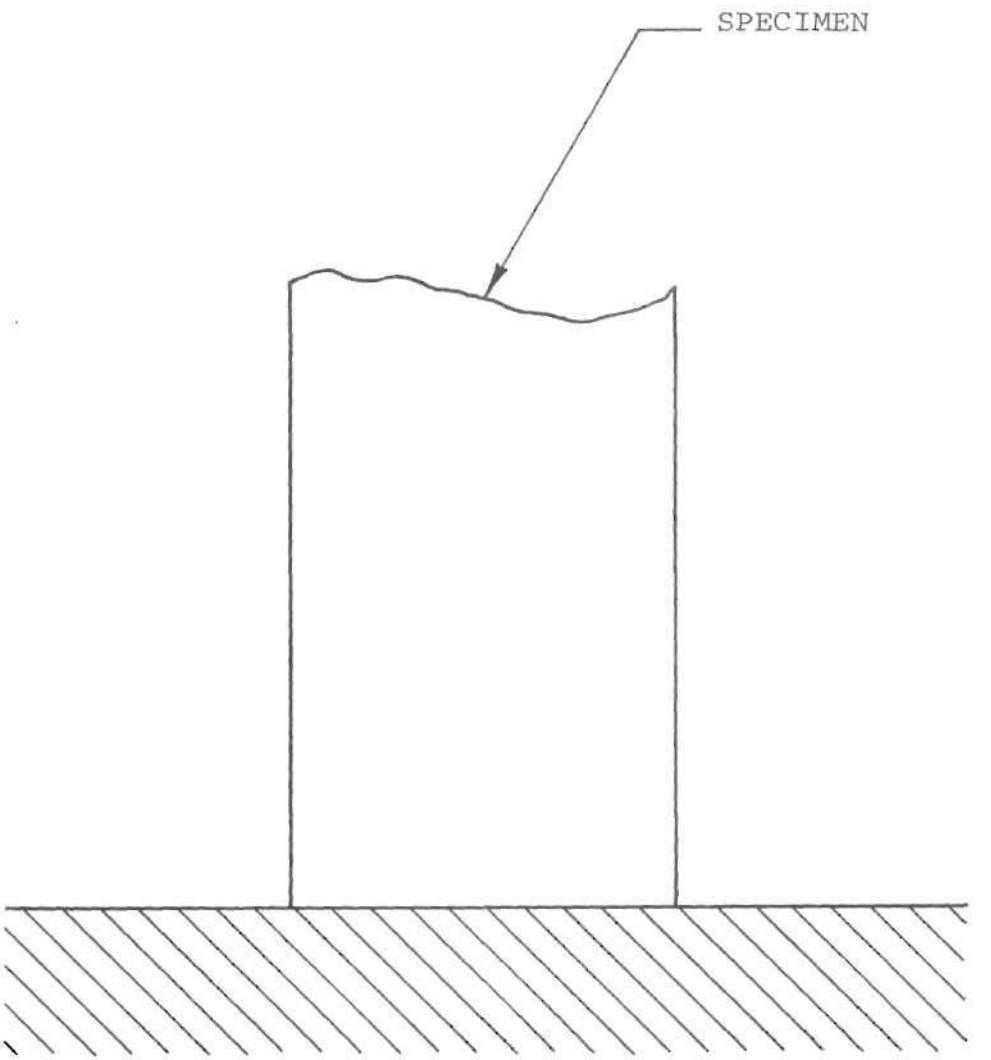

Figure 7. Flat End Arrangement

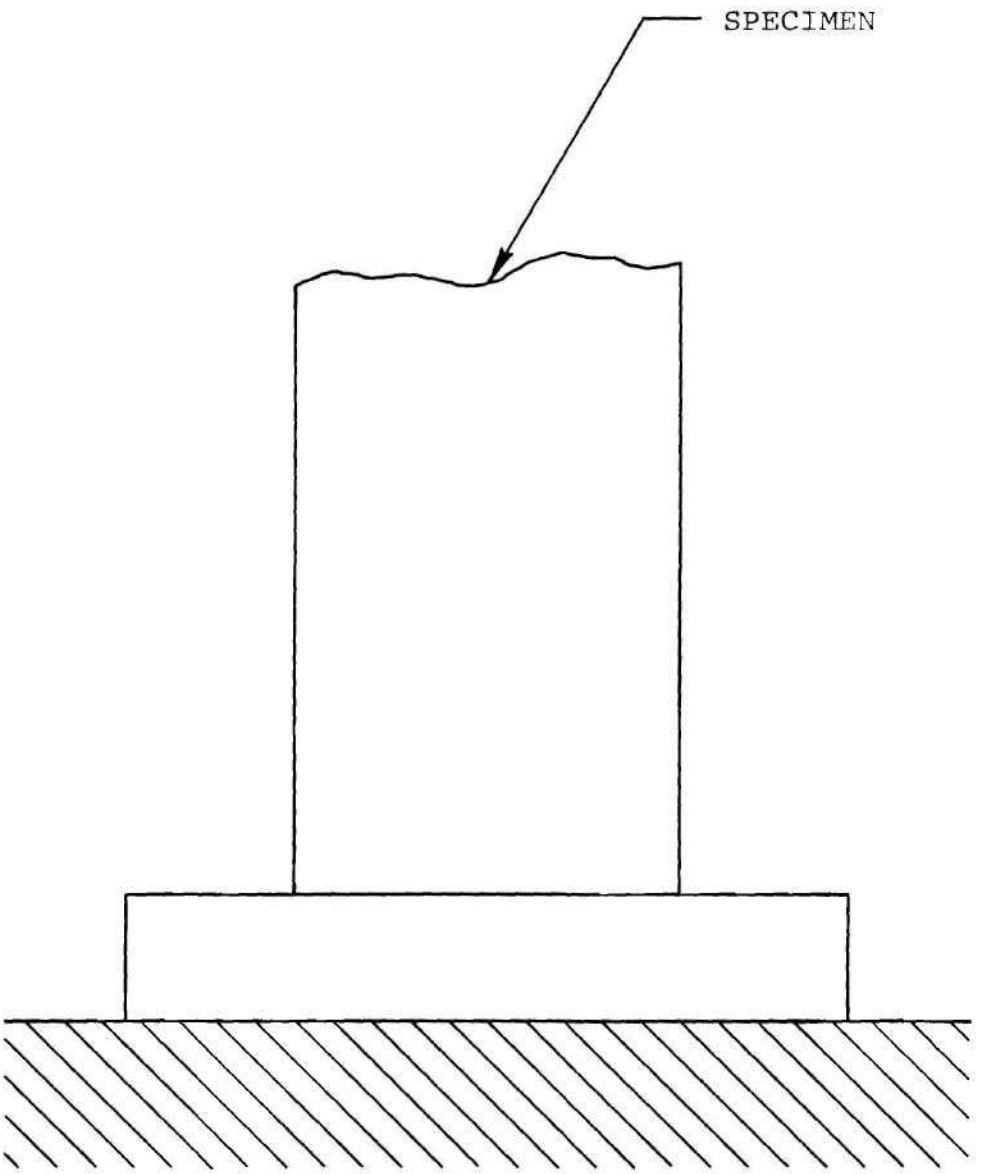

Figure 8. Flange Arrangement

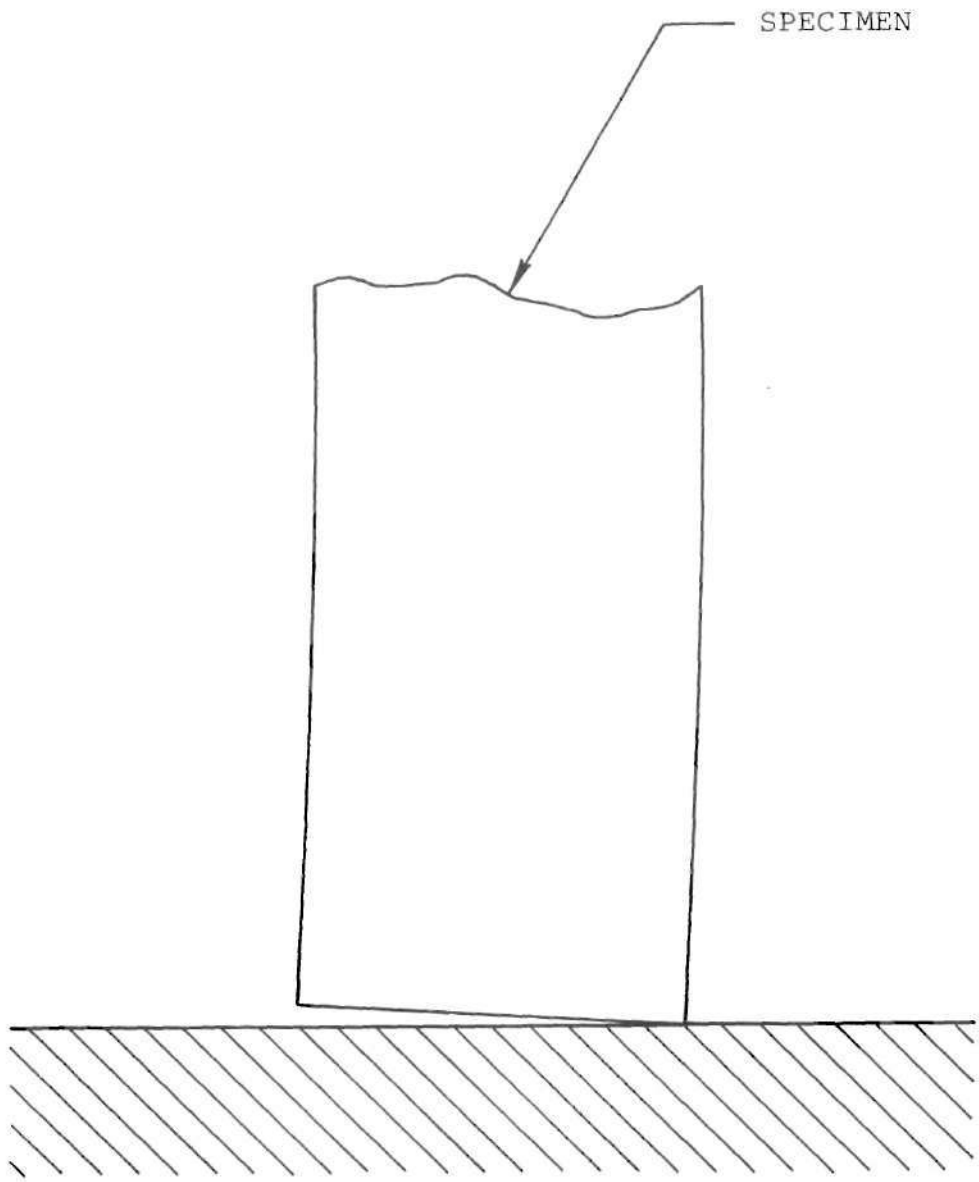

Figure 9. Tilt of Specimen with Flat Ends

developed at the University of Washington in 1926. It is shown in Figure 10, and it has a capacity of 500,000 pounds. It is clear from the figure that the device consists mainly of a semi-cylindrical loading block and a concave base, the radius being such that the intersection of the neutral axis with the plane of the column end was at the center of curvature of the fixture. The annular space between the base and the loading block was filled with a single layer of steel rollers whose diameters were 1.5 inches. The radius of the loading block was 6 inches. A friction test indicated a coefficient of friction of .002, and the device performed very satisfactorily. Tests show, however, that extreme care should result in a reduction in the friction coefficient to .0006.

It is apparent that friction could be reduced very much more if the steel rollers were replaced by a thin film of oil under pressure. Such a device is shown in Figure 11.

In 1938 Osgood (15) carried out an investigation of the column strength of tubes elastically restrained against rotation at their ends. This fixture consisted of essentially a carrier with a knife edge which bore on a seat on a stationary support clamped to one of the test machine platens, as shown in Figure 12. Rotation about the knife edge was restrained by the helical springs, the degree of restraint being adjustable by changing the active lengths of the springs. Since the springs were active only in compression, they were pre-loaded by means of wing nuts. The fixture was provided with means for holding the end of the test specimen in position in the carrier and moving it horizontally under low loads in a direction perpendicular to the knife edge.

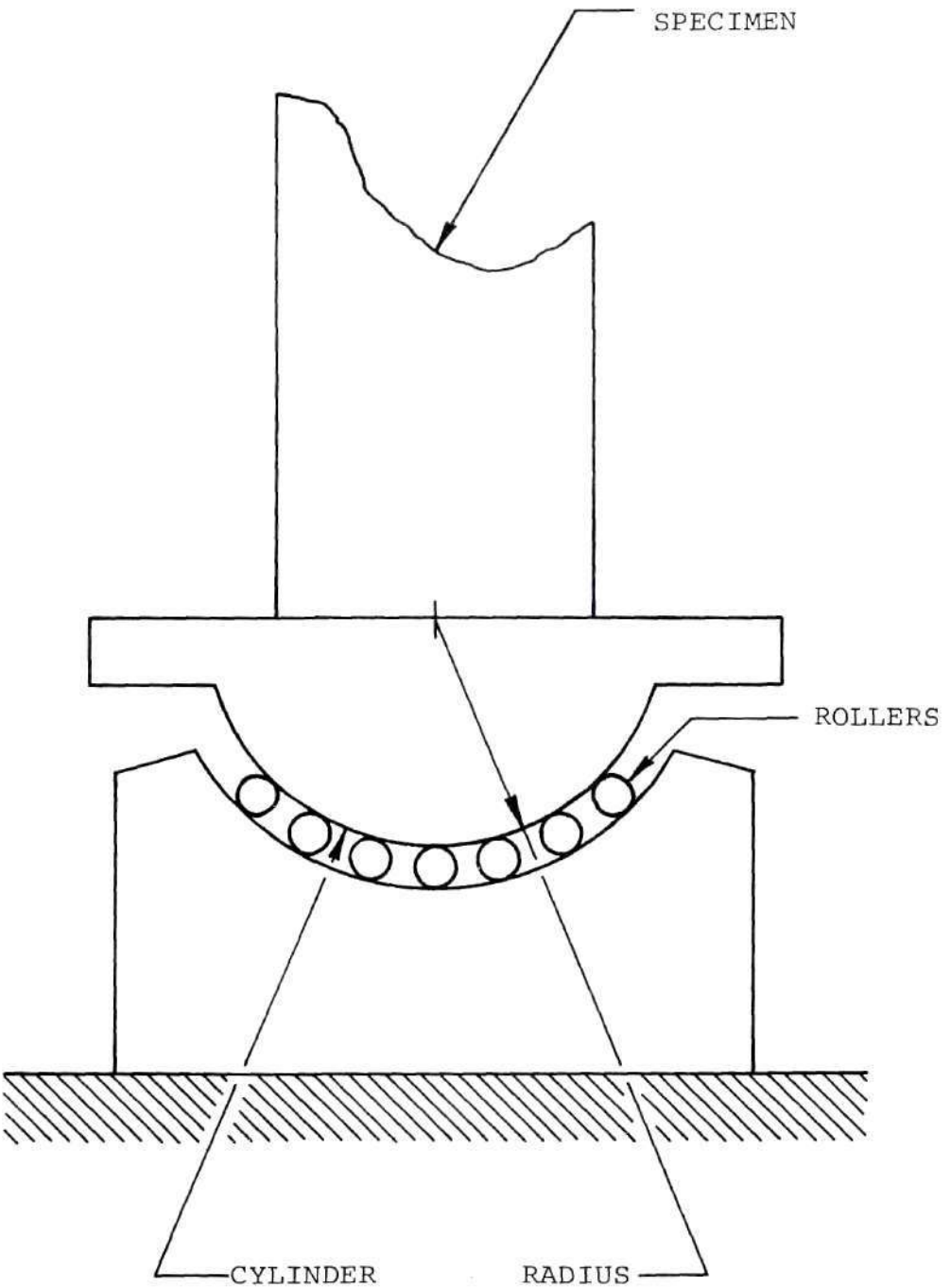

Figure 10. University of Washington Roller System

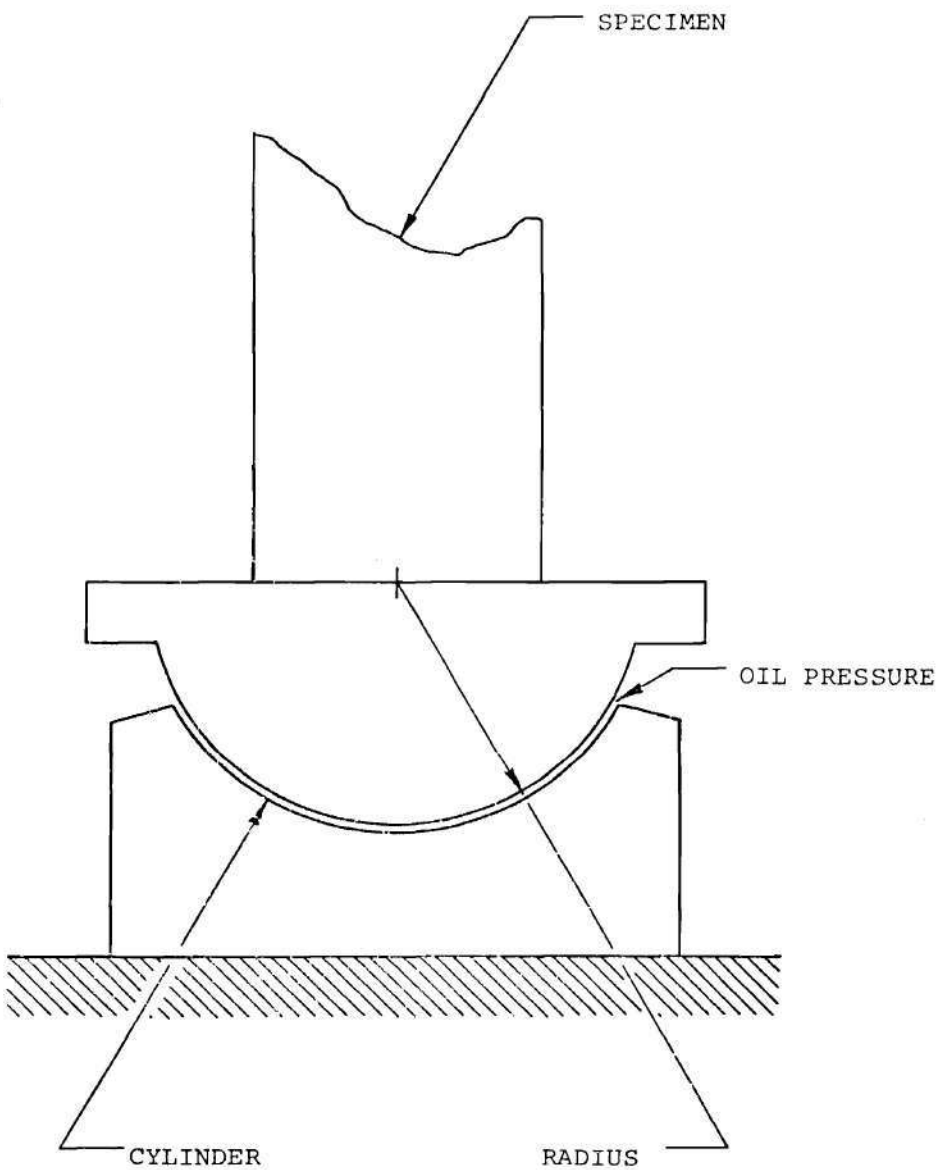

Figure 11. Hydraulic End Fixture

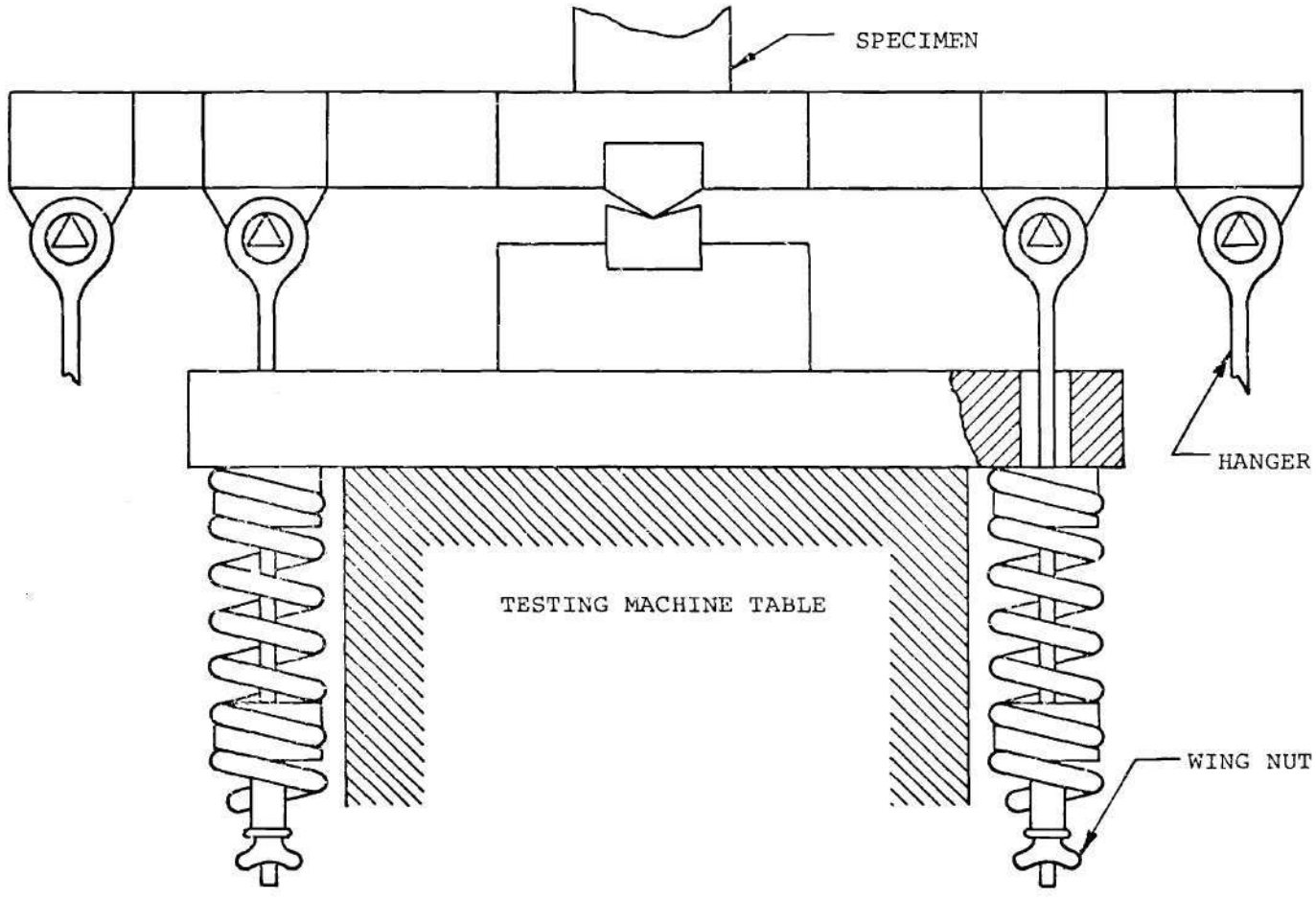

Figure 12. Diagram of the Apparatus for Procuring Elastic Restraint at End of Column

This is the well-known "centering under load" technique, which has the purpose of ensuring that the load is centrally applied and that the condition shown in Figure 9 does not occur.

In 1939 Barlow (16) made a logical and simple device for testing light columns. From Figure 13, it is seen that each unit consisted of a round hardened steel bar supported between two ball bearing assemblies. At the mid-point of the bar was ground a flat in whose surface lay the axis of rotation of the assembly. The flexural rigidity of the loading bar was such that an angular deflection of 1.2 degrees could occur under a load of 24,000 pounds, while the bearing would not bind until this angle reached 1.5 degrees. Since the maximum test load was 8000 pounds, the device worked well. Like the majority of knife edge or roller assemblies, this end fixity device was restricted to a single degree of freedom. However, in addition to the lower rotational restraint achieved, the device had other advantages. The first of these was that no corrections for effective free length were necessary; the second was that the pivot axis could be statically balanced for precision tests. Thirdly, the use of commercial ball bearing assemblies permitted the use of high-quality parts at very low cost.

The restriction to a single degree of freedom was lifted in subsequent research (17). Two sets of half bearings resulted in a fixture having two degrees of freedom. The new device was entirely similar to the old, with the important exception that the half bearings enabled the testing of specimens of essentially zero length via the simple expedient of assembling the base castings and the accompanying half bearings around a cylindrical steel bar. In this way the friction

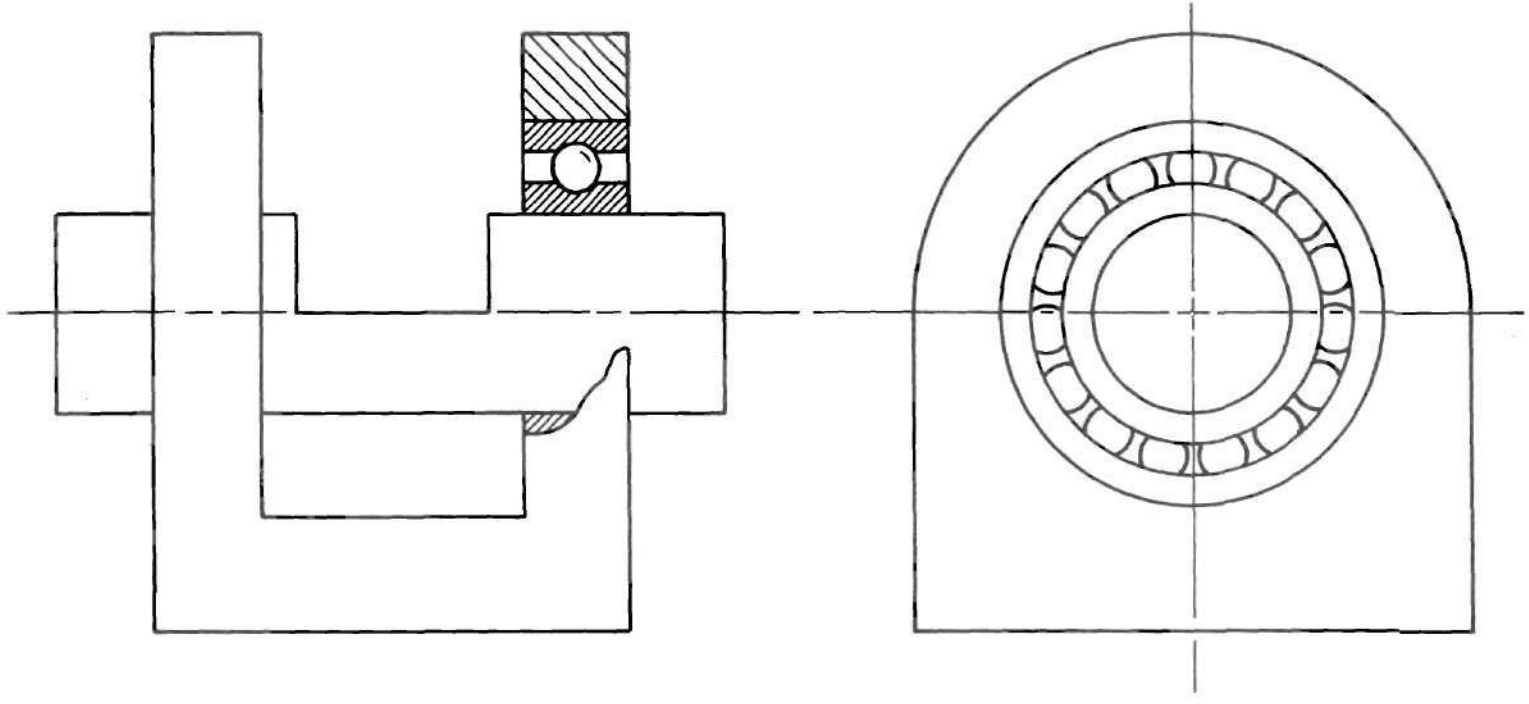

Figure 13. Barlow's End System for Light Loads (Single Degree of Freedom).

characteristics of the device could be evaluated by determining the torque required to start rotation of the bar under various compressive loads of the assembly. This test was performed about one axis only, owing to the extreme freedom of movement of the assembly. Friction in the fixture is manifested in an eccentricity of loading, and Barlow reports that eccentricities of .0039 inch at 100 pounds and .00595 inch at 6000 pounds were measured, concluding that these were negligible. This device is shown in Figure 14.

The next major development appears to have been due to Templin (18), who devised a system of hydraulically-supported spherically-seated compression test machine platens. The design was done with an eye to six basic requirements set forth by Templin for suitable fixtures for making round-end tests of column specimens:

1. There should be three degrees of freedom,

2. The device should possess as low resistance to rotation as possible,

3. The method should be applicable to large total load systems,

4. Distortion should be minimal during use,

5. The device should apply either uniform axial loads or loads with prescribed eccentricities,

6. It should be reasonable in cost, simple to install, and easy to maintain.

A drawing of the resulting device is shown in Figure 15.

In addition to satisfying the above requirements, the Templin device had some other interesting features. The fixture could be changed from near-zero to near-infinite rotational restraint through

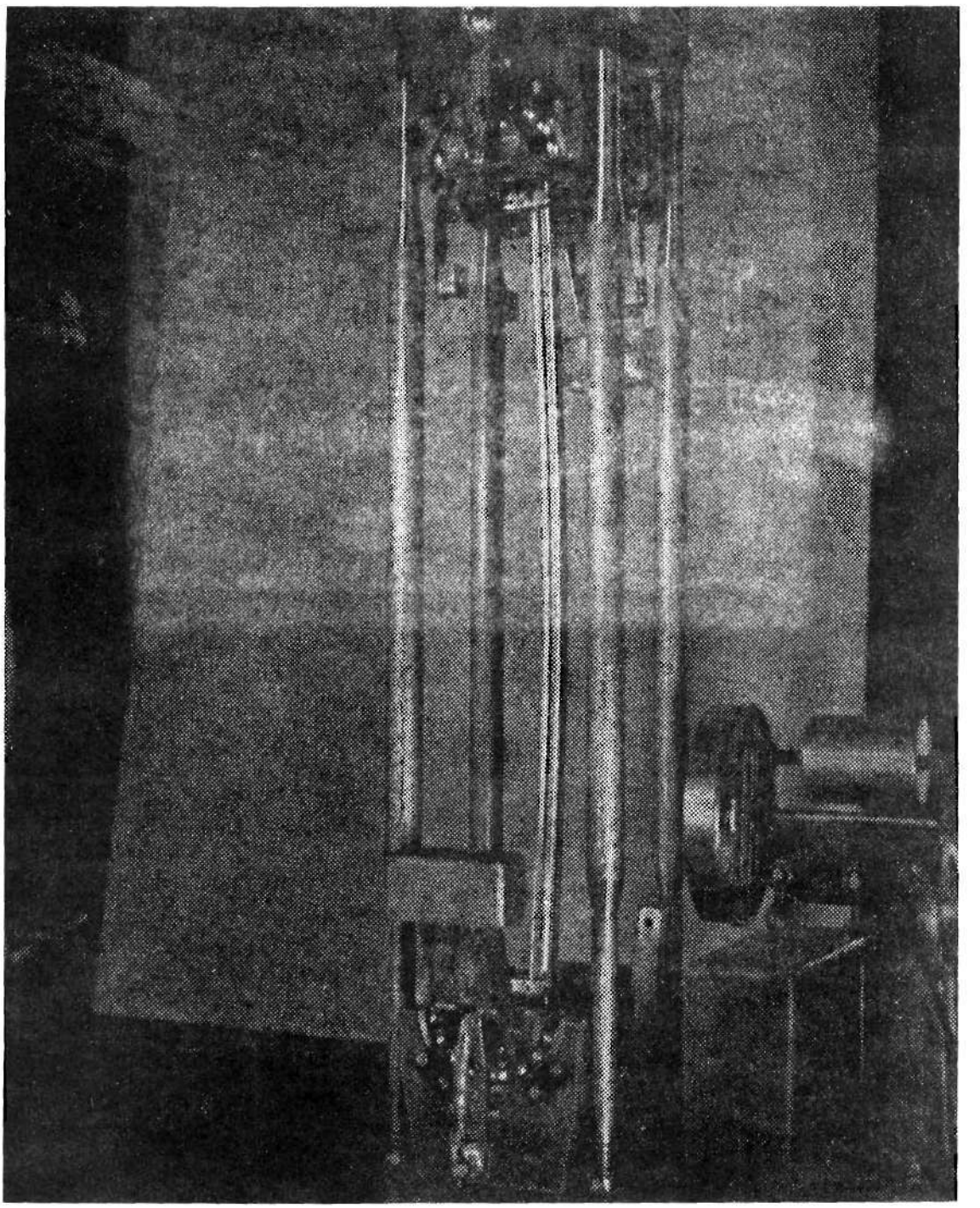

Figure 14. Barlow's Two Degree of Freedom Pin End Fixture

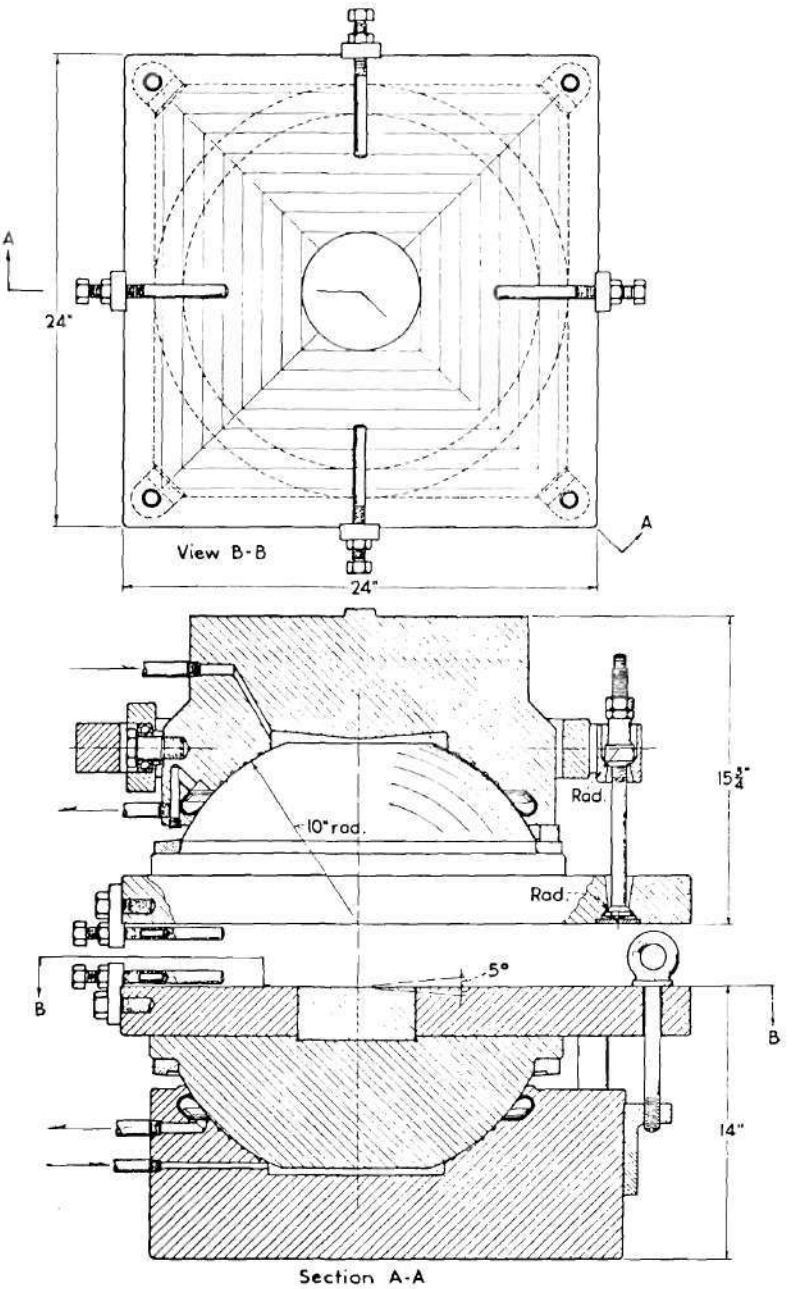

Figure 15. Assembly Drawing of Templin's Device

the simple expedient of inserting four distance pieces between the base plate and the platen; errors in parallelism between upper and lower platens could be corrected readily by making the distance pieces adjustable. Furthermore, it was found that the testing machine, being of the hydraulic type, could supply the oil to the test fixture at the proper pressure, thus eliminating the need for a separate hydraulic system. Driving the test fixture with the test machine hydraulic system decreased the strain rate capability of the machine, but this is of little consequence in quasi-static testing. The platens had attachments for positioning specimens with respect to the platens, as well as attachment points for transducers.

To evaluate the frictional characteristics of his device Templin performed a test essentially the same as that done by Barlow. The results are shown in Figure 16. The differences in behavior in the two directions are ascribed to slight errors in centering the fixtures. There can be little doubt that the device was of good quality compared with most others which preceded it.

In 1959 Goldberg and Lenzen (19) published the description of a roller fixture for pin-end column tests. The geometric details are clear from Figure 18. The rollers and base blocks were made of Ryalloy tool steel tempered to a Rockwell "C" scale hardness of 57. Foppl's (20) formula indicates that under a compressive load of 300,000 pounds and a contact length of 8 inches, the maximum bearing stress was 215,000 psi, considerably less than the ultimate stress of 300,000 psi arrived at by conversion from the Rockwell hardness. Thus bearing failure was avoided. The rollers were keyed to the blocks by a tooth

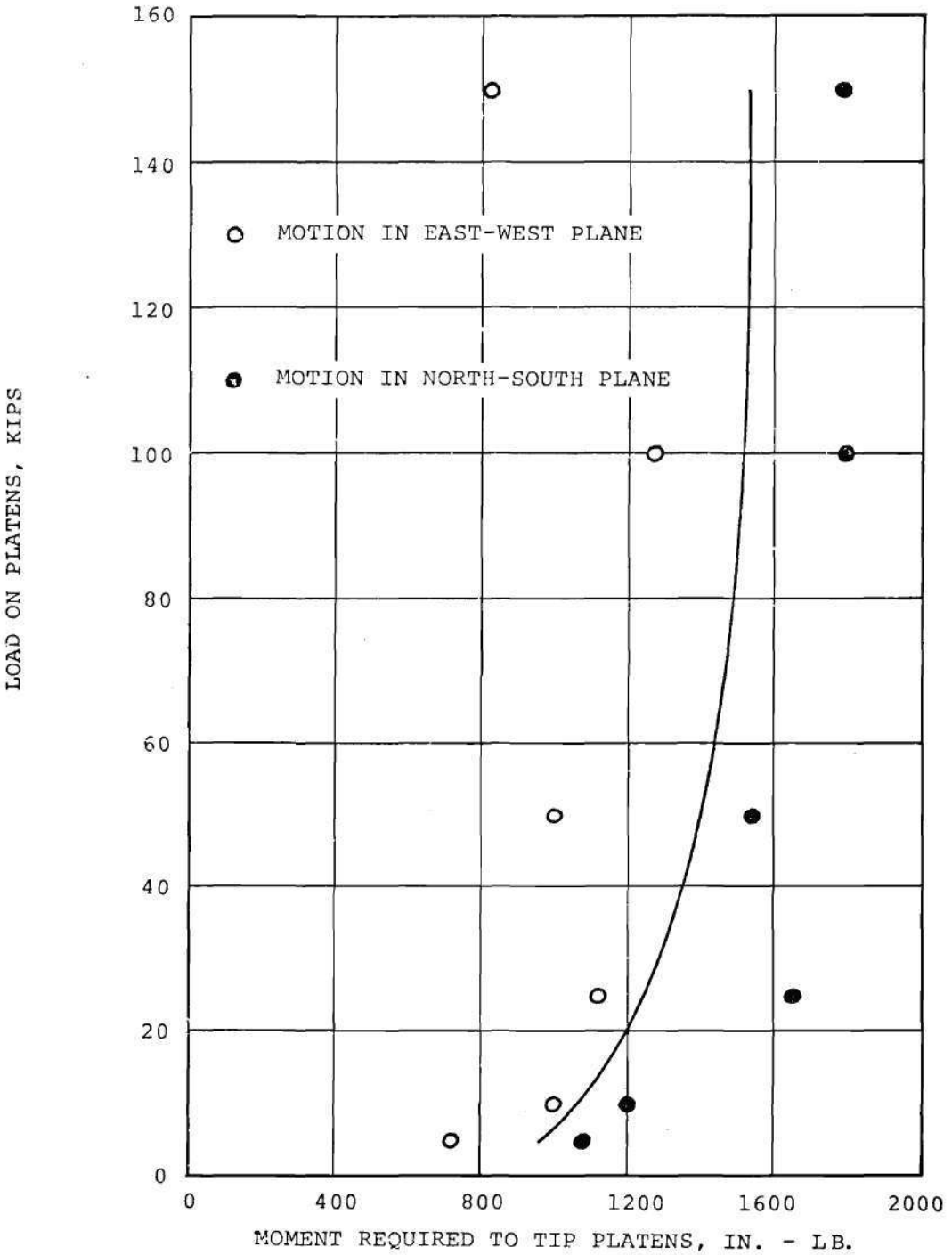

Figure 16. Resistance to Tipping of Templin Fixture When Functioning as a Complete Sphere Under Load

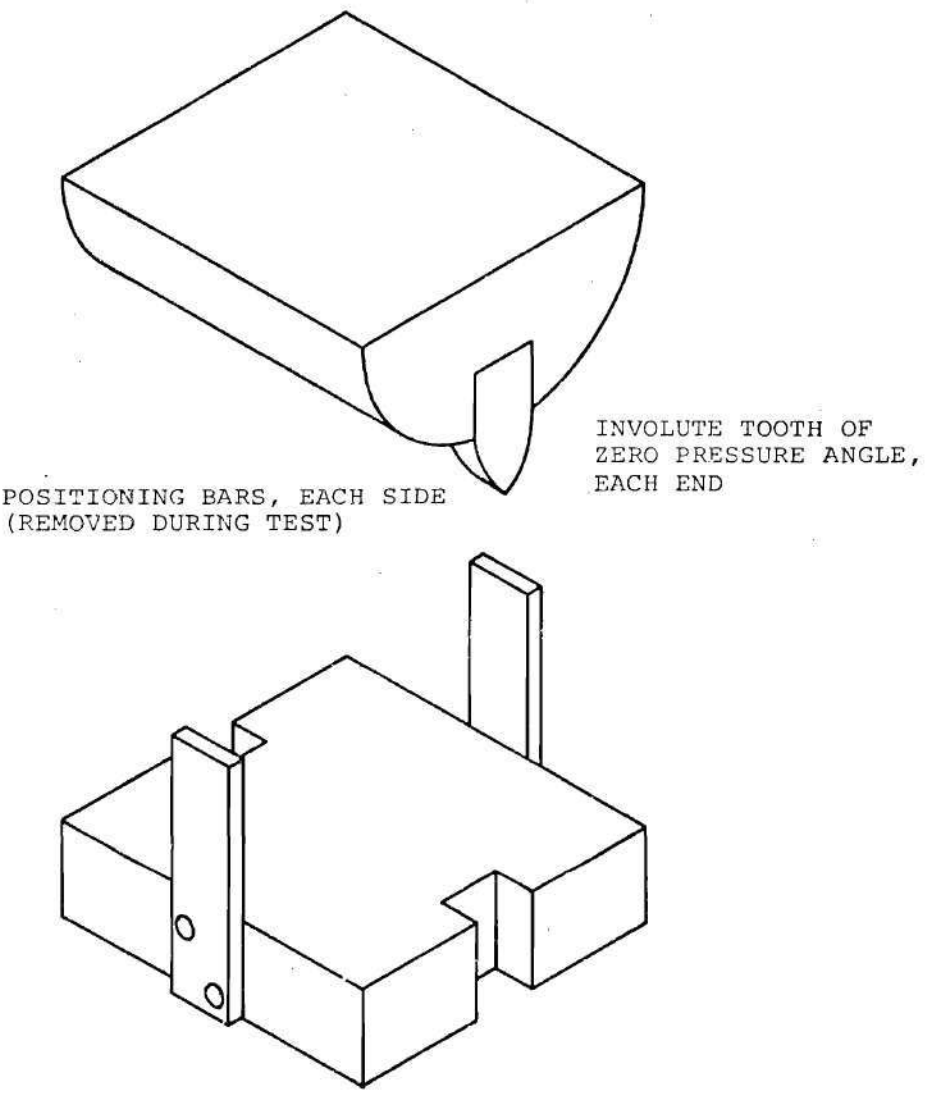

Figure 18. Fixture for Pin End Column Tests (Goldberg and Lenzen).

at each end, these teeth being involute curves of zero pressure angle. They resisted relative translation as long as the angular displacement of the roller was less than 22.5 degrees.

It is interesting to compare this device's rotational restraint, shown in Figure 17, with that of Templin's fixture. Scatter in the data precludes any definite conclusions, but it may be said that this apparatus was at least competitive with that of Templin, particularly at lower load levels.

More recently, Lehigh University carried out considerable research on steel structures for large civil engineering applications. The latest standard column end fixture used at their Fritz Engineering Laboratory (21,22) is shown schematically in Figure 19. The device was basically similar to that of Goldberg and Lenzen, but being designed specifically for large structures, its load capacity was considerably higher; viz., two million pounds. The material used in the roller and base block was special tool steel heat-treated to 70-80 Scleroscope surface hardness. The geometry was again dictated by the necessity of avoiding bearing failure; with a roller radius of ten inches, the cylinder length came out to be 24 inches.

It is evident from Figure 19 that the apparatus consists essentially of a column base plate (to which the column was welded), a fixture platen that connects the column base plate to the cylindrical bearing block, the flat bearing block, an adjusting assembly composed of sliding height-adjustment wedges and a small cylindrical bearing, and a base. Top and bottom fixtures were identical. The need for obtaining uniform contact pressure along the cylinder-bearing block

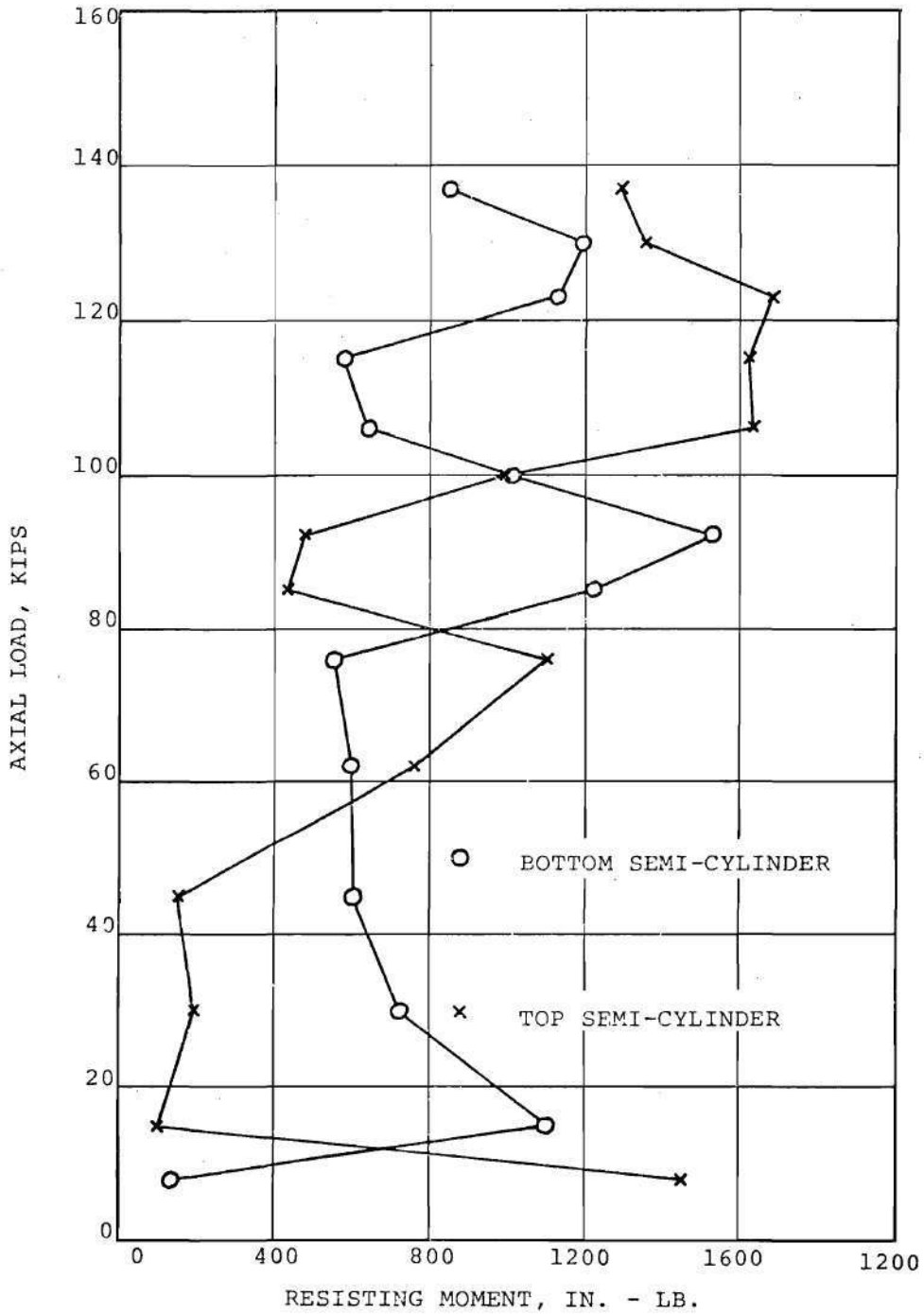

Figure 17. Resistance of Semicircular Ends to Rotation When Subjected to Axial Load (Goldberg and Lenzen).

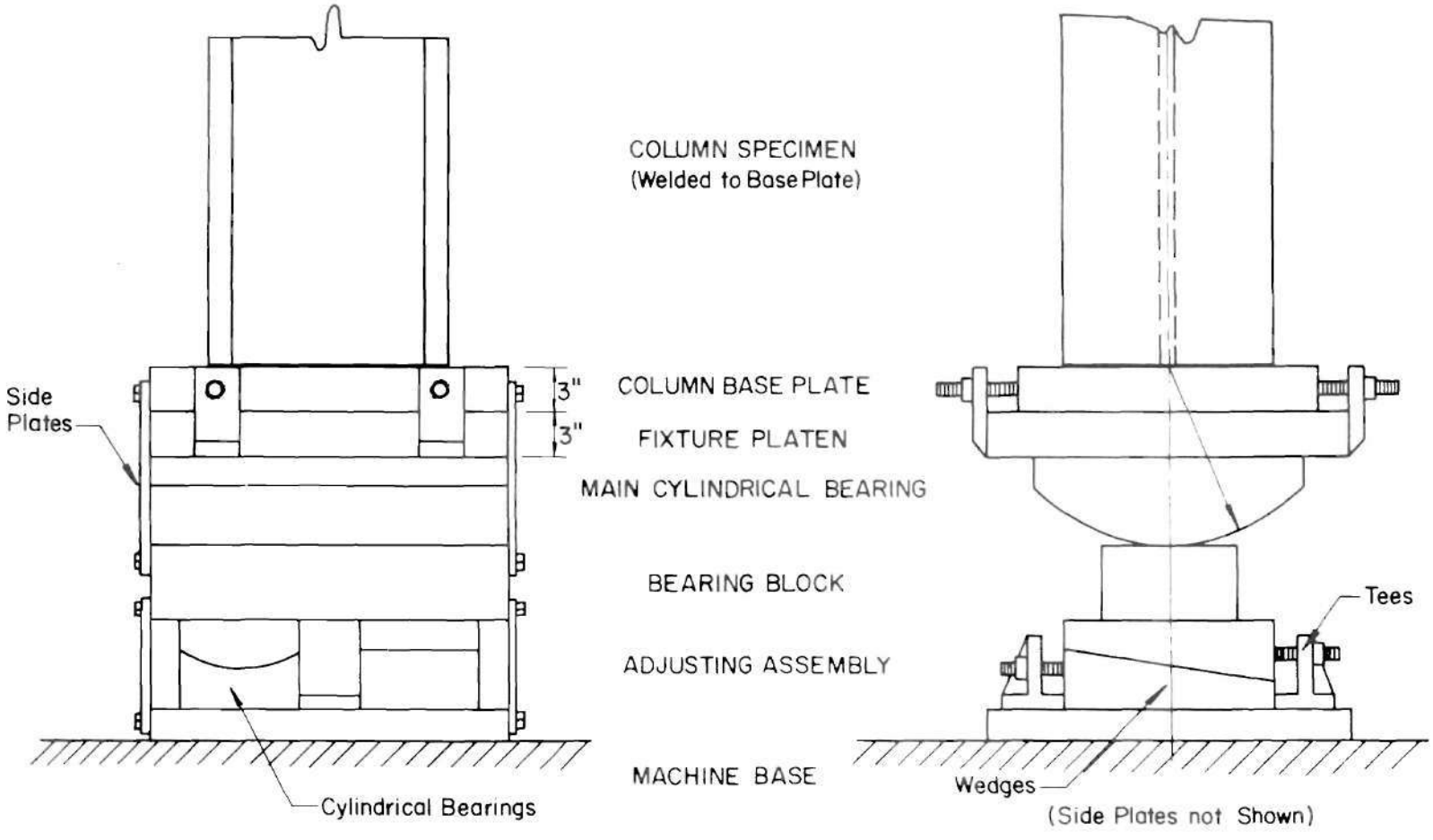

Figure 19. Standard Column End Fixture at Fritz Engineering Laboratory.

interface and for neutralizing lack of normality between the column axis and the testing machine table was satisfied by the adjusting assembly. As the height of the wedge adjustment changed, the end plane of the column rotated around the cylindrical bearing. The column base plate could be slid relative to the fixture platen, permitting the use of the well-known "centering under load" technique to minimize eccentricity.

Tests were carried out to evaluate the rotational restraint actually present under axial load. For low load ranges, a hysteresis check was made in a load-unload cycle. No hysteresis was observed. For high load ranges, a hydraulic jack was mounted parallel to the column between the base plates, such that additional bending and axial stresses could be superposed on the existing load states. The results are shown in Figure 20.

In methods of adjustment and alignment, the above fixture was quite similar to one used earlier at Lehigh University and described in lucid detail by Adams and Galambos (23) and by Beedle, Ready, and Johnston (24). Only the means of allowing rotation was dissimilar; this device utilized a double knife edge. The test assembly is shown schematically in Figure 21 and pictorially in Figure 22. Steel structural members of full-scale building size were tested in the machine, the point of departure from previous methods being that end moments were applied rather than minimized. The chief criterion regulating the geometry of the end fixture was that the point of end rotation and application of axial load, the center of moment, the point of lateral support (the support being necessary to equilibrate the

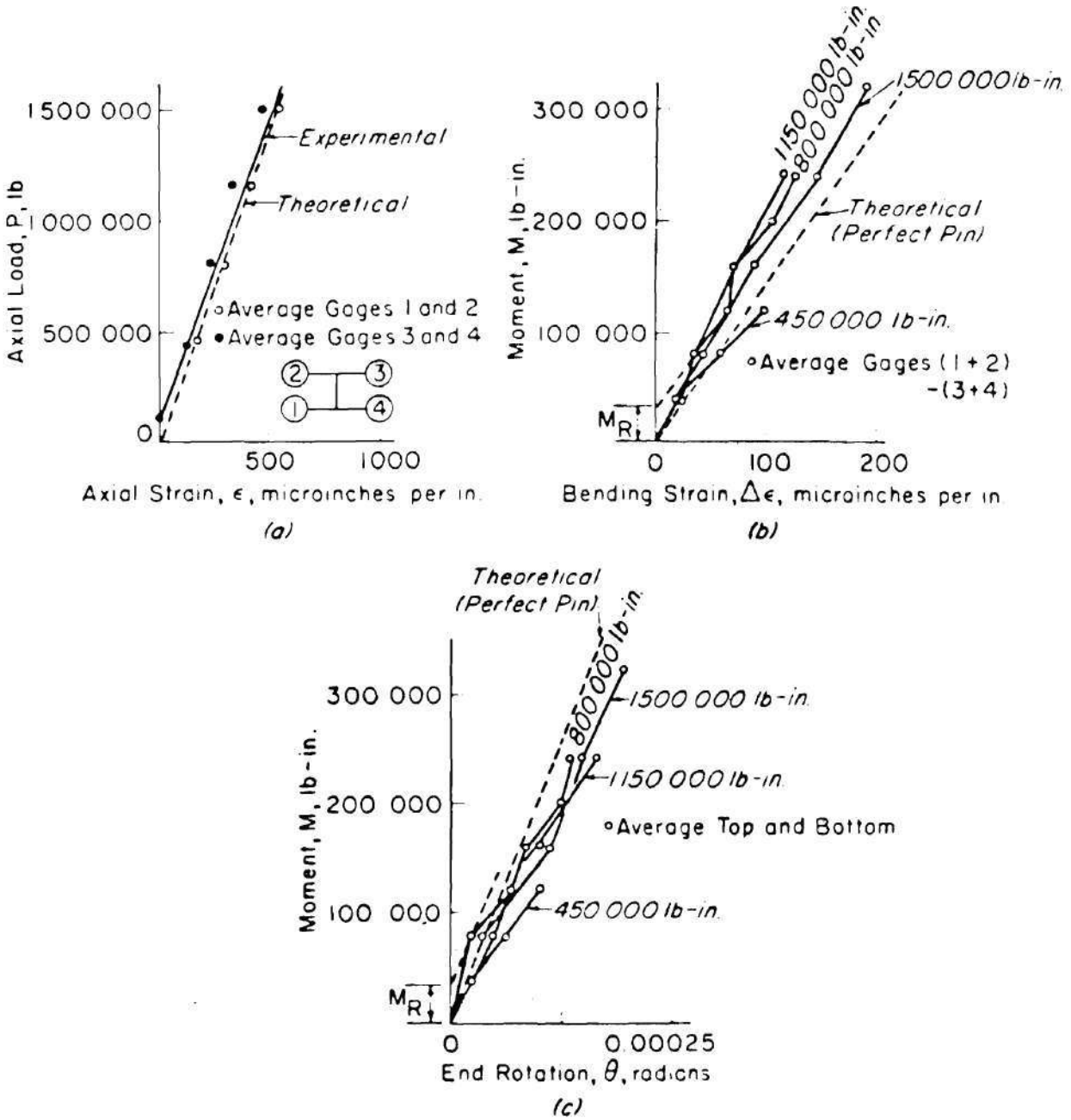

Figure 20. Performance of the Apparatus Shown in Figure 19

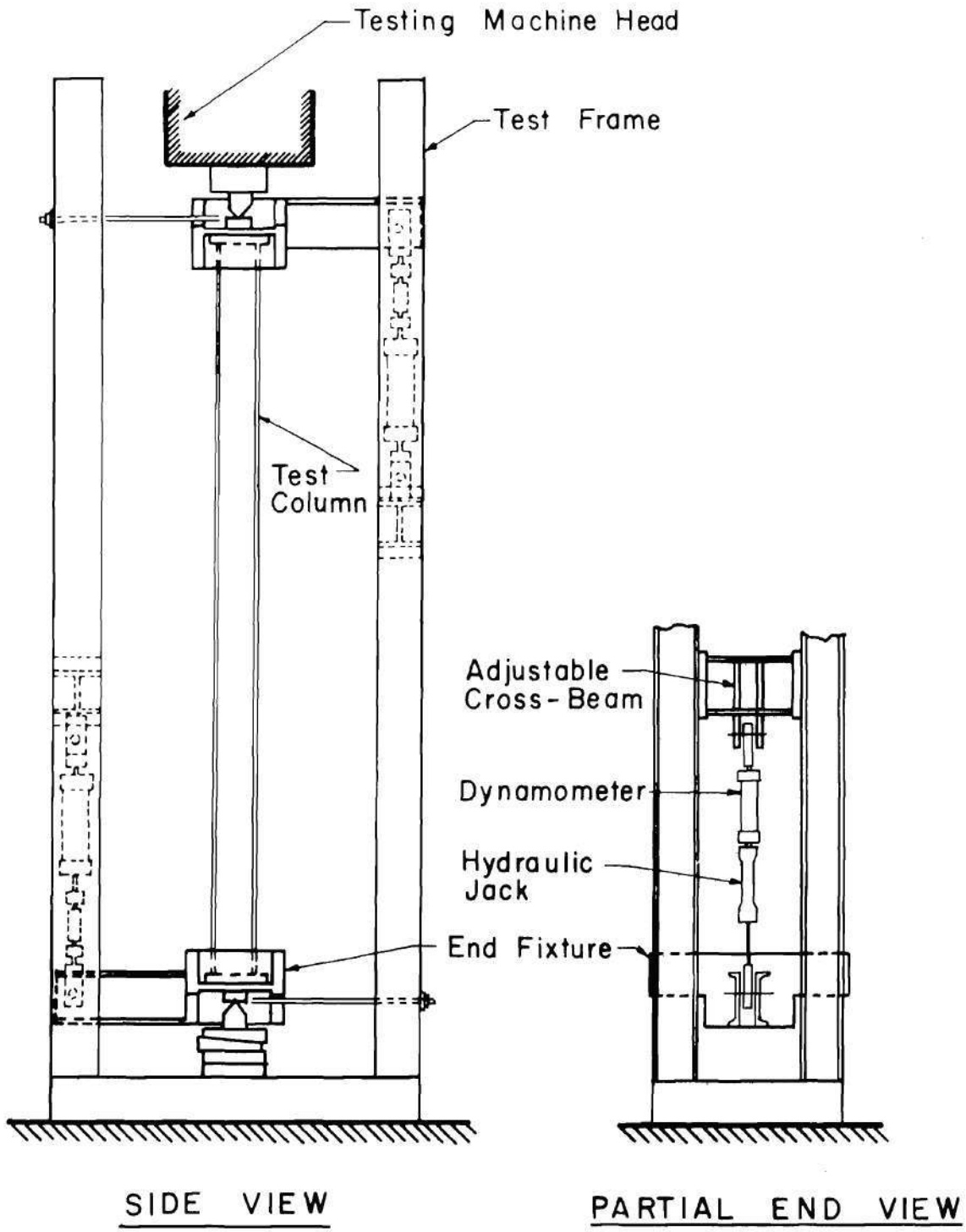

Figure 21. Test Assembly for Unbraced Columns.

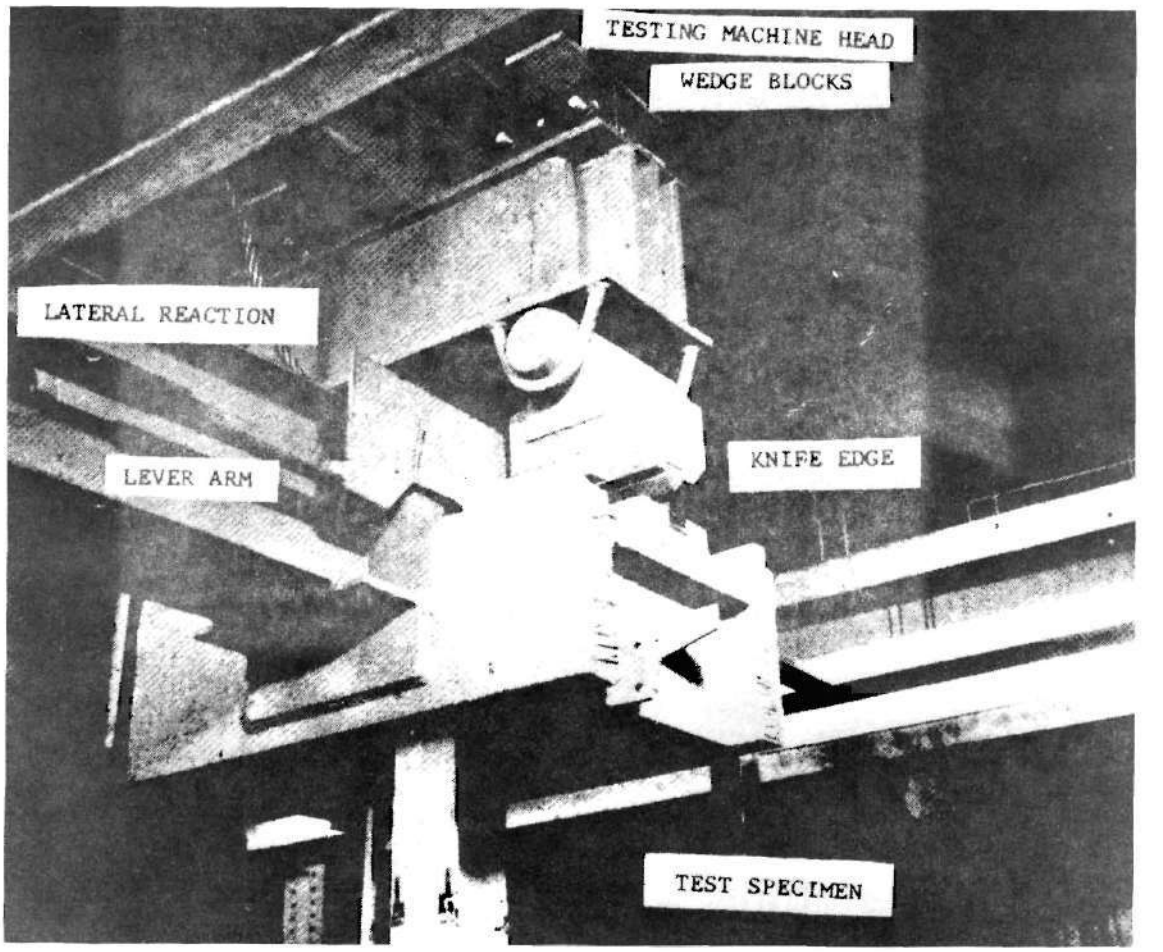

Figure 22. Upper End Fixture of Apparatus Shown in Figure 21 (Adams and Galambos).

applied end moments), and the end of the actual test specimen lie as nearly as possible in the same plane. This condition was reasonably satisfied in all but the last requirement, the end of the column being almost six inches above the knife edge. It was thus necessary to use an adjusted column length in the data analysis.

Application of moments to the end of the column was accomplished via an arm mounted at the end of the specimen, perpendicular to its axis. Each arm was driven at the outboard end by a tension-compression hydraulic jack that was mounted on the test frame. Alignment was accomplished by centering the column carefully on the end fixtures and then positioning the fixtures equidistantly from the vertical screws of the testing machine. The knife edge seats tended to automatically position the knife edge blocks, which could be moved with respect to the adjusting wedges. Alignment was checked with strain gages and levels; leveling under load was used sparingly. It was deemed that alignment was not as critical as in other tests because of the presence of the applied end moments.

Displacements were initially measured by observing the relative motion of a graduated scale fixed to the column and a taut wire hanging from a fixed point. Subsequently, dial gages were used for both lateral deflection and, in conjunction with a micrometer lead screw and a leveling bar, end rotation measurement.

Three different tests were described: axial load alone, with both ends free to rotate; axial load in combination with a moment applied at one end, with the opposite end pinned; and axial load with one applied end moment, with the opposite end clamped. In the last

case, clamping was obtained by having the hydraulic jack supply enough force to the end of the moment arm to drive the measured end rotation to zero. The general testing technique was to apply a given axial load and to hold it constant while varying the applied end moment. Since the application of end moments altered the axial load in the column, the two quantities were alternately adjusted until each attained the desired values. Then the moment was incremented and the process repeated. Lateral displacements at the end of the beam were neutralized by applying appropriate forces to the lateral supports.

One of the main objectives of the test series was to compare measured carry-over moments with those predicted by analysis. Inasmuch as the agreement was good, the authors concluded that friction in the knife edges was minimal. To verify this conclusion they conducted moment-reversal tests at the upper knife edge and observed no detectable hysteresis. Their results are given in Figure 23.

At this point there exists a natural inclination to extend the results of column tests to two-dimensional structures -- plates and shells. The complication, of course, is that boundary conditions are now prescribed along a line, rather than at a point. Nevertheless, some experimental studies (25-36) have been undertaken, and they amply illustrate the difficulties that exist in treating even the simplest of cases: uniform, homogeneous, isotropic, flat rectangular plates simply-supported along two edges. When sandwich plates are considered, the complexity of boundary restraint is greatly compounded, a point that is strongly made by Benson and Mayers (37). For thin shells, moreover, this approach of trying to duplicate in the laboratory all the

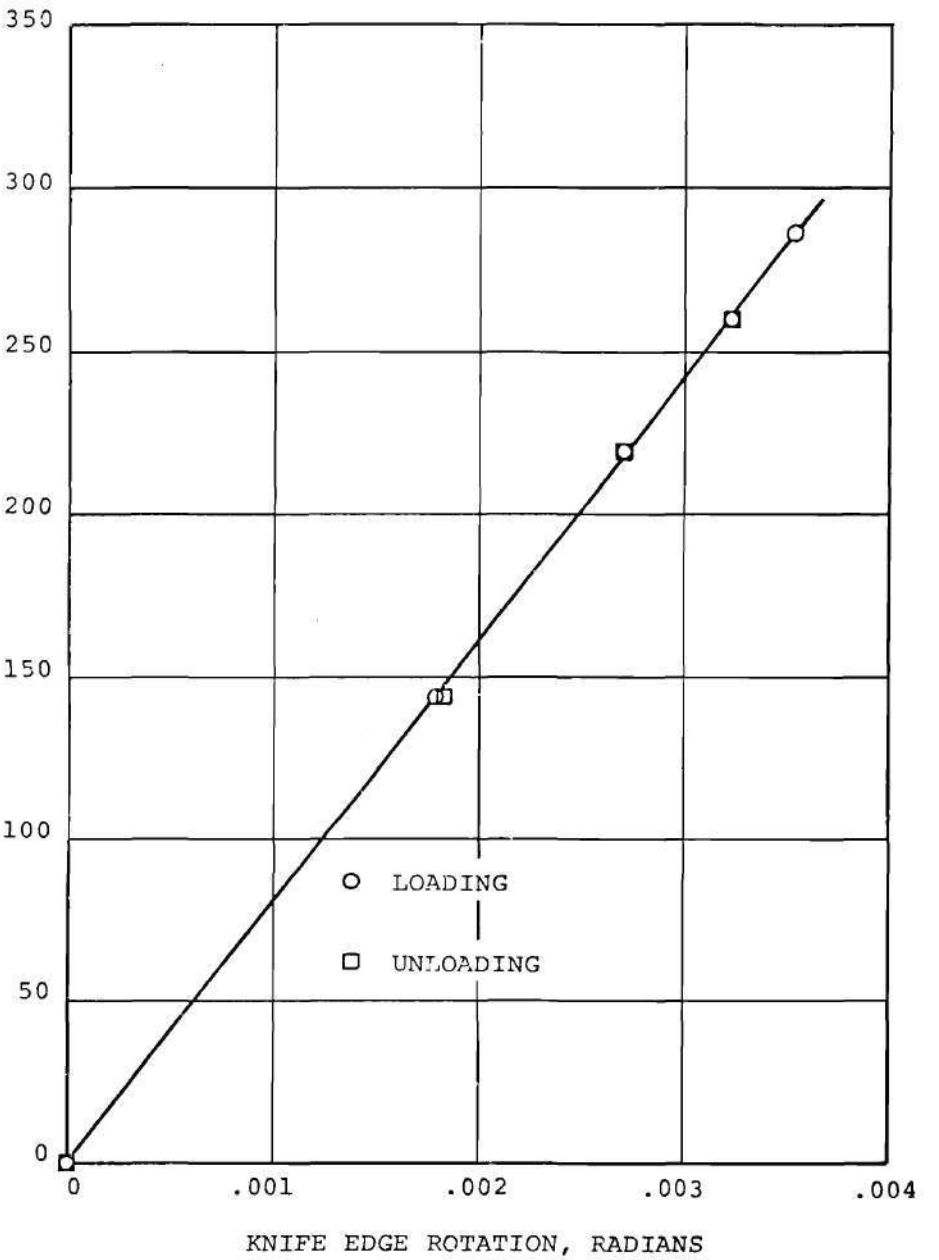

Figure 23. Performance of the Device Shown in Figures 21 and 22.

boundary conditions obtained by analysis meets with staggering difficulties, since at least some of the boundaries are curved lines. Thus, boundary condition studies for shells have tended to be analytical in nature. While most of these investigations are fairly recent (38-42), the earlier recognition of the significance of boundary effects by Love (43) and Southwell (44) cannot be ignored.

Expanded Disucssion of Problems Associated with Pin End Fixtures

Let us consider the case of a spherical column fixture bearing on a plane surface. The first issue of importance is that of the contact stresses. These can cause rupture of the ball or bearing failure of the surface or both. We may recall that Hodgkinson noted difficulties in this regard. Some information on the contact stress levels can be obtained from the work of Hertz (20). If we assume the following material properties; viz.,

$$\begin{aligned} &\text{Modulus of elasticity} && = E && = 30\text{x}10^{6} \\ &\text{Poisson's ratio} && = \nu && = .3 \\ &\text{Maximum compressive stress} && = \sigma_{max} && = 210{,}000 \text{ psi} \end{aligned} \tag{1}$$

then, following Hertz, we may compute that the spherical diameter must be 82.5 inches for an applied load of 300,000 pounds. Such a large diameter presents problems both with regard to manufacture and to operation. Furthermore, there are difficulties with the precise definition of effective length, and with sideslip during relatively large rotations. In addition, at higher load levels the rotational

resistance due to flattening of the spherical surface becomes so high that infinite, rather than zero, rotational restraint is approached. According to Wagner (45) agreement with the Euler curve is thus precluded. In fact, the resulting error may be as high as 100 per cent if the effective length is assumed to be the distance between the centers of the hemispherical ends.

It is apparent from the Hertz equation that one method of reducing the high contact stresses is to make the bearing block a hemispherical surface rather than a plane. In this case, if the diameter of the ball and socket are equal, the contact stresses are reduced for a given diameter so that the ball size can become reasonable. However, the frictional forces become prohibitive. It is for precisely this reason that the hydraulic fluid bearing becomes so attractive when a hemispherical seating is used. In this case, the hemisphere size can be substantially reduced, and error in determination of the effective column length is similarly minimized.

Another means of reducing the contact stress is to replace the hemispherical surface, when used with a plane, with a semi-cylindrical rolling surface. In this case, we compute from Hertz' equations that a diameter of 8.88 inches suffices. This is far more reasonable from a manufacturing point of view than the 82.5 inch diameter hemisphere. There remain the problems of sideslip and friction, but these can be overcome, as is evident in the work of Goldberg and Lenzen. Their roller fixture and that of the University of Washington appear to be superior to the Lehigh device in that sideslip was prevented, thus greatly simplifying the question of effective strut length.

Effective length questions also arise in the case of the knife-edge fixture; since in this type of device rotation must occur about some point other than the intersection of the neutral axis and the end plane of the specimen, it is clear that the length between inflection points will not correspond to the nominal length of the column. Thus, even if the knife edges were considered friction-free, it was desirable to derive applicable mathematical expressions for the purpose of analyzing experimental results of knife-edge tests. Such expressions have been formulated (45). As before, the radii of the knife edge and that of the seat must be chosen in accordance with the Hertzian equations. It is necessary that the knife edge be sufficiently long to allow appreciably different radii in the edge and the carrier. The reason for this can be discerned from Figure 24, where it is apparent that if the radii are equal, or nearly equal, the fixture behaves like the pin device, with correspondingly high friction levels. Wagner showed that if the end of the strut rotates through an angle θ as a result of the axial load, the line of action of the force intersects the axis of the strut at the point A, which is separated from the contact point of the knife edges by the distance

$$\frac{\Delta L}{2} = \frac{1}{\frac{1}{r_2} - \frac{1}{r_1}} \quad . \tag{2}$$

The length L - ΔL is therefore to be regarded as the buckling length. A criterion for the difference between the radii r_2 and r_1 is that the

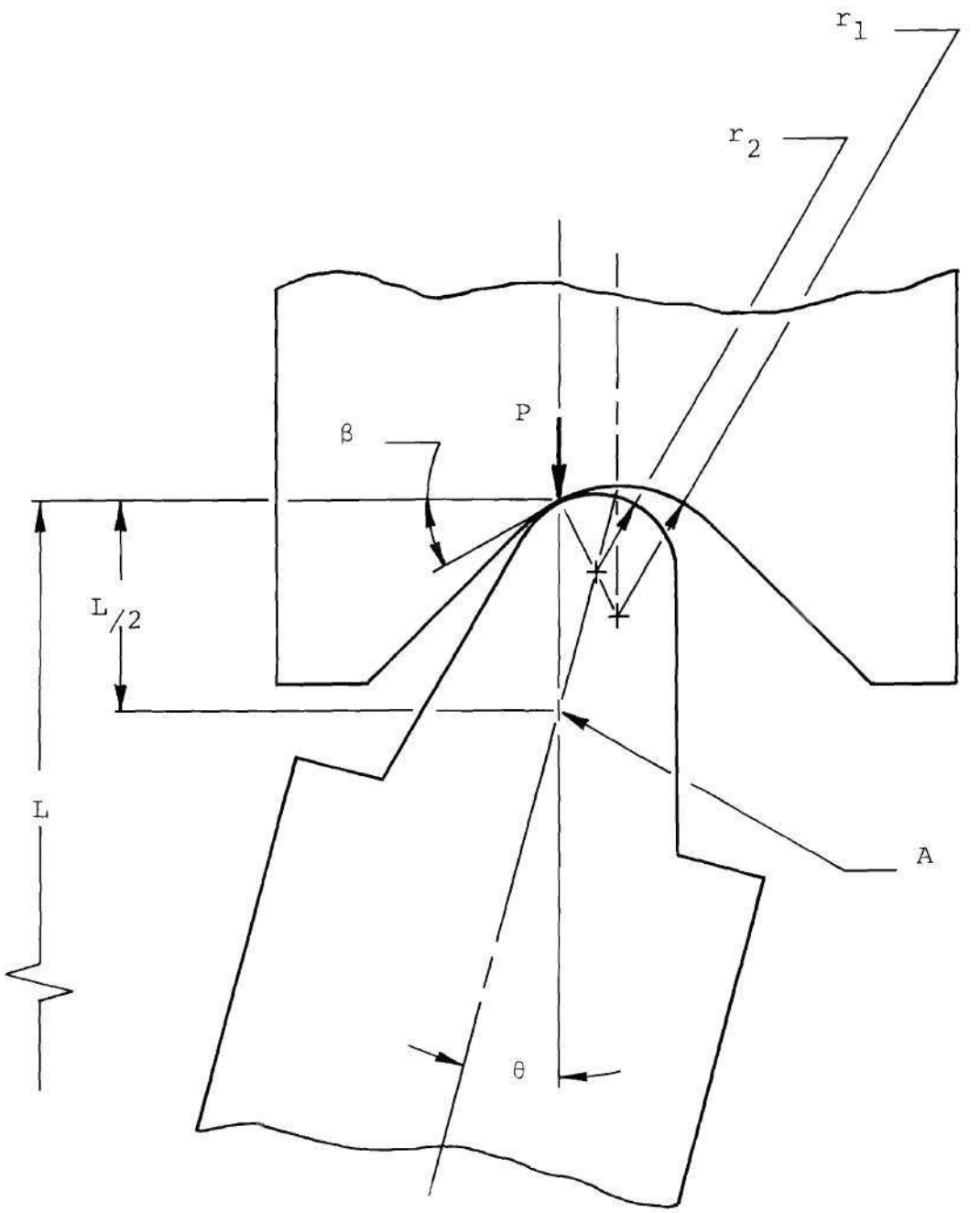

Figure 24. Geometry of Knife Edge System

angle β be at all times smaller than the angle of friction. Obviously, if this condition is not met, the knife edge will slip in the carrier as mentioned previously, and the otherwise simple relation will be obscured.

When there are rigid fixtures, or carriers, at the ends of the specimen, the effective length situation is somewhat more complex. A rational method for dealing with rigid portions of equal length at freely supported ends has been presented by Engesser (46). Nater (47), Usinger (48), and Leduc (49) have treated the problem of the straight elastic column elastically restrained against rotation at its ends while Bleich (50) has made similar studies for the inelastic case. Another treatment was presented by Osgood (15), and that work will be summarized here.

The familiar governing differential equation for the column is

$$\frac{d^2w}{dx^2} = \frac{M}{EI}. \tag{3}$$

With reference to Figure 25, the bending moment M at any section may be expressed as

$$M = M_0 + F(S_0 + x) - Pw. \tag{4}$$

The appropriate boundary conditions are

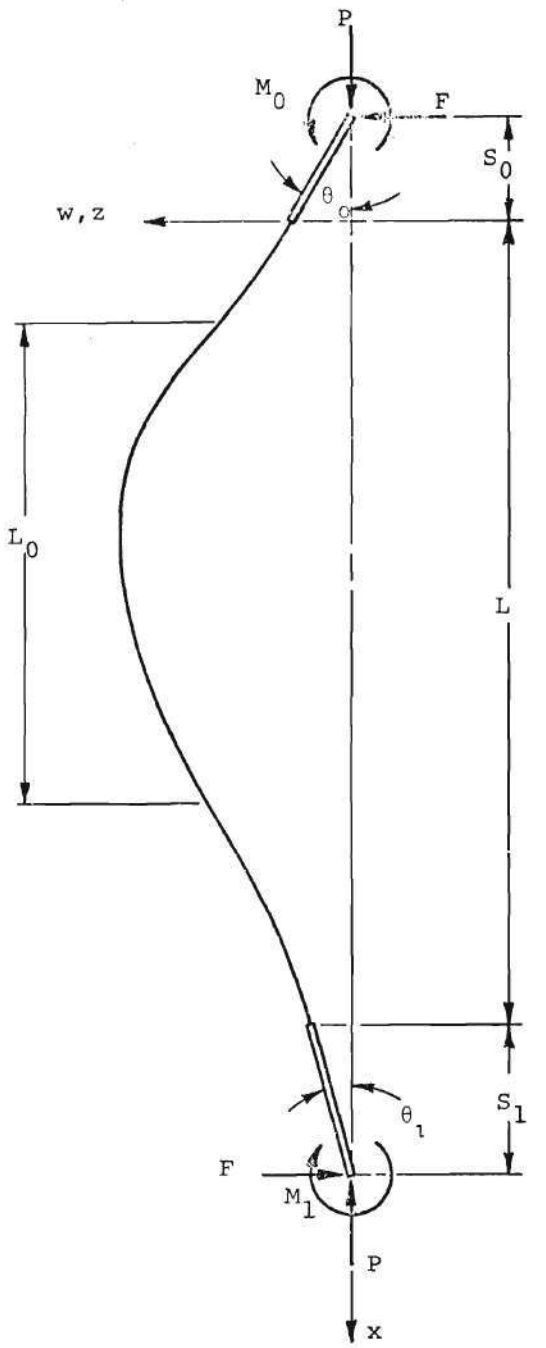

Figure 25. Deflected Center Line of Column.

$$x = 0: \quad \frac{dw}{dx} = \theta_0, \quad w = S_0\theta_0; \tag{5}$$

$$x = L: \quad \frac{dw}{dx} = \theta_1, \quad w = -S_1\theta_1.$$

Solution of the above boundary-value problem yields four linear homogeneous equations in θ_0, θ_1, and two constants of integration. The existence of a non-trivial solution for w requires the vanishing of the determinant of the coefficients in the system of equations.

If the non-dimensional variables

$$\varphi = L \sqrt{\frac{P_{cr}}{EI}} \tag{6}$$

$$\alpha_0 = \frac{k_3}{PL\left(1 + \frac{S_0}{L} + \frac{S_1}{L}\right)} \tag{7}$$

$$\alpha_1 = \frac{k_2}{PL\left(1 + \frac{S_0}{L} + \frac{S_1}{L}\right)} \tag{8}$$

are introduced, the characteristic equation may be written in the form

$$\left\{1 + \alpha_0 + \alpha_1 - \varphi^2\left[\frac{S_0 S_1}{L^2} - \frac{S_1}{L}\left(1 + \frac{S_1}{L}\right)\alpha_0 \right. \right. \tag{9}$$

$$\left. - \frac{S_0}{L}\left(1 + \frac{S_0}{L}\right)\alpha_1 + \left(1 + \frac{S_0}{L} + \frac{S_1}{L}\right)\alpha_0\alpha_1\right]\Big\} \sin\varphi$$

$$- \varphi\left[\alpha_0 - \frac{S_0}{L} + \alpha_1 - \frac{S_1}{L} + 2\left(1 + \frac{S_0}{L} + \frac{S_1}{L}\right)\alpha_0\alpha_1\right]\cos\varphi$$

$$+ 2\left(1 + \frac{S_0}{L} + \frac{S_1}{L}\right)\alpha_0\alpha_1\varphi = 0$$

For the special case $S_0 = S_1 = S$ and $\alpha_0 = \alpha_1 = \alpha$, we can introduce the non-dimensional variables

$$\rho = \left(1 + \frac{2S}{L}\right) - \frac{S}{L} = \frac{k}{PL} - \frac{S}{L}; \tag{10}$$

$$\rho' = \frac{\alpha - \frac{S}{L}}{1 + \frac{2S}{L}} = \frac{\frac{k}{PL} - \frac{S}{L}\left(1 + \frac{2S}{L}\right)}{\left(1 + \frac{2S}{L}\right)^2} \tag{11}$$

Substitution into equation (9) and collecting terms gives

$$\left(\frac{1 + \cos\varphi}{\sin\varphi} + \rho\varphi\right)\left[\left(1 + 2\rho'\right)\left(1 - \cos\varphi\right) - \rho'\varphi\sin\varphi\right] = 0. \tag{12}$$

It is noteworthy that values of φ equal to integer multiples of 2π make the left-hand side of equation (12) indeterminate. However, insertion of these values into equation (9) excludes them as possible solutions. Two other possibilities arise when each of the two factors in equation (12) vanishes. Equating the first factor to zero gives rise to $\theta_0 = -\theta_1$, while the vanishing of the factor on the left yields $\theta_0 = \theta_1$. It is apparent that the first and second cases correspond to the first and second modes, respectively; hence we are interested only in the first solution. The vanishing of the first factor may be rewritten

$$\cot \frac{\varphi}{2} + \rho\varphi = 0. \tag{13}$$

The solution to this equation is simplified further if we introduce the new variables

$$s = \frac{\varphi}{\sin\varphi} - 1; \tag{14}$$

$$t = 1 - \frac{\varphi}{\tan\varphi}. \tag{15}$$

Equation (13) then becomes

$$t + s = -\frac{1}{\rho}. \tag{16}$$

Tables of t + s are available in Reference (31).

Another special case is represented by the conditions $\alpha_0 = 0$ and

$S_0 = S_1 = S$. Introduction of the new non-dimensional variable

$$\rho'' = \frac{\alpha_1 - 2SL}{1 + \frac{2S}{L}} = \frac{\frac{k_2}{PL} - \frac{2S}{L}\left(1 + \frac{2S}{L}\right)}{\left(1 + \frac{2S}{L}\right)^2} \tag{17}$$

into equation (9) simplifies it to the form

$$t = -\frac{\varphi^2 S}{L}\left(1 + \frac{S}{L} + \frac{S}{\rho'' L}\right) - \frac{1}{\rho''}\,, \tag{18}$$

which, by trial and error, may be solved for the eigenvalue φ with the aid of Table 8 in Reference 15.

Finally, if $S_0 = S_1 = 0$, equation (9) may be expressed in the form

$$\alpha_0\alpha_1(t^2 - s^2) + (\alpha_0 + \alpha_1)\, t + 1 = 0. \tag{19}$$

Zimmerman (51) gives this equation and Prager (52) presents it in a modified form. Both assume it to apply for elastic buckling only. It has also been published in a paper by Osgood (53). The equation may be solved directly by means of the nomogram, Figure 26, the idea for which it attributed to L. B. Tuckerman by Osgood.

In order to use the nomogram, a straight line is run through the points of the circle determined by the values of α_0 and α_1 read on the

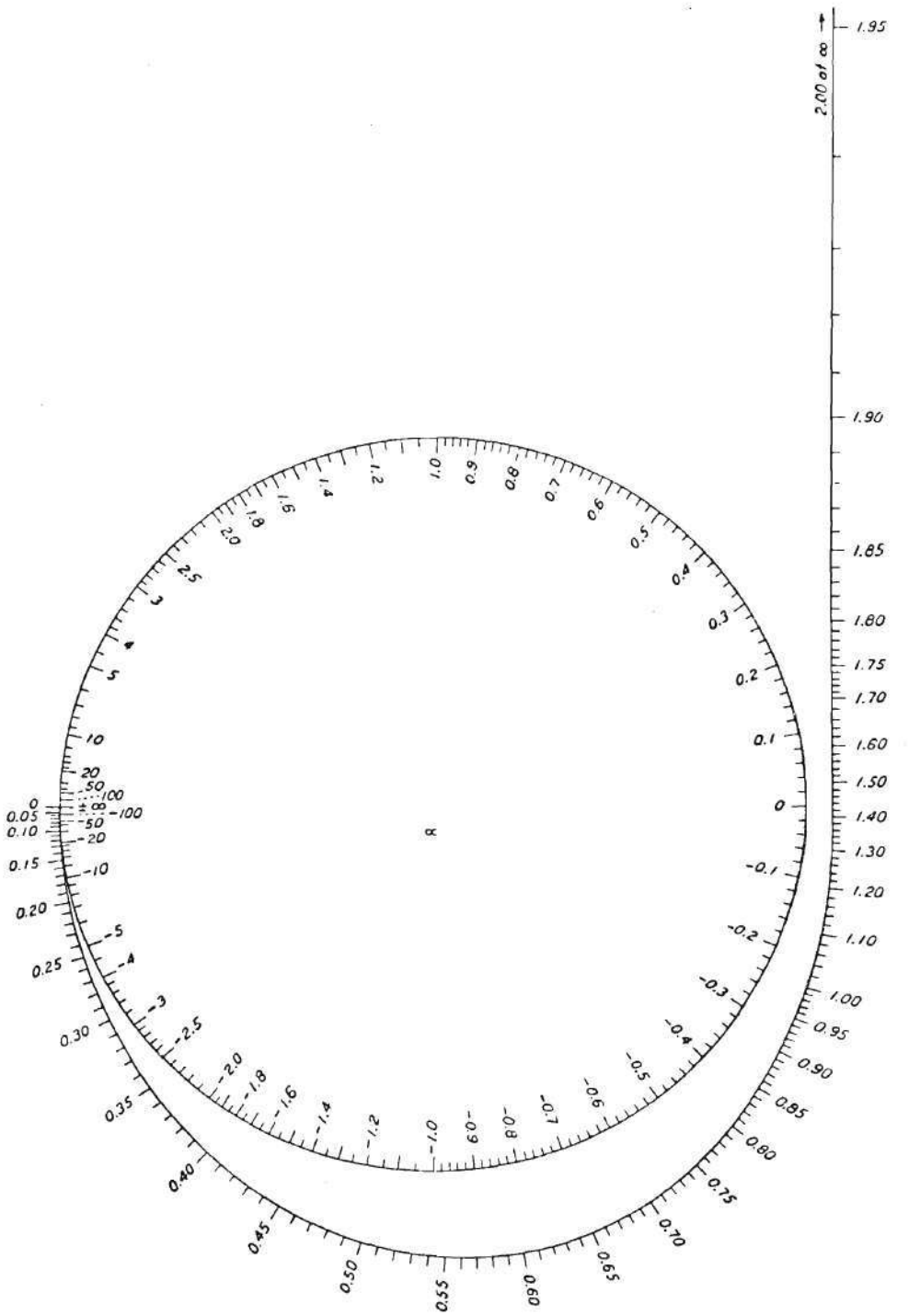

Figure 26. Nomogram for Determining ϕ/π

circular scale. This line will intersect the spiral curve in at least one point. The value of φ/π corresponding to this point, or the lower value if there are two intersections, read on the scale of the spiral curve, will be the lowest value for which buckling can occur. In the case of the two points of intersection, the higher value of φ/π corresponds to an unstable condition of equilibrium.

Once having found φ, it is a simple matter to find the distance between inflection points L_0; i.e., the effective length for the pin-end condition. Noting that the axial load is uniform along the length of the column, we have

$$P_{cr} = \frac{\pi^2 EI}{L_0^2} \quad . \tag{20}$$

Recalling that

$$\varphi = L\sqrt{\frac{P_{cr}}{EI}} \quad . \tag{21}$$

subsititution gives

$$L_0 = \frac{\pi L}{\varphi} \quad . \tag{22}$$

CHAPTER III

DETERMINATION OF BUCKLING LOADS FOR ACTUAL STRUCTURES

We have thus far illustrated the difficulties the experimentalist has faced in verifying the results obtained from analysis, and the techniques employed to surmount these difficulties. In all cases, the goal was to make the boundary restraint as nearly ideal as possible; knowledge of the actual boundary conditions was directly related to the success of this endeavor.

In many instances, however, the experimentalist finds himself in a very different situation. The interface between a component and the rest of a structural system may present such lack of ideality, or such complexity, or both, that analysis is unable to assess the degree and type of boundary restraint. If, in attempting to predict the buckling load of such a structure, the boundary restraint can be measured experimentally, its effect on buckling can be computed by analysis. In many cases this is impossible; having at hand only the test techniques discussed so far, the experimentalist has no alternative to buckling the structure and recording the maximum load. If the buckling process is elastic, no harm is done to the specimen, and the desired information is obtained.

In general, however, the sudden growth of deformations associated with buckling precludes the survival of the specimen in its virgin state. Thus, in the absence of non-destructive test techniques, there is no

way of knowing the buckling load for practical structures with realistic end restraint without ruining the specimen.

It should be pointed out at this time that the success of any test depends on its ability to distinguish the variable of interest from all others. In the case of the non-destructive test for end fixity, we must be mindful of the fact that buckling is also affected by deviation from ideality of many factors other than boundary conditions, such deviations being lumped under the term "imperfections" (in structural form, loading action, etc.)

The inevitability of imperfections has been generally recognized by analysts since Young and, of course, by all experimentalists. Christie appears to have been the first to compensate for imperfections in a test column by shifting the ends of the column relative to the supports. The tests of von Karman (13) show that slight imperfections such as small initial curvatures do not affect the strength of pin-ended columns when centered under load. Zimmerman (51) has also shown this result theoretically and Rein (54) has confirmed his work in a careful series of tests.

Nonetheless, the most important feature of the presence of imperfections is the effect on the motions normal to the loading direction. In 1807 Young discovered the relationship between the elastic lateral deflection at the mid-point of an imperfect column under axial compression, the compressive force, and the classic instability load for the perfect strut. By the end of the century it had become common engineering knowledge, and it has played a central role in column testing to this date.

The first use of the formula to interpret test data on columns was by Ayrton and Perry (4) in 1886, in the first verification of Euler's (2) work. Their paper was largely ignored, and it was not until R. V. Southwell (5) published his work that the methodology that bears his name became routine for the strut problem.

The analytical derivation of the formula that forms the basis of the technique is most straightforward. It consists of equating the coefficients for various harmonics when similar Fourier series for initial and elastic deflections are inserted in the appropriate differential equation of equilibrium. The result is

$$a_n = \frac{e_n}{\frac{P_n}{P} - 1} , \quad (N = 1,2,\ldots) \tag{23}$$

where the denominator is actually a load-dependent magnification factor. It is evident that if the eigenvalues P_n are widely separated, and if the load P is a substantial portion of the lowest eigenvalue P_1, the first term in the Fourier series for the elastic deflection predominates, giving

$$a_1 = \delta , \tag{24}$$

where δ is an elastic displacement measured at a suitable location (55) (the mid-point, in the case of the symmetric strut). We thus have

$$\delta \left(\frac{P_1}{P} - 1 \right) = e_1 \ . \tag{25}$$

Slight rearrangement gives

$$\delta = P_1 \left(\frac{\delta}{P} \right) - e_1 \ , \tag{26}$$

and we observe that δ and δ/P are linearly related. Thus, a plot of δ versus δ/P will have for its slope the critical load of the perfect specimen, and for its δ-intercept the quantity $-e_1$, which is a measure of initial imperfection. Other linear representations are possible, but this one is the most common. It is apparent that through the use of the slope and intercept of this plot, we have successfully separated the influence of imperfections from boundary effects.

To confirm his formula Southwell analyzed von Karman's data on centrally compressed columns. The results, Figure 27, were excellent in that the maximum deviation of the critical load derived by the technique from the classical critical load was 2.5 per cent. Similar agreement was reached when Robertson's data from experiments with specified loading eccentricities was analyzed.

Although this approach was specifically generated for the strut, it is much broader. A general view of its applicability to columns and plates was given by Horton, Cundari, and Johnson (56), while an outline of its potential to shell bodies has been presented by Horton

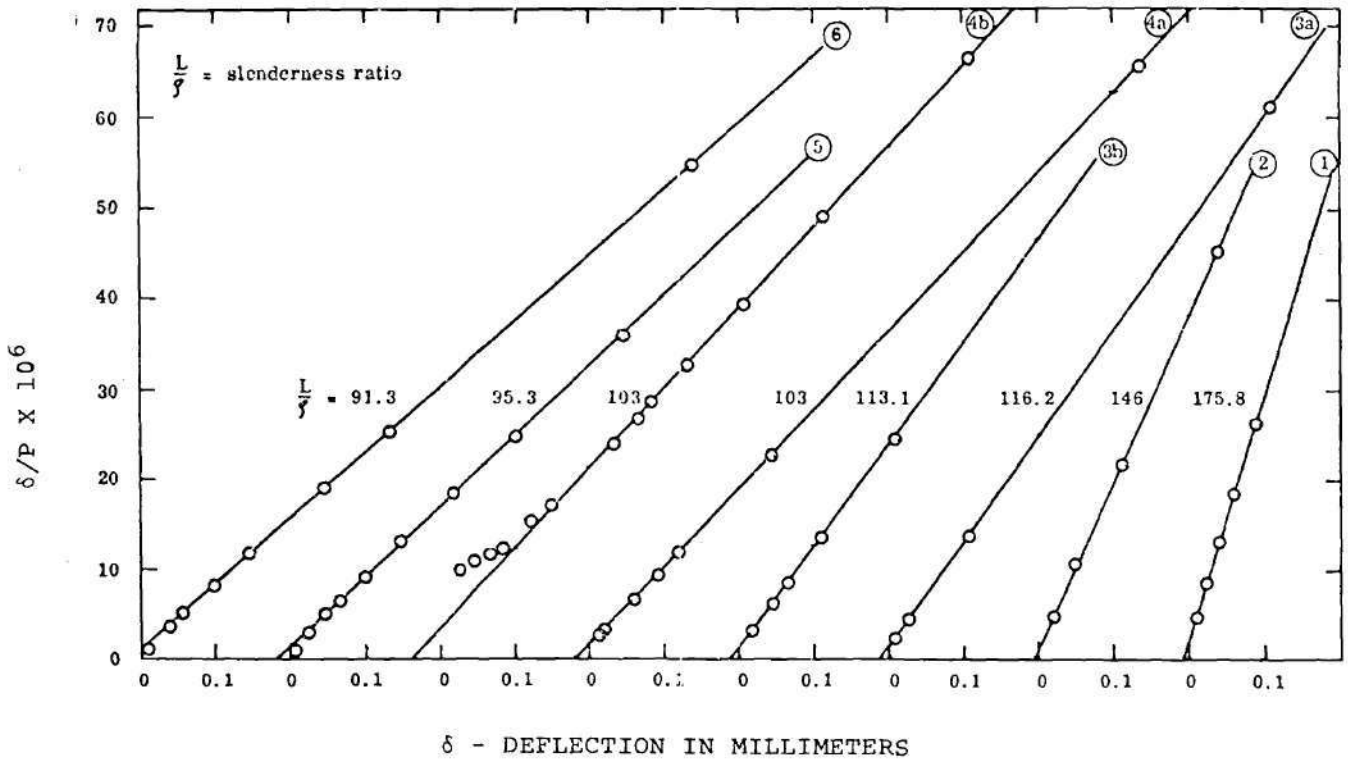

Figure 27. von Karman Data on Compressed Columns Plotted in the Linear Form by Southwell

and Cundari (57).

It is clear that the Southwell plot represents a great improvement in the state of affairs regarding buckling load prediction. Once the critical load has been established from a Southwell plot, the end fixity coefficient is immediately known, and a glance at equation (26) shows that the effects of imperfections have been isolated.

CHAPTER IV

NON-DESTRUCTIVE TESTS FOR THE DETERMINATION OF END FIXITY

General Discussion

We have discussed the Southwell plot as a means of experimentally determining the buckling loads of actual structures in realistic environments. While we have pointed out that the technique gives an experimental assessment of boundary effects (end fixity coefficient) and distinguishes those effects from the influence of imperfections, we have stopped short of labeling the Southwell plot a non-destructive test method. The reasons are contained in the assumptions under which equation (24) is valid. The first condition is that the eigenvalues are widely separated. If this is not met, as in the case of the circular cylindrical shell under axial compression, the interpretation that should be given the results of the method is unclear, even though the procedure is experimentally workable (58). More important, however, is the second requirement; viz., that the load P be a "substantial" portion of the lowest eigenvalue P_1, "substantial" referring to that load beyond which the deflected shape resembles the buckle shape. Aside from the experimental difficulty pursuant to the application of a large load, the important consequence of this assumption is that a destabilizing load approaching the instability level is required to obtain information on the buckling load. Thus, there is the clear and present danger that unanticipated buckling will occur before any trends

are indicated by the Southwell plot; a test in which there is a probability (albeit small for some structures) of specimen destruction can hardly qualify as a satisfactory non-destructive test technique.

It is interesting to note that the method depends on the growth under axial load of lateral deflections, which is in turn dependent on the structure being either highly flexible, or significantly imperfect, or both. We thus have the situation in which the highest-quality, most expensive specimens, the specimens we would most like to protect from destruction, have the greatest likelihood of meeting that fate.

The direction we should take in searching for a suitable non-destructive test is fairly clear. Noting the danger in the Southwell method of energizing the structure with a destabilizing load, it is apparent that we must be able to predict behavior in destabilizing environments by subjecting the system to non-destabilizing loads. The best type of member to consider in starting such a search is the beam, with suitable energizers being lateral forces.

The process is perhaps best initiated by making a few simple observations. We note that the critical load for a reasonably slender column under axial compression is given by

$$P_{cr} = \frac{\pi^2 EI}{L^2} \tag{27}$$

when the column is pinned at both ends. If the end rotational restraint is changed from zero to infinite (a "clamped" or "fixed end" condition) the critical load then becomes

$$P_{cr} = \frac{4\pi^2 EI}{L^2} \quad . \tag{28}$$

Now consider the same simple member under a non-destabilizing concentrated load applied laterally (normal to the direction of the destabilizing load) at its midpoint, in the absence of the axial load. The failure mode is changed from the geometric failure (buckling) to a material failure. As long as this failure is not approached, the lateral deflection is linear with the load; the flexibility coefficients for the two cases are given by

$$\frac{\delta}{Q} = \frac{L^3}{48EI} \text{ (pinned)} \tag{29}$$

and

$$\frac{\delta}{Q} = \frac{L^3}{192EI} \text{ (clamped)} \quad . \tag{30}$$

It is to be noted that changing the boundary restraint from zero to infinite causes the critical load to increase by a factor of four, while causing the flexibility coefficient to decrease by an identical factor. The question to be resolved is whether this is merely an interesting coincidence or a particular manifestation of a basic phenomenon.

The best mathematical expression of this observation is given

when we consider the product of the critical load and the flexibility coefficient. We have

$$P_{cr}\left(\frac{\delta}{Q}\right) = \frac{\pi^2 L}{48} . \tag{31}$$

In other words, the product of the critical load and the flexibility coefficient is a constant for all geometrically similar specimens, regardless of whether the ends are pinned or clamped. It is to be noted that the only geometric factor in the constant is very easily measured.

The importance of this relationship, if it can be extended to other cases, is clear. It provides the simplest possible method of determination of the critical load, and hence the end fixity coefficient, from easily determined quantities.

It is important to note that the two examples given so far have certain features in common:

1. The bodies are geometrically uniform;
2. They are symmetrical;
3. They are devoid of intermediate lateral support;
4. They have ideal end restraint (zero or infinite).

To extend the concept further, we begin by systematically removing these conditions, in the order of their presentation.

P-Delta Approach

Nonuniform Columns

For a first example, we consider the strut depicted in Figure 28a. This strut is nonuniform, the two segments having different cross-section areas. The analysis that follows also appears in a paper by Horton, Craig, and Struble (59).

According to Case (60) the critical load for a strut unsymmetrical about the center is given by

$$\frac{2}{P_{cr}} = \frac{1}{P_a} + \frac{1}{P_b}, \tag{32}$$

where P_a is the buckling load of a strut with two halves like OA, and P_b is the buckling load of a strut with two halves like OB. Furthermore, it requires only a very simple calculation to show that the flexibility coefficient for the composite beam, centrally loaded, is given by

$$2\left(\frac{\delta}{Q}\right) = \left(\frac{\delta}{Q}\right)_a + \left(\frac{\delta}{Q}\right)_b, \tag{33}$$

where the subscripts again refer to each half considered as a full beam. Combination of equations (32) and (33) yields

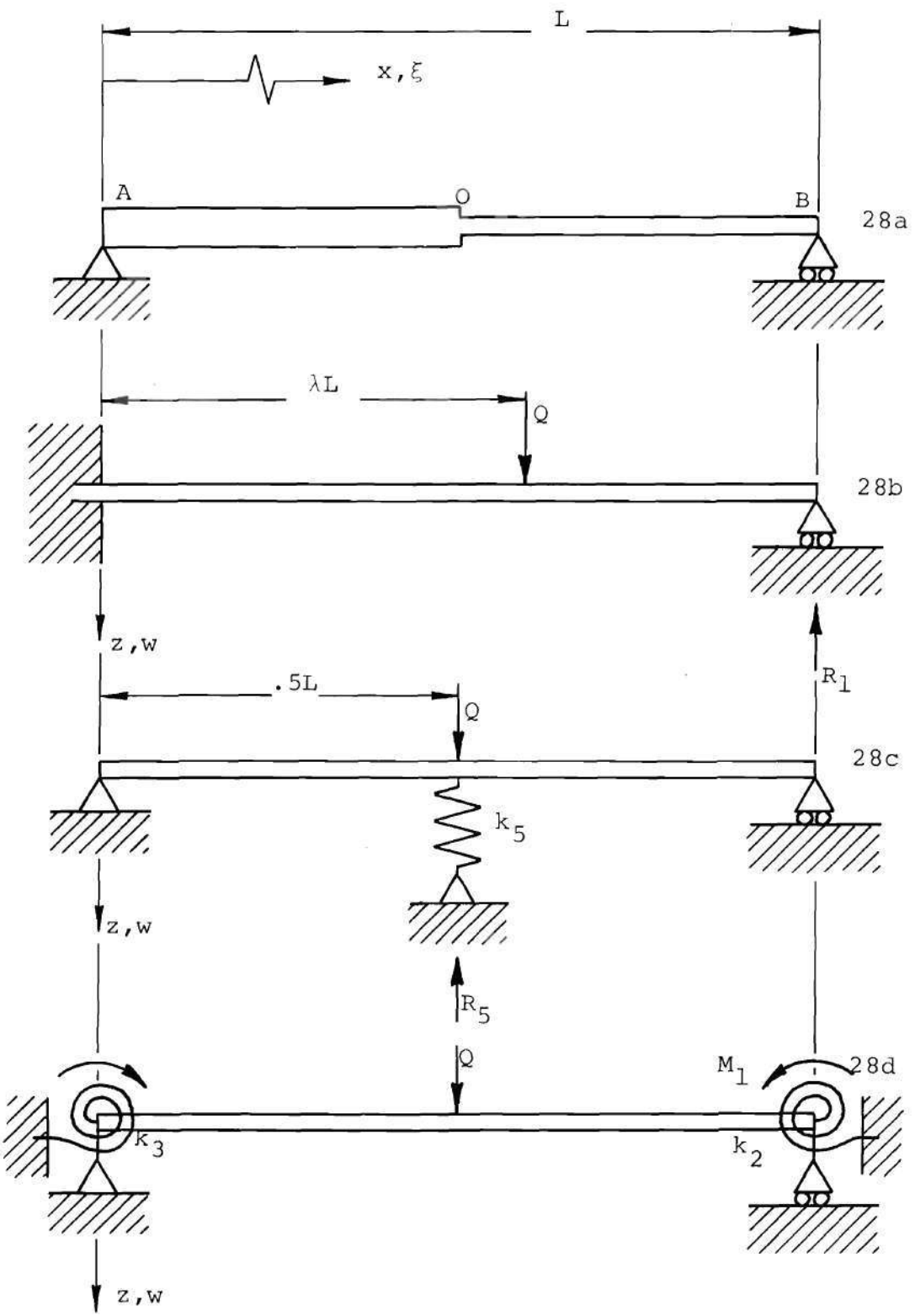

Figure 28. Diagram of Several of the Beam Configurations Studied.

$$P_{cr}\left(\frac{\delta}{Q}\right) = \frac{P_a P_b\left[\left(\frac{\delta}{Q}\right)_a + \left(\frac{\delta}{Q}\right)_b\right]}{P_a + P_b} \tag{34}$$

$$= \frac{\left[P_a\left(\frac{\delta}{Q}\right)_a\right]P_b + P_a\left[P_b\left(\frac{\delta}{Q}\right)_b\right]}{P_a + P_b} .$$

Substitution of equation (31) at this point results in

$$P_{cr}\left(\frac{\delta}{Q}\right) = \frac{\pi^2 L}{48} . \tag{35}$$

It is apparent from the preceding that the conditions of complete uniformity and symmetry of the structure are not essential. It is now possible to further generalize our results by considering a case lacking not only uniformity and symmetry in the body, but in the boundary restraint as well. In particular, consider the clamped-pinned beam shown in Figure 28b. The section stiffness EI is variable and is given by

$$EI = EI_0(1 - a^2\xi^2). \tag{36}$$

where $\xi = x/L$, and where a is called the taper ratio.

The case a = 0 (uniform EI) is best treated individually. From Roark (61) we see that

$$P_{cr} = 2.05 \frac{\pi^2 EI}{L^2} , \tag{37}$$

and that the flexibility coefficient at the point of application of the load, hereafter referred to as the load-point flexibility coefficient, is given by

$$\frac{\delta}{Q} = .00911 \frac{L^3}{EI} . \tag{38}$$

The product of this coefficient and the critical load is

$$P_{cr}\left(\frac{\delta}{Q}\right) = .897 \frac{\pi^2 L}{48} . \tag{39}$$

Clearly, we have an error that exceeds 10 per cent; to improve on this we require a larger flexibility coefficient. With this in mind, we note that if the beam is loaded such that the load-point flexibility coefficient is maximized, that quantity is given by

$$\left(\frac{\delta}{Q}\right)_m = .00984 \frac{L^3}{EI} , \tag{40}$$

and the usual product becomes

$$P_{cr}\left(\frac{\delta}{Q}\right)_m = .968 \frac{\pi^2 L}{48} . \tag{41}$$

The error has been reduced considerably.

In dealing with future cases, we tentatively establish the rule that the beam be loaded at the point of maximum load-point flexibility. Of course, the test of such a load location criterion is its ability to load to accurate prediction of buckling loads.

With regard to the beam unsymmetric about the mid-point, it is to be noted that when the ratio of the two section stiffness is zero or unity (the two limiting cases), the maximum load-point flexibility is located at the mid-point, and those results are undisturbed. For intermediate cases, it is doubtful that the minor deviations of the maximum flexibility location from the mid-point will seriously affect the results.

Returning to the problem of the parabolically-tapered beam, it can be shown (62) that the system has a critical load which is given by

$$17.79 \frac{EI_0}{L^2} < P_{cr} < 17.88 \frac{EI_0}{L^2} \tag{41}$$

when $a^2 = 1/3$, which is greater than that usually found in practical application. The analysis of this structure is conveniently done with the well-known dummy load method.

The first requisite is to obtain the actual moment distribution, which is dependent on the unknown force R_1 at the end of the beam. Toward this objective, the internal complementary work is given by

$$U^* = \frac{Q^2 L^3}{2} \int_0^1 \frac{\left[\frac{M(\xi)}{QL}\right]^2}{EI(\xi)} \, d\xi, \tag{42}$$

where M is the actual moment distribution. Since the reactions do no work, the complementary potential is given by an expression identical to (42). In terms of the unknown redundant R_1, the moment distribution is given by

$$\frac{M(\xi)}{QL} = \begin{cases} \left(\frac{R_1}{Q}\right)(1-\xi) + \xi - \lambda & 0 < \xi < \lambda. \\ \left(\frac{R_1}{Q}\right)(1-\xi) & \lambda < \xi < 1. \end{cases} \tag{43}$$

Substitution of (43) and (36) into (42) gives

$$W^* = \frac{L^3}{2EI_0} \int_0^\lambda \frac{\left[\left(\frac{R_1}{Q}\right)^2 (1-\xi)^2 - 2\left(\frac{R_1}{Q}\right)(1-\xi)(\lambda-\xi) + (\lambda-\xi)^2\right]}{1 - a^2\xi^2} \, d\xi$$

$$+ \frac{L^3}{2EI_0} \left(\frac{R_1}{Q}\right)^2 \int_\lambda^1 \frac{(1-\xi)^2}{1-a^2\xi^2} \, d\xi, \tag{44}$$

or

$$\frac{W^*}{\frac{L^3}{2EI_0}} = \left(\frac{R_1}{Q}\right)^2 \int_0^1 \frac{(1-\xi)^2}{1-a^2\xi^2}\, d\xi - 2\left(\frac{R_1}{Q}\right) \int_0^\lambda \frac{(1-\xi)(\lambda-\xi)}{1-a^2\xi^2}\, d\xi \qquad (45)$$

$$+ \int_0^\lambda \frac{(\lambda-\xi)^2}{1-a^2\xi^2}\, d\xi.$$

Now the force at the end is that R_1, among all R_1's in equilibrium with the lateral load Q, which permits compatible deformations of the structure; equivalently,

$$\frac{\partial\left(\frac{W^*}{\frac{L^3}{2EI_0}}\right)}{\partial\left(\frac{R_1}{Q}\right)} = 0. \qquad (46)$$

Carrying out the indicated differentiation of (45) and solving for R_1/Q, we have

$$\left(\frac{R_1}{Q}\right) = \frac{\int_0^\lambda \frac{(1-\xi)(\lambda-\xi)}{1-a^2\xi^2}\, d\xi}{\int_0^1 \frac{(1-\xi)^2}{1-a^2\xi^2}\, d\xi} \qquad (47)$$

Expansion of the integrands of (47) would show that we are dealing with

three basic integrals, which may be considered as functions of the upper limit of integration. Specifically, we have

$$B_0(\zeta) = \int_0^{\zeta} \frac{d\xi}{1-a^2\xi^2} = \frac{1}{2a} \ln\left(\frac{1 + a\zeta}{1 - a\zeta}\right) \tag{48a}$$

$$B_1(\zeta) = \int_0^{\zeta} \frac{\xi d\xi}{1-a^2\xi^2} = -\frac{1}{a^2} \ln \sqrt{1 - a^2\zeta^2} \tag{48b}$$

$$B_2(\zeta) = \int_0^{\zeta} \frac{\xi^2 d\xi}{1-a^2\xi^2} = \frac{1}{a^3} \ln\left(\frac{1 + a\zeta}{\sqrt{1-a^2\zeta^2}}\right) - \frac{\zeta}{a^2} . \tag{48c}$$

Substitution of equations (48) into (47) gives

$$\frac{R_1}{Q} = \frac{\lambda B_0(\lambda) - (\lambda+1) B_1(\lambda) + B_2(\lambda)}{B_0(1) - 2B_1(1) + B_2(1)} , \tag{49}$$

or

$$R_2 \left(\frac{R_1}{Q}\right) = \lambda B_0(\lambda) - (\lambda+1) B_1(\lambda) + B_2(\lambda), \tag{50}$$

where

$$R_2 = B_0(1) - 2B_1(1) + B_2(1). \tag{51}$$

Since the lateral deflection is desired for one location (the load-point) only, a convenient technique is the well-known dummy load method. In this case, the dummy, or unit, load is applied in the same location as the actual load; a suitable equivalent structure is the cantilever beam shown in Figure 33a. It follows that the moment distribution due to the dummy load is given by

$$\frac{M_d(\xi)}{L} = \begin{cases} \xi - \lambda & 0 < \xi < \lambda \\ 0 & \lambda < \xi < 1 \end{cases} . \tag{52}$$

The load-point deflection is given by

$$\delta = \int_0^L \frac{[M(x)][M_d(x)]}{EI(x)}\, dx, \tag{53}$$

or

$$\delta = QL^3 \int_0^1 \frac{[M(\xi)/QL][M_d(\xi)/L]}{EI(\xi)}\, d\xi. \tag{54}$$

Substitution of equations (52) and (43) into (54) yields

$$\delta = \frac{QL^3}{EI_0} \int_0^\lambda \frac{[(R_1/Q)(1-\xi) + \xi - \lambda](\xi-\lambda)}{1-a^2\xi^2}\, d\xi. \tag{55}$$

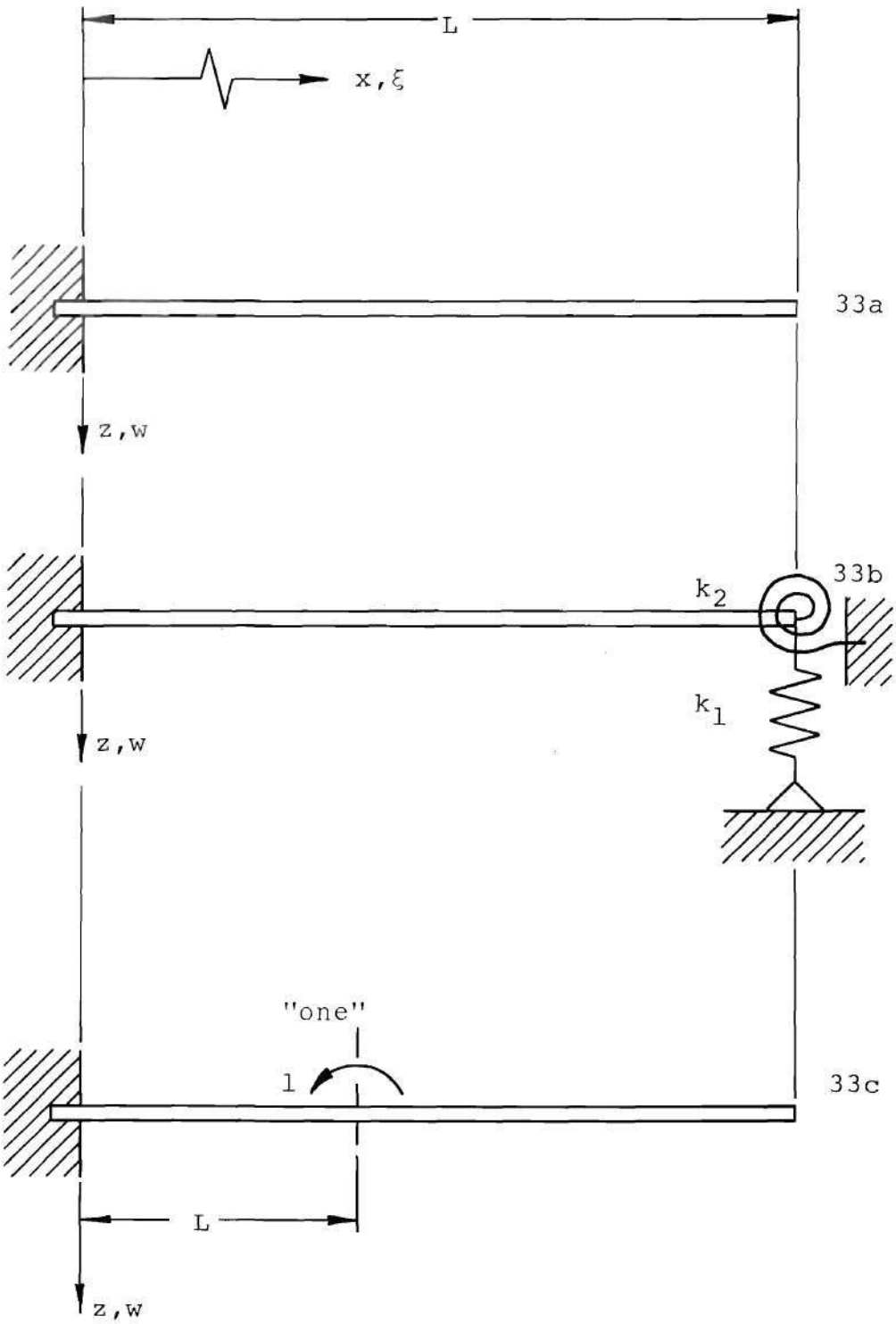

Figure 33. Diagram of Several of the Beam Configurations Studied

Integration is easily accomplished by expanding the integrand and substituting equations (48) into the result; this leads to

$$\frac{\frac{\delta}{Q}}{\frac{L^3}{EI_0}} = \left(\frac{R_1}{Q}\right)[-\lambda B_0(\lambda) + (\lambda+1)B_1(\lambda) - B_2(\lambda)] \tag{56}$$

$$+ \lambda^2 B_0(\lambda) - 2\lambda B_1(\lambda) - B_2(\lambda).$$

The above can be simplified by comparison of the first term on the left hand side with equation (50). We thus have

$$\frac{\frac{\delta}{Q}}{\frac{L^3}{EI_0}} = -\left(\frac{R_1}{Q}\right)^2 R_2 + \lambda^2 B_0(\lambda) - 2\lambda B_1(\lambda) + B_2(\lambda). \tag{57}$$

Since the maximum value of (57) is sought, it is necessary to differentiate the above. This is simplified considerably if we recall that the functions B_1 are defined by integrals and hence are amenable to differentiation by Leibnitz' rule, the derivatives simply being the integrands evaluated at the upper limit of integration. This leads to a simple result when equation (50) is differentiated; viz.,

$$R_2 \frac{d}{d\lambda}\left(\frac{R_1}{Q}\right) = B_0(\lambda) - B_1(\lambda). \tag{58}$$

Now, differentiating equation (57) and substituting equation (58) into the result leads to

$$\frac{d}{d\lambda}\left[\frac{\frac{\delta}{Q}}{\frac{L^3}{EI_0}}\right] = 2B_0(\lambda)\left(\lambda - \frac{R_1}{Q}\right) + 2B_1(\lambda)\left(\frac{R_1}{Q} - 1\right) \tag{59}$$

The maximization of (57) is equivalent, of course, to the vanishing of (59). It is apparent from the logarithmic nature of B_0 and B_1 that the root λ_m cannot be found in closed form; a suitable numerical scheme is Newton's method. In this approach, the derivative of equation (59) is needed. Accordingly, the second derivative of the reaction coefficient R_1/Q is obtained from equation (58) as

$$R_2 \frac{d^2}{d\lambda^2}\left(\frac{R_1}{Q}\right) = \frac{1 - \lambda}{1-a^2\lambda^2} . \tag{60}$$

Differentiation of (59) and substitution of (60) gives

$$\frac{d^2}{d\lambda^2}\left[\frac{\frac{\delta}{Q}}{\frac{L^3}{EI_0}}\right] = 2\left(\frac{R_1}{Q}\right)\left[\frac{\lambda-1}{1-a^2\lambda^2}\right] - \frac{2}{R_2}\left[B_0(\lambda) - B_1(\lambda)\right]^2 + 2B_0(\lambda). \tag{61}$$

The iteration was accomplished with a Hewlett-Packard digital computer. The program, found in Appendix I, was written and executed in the Hewlett-Packard BASIC language. The maximizing λ and the

flexibility coefficient at that point were found to be

$$\lambda_m = .599192; \tag{62}$$

$$\frac{\frac{\delta_m}{Q}}{\frac{L^3}{EI_0}} = 0.0108852. \tag{63}$$

Thus

$$P_{cr}\left(\frac{\delta_m}{Q}\right) = .951\,\frac{\pi^2 L}{48}\,. \tag{64}$$

The error between this result and that established in equation (31) is less than 5 per cent, which is excellent from a practical point of view.

Intermediate Lateral Support and Higher Modes

It is often necessary to enhance the load-carrying capacity of a beam by increasing the number of support locations. While it is clear that in general the behavior in destabilizing load environments would be considerably altered by ideal (i.e., infinite restraint) added support, an equally true, and more useful, statement can be made for non-ideal support augmentations. Their prevalence requires that we determine whether our test technique is valid for such cases.

As an example, consider a beam supported by a central lateral spring, as shown in Figure 28c. Due to symmetry, the location of the

maximum load-point flexibility coefficient is the beam mid-point. It is shown in Appendix II that the flexibility coefficient there is given by

$$\bar{\delta} = \frac{1}{K_5+48} \cdot \tag{65}$$

It is furthermore shown that for symmetric buckling, which occurs for

$$K_5 \leq 16\pi^2, \tag{66}$$

the buckling load ratio R is the root of the characteristic equation

$$1 - \frac{8}{\pi^4} K_5 \sum_{\text{odd}}^{\infty} \frac{1}{n^2(R-4n^2)} = 0. \tag{67}$$

The root-finding scheme is outlined in the computer program included in Appendix II. Buckling load prediction, using equations (31) and (65), was also incorporated in the program, and the results of the computer calculations are shown in Figure 29. The error in buckling load prediction using a lateral load is plotted against the spring stiffness K_5, and it is seen that the error is generally very small, rising to 6.33 per cent at the transition from the first to the second buckle mode. Beyond that point, the error drops abruptly to zero if the test engineer uses as an upper bound in his predictions the second-

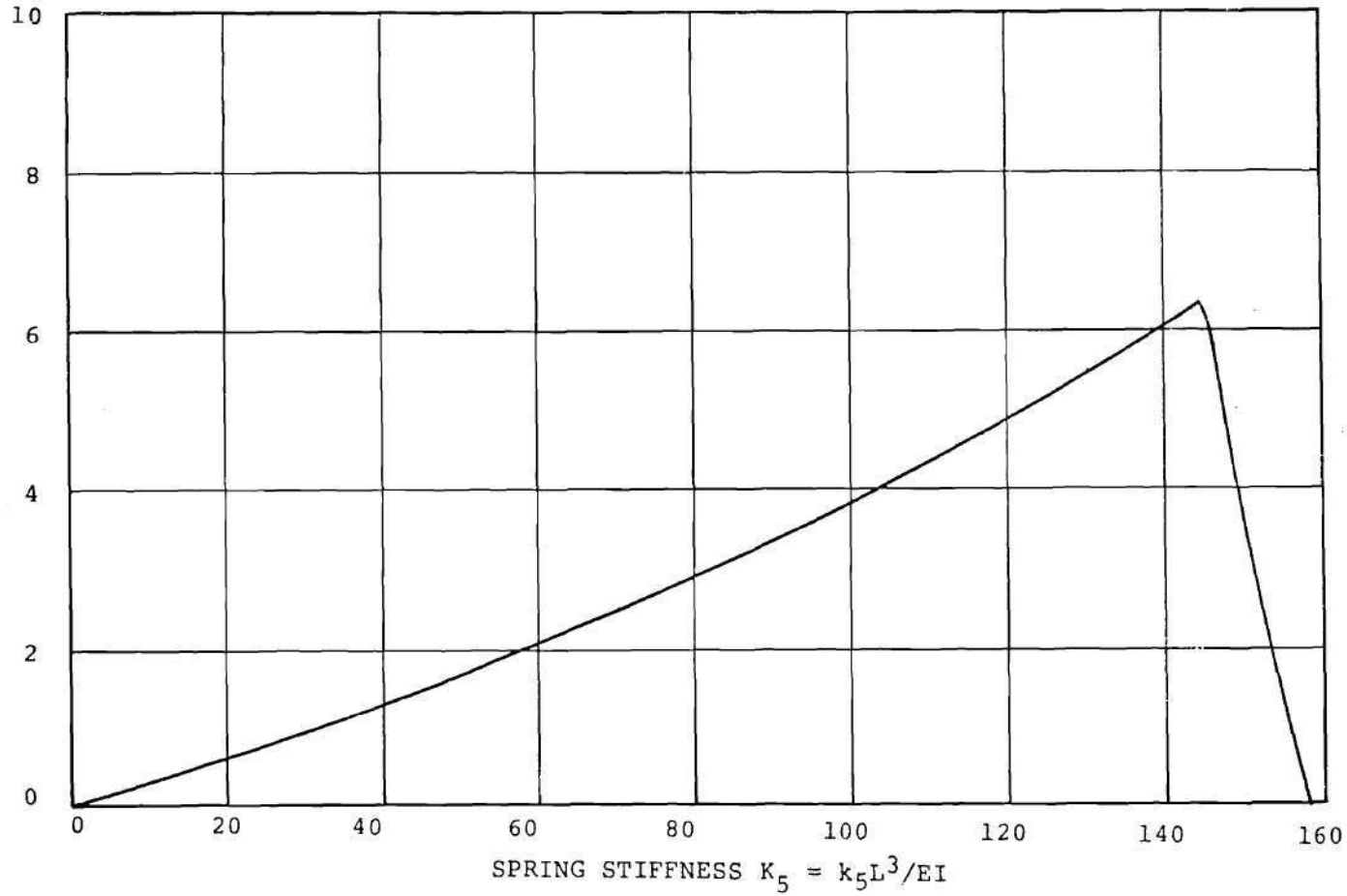

Figure 29. Variation of Buckling Load Prediction Error with Spring Stiffness K_5 for Configuration 28c

mode buckling load.

The use of the upper bound is unnecessary, however, if we modify our results somewhat. For the antisymmetric (second mode) case, there is obviously an inflection point at $x = L/2$, and the flexibility at the load point must have a maximum elsewhere. Indeed, maximization occurs midway between the ends and the center support; consider, then, the simultaneous application of a point load Q at one of the maximum points and an equal and oppositely-directed load at the other. The deflection at each location is

$$\delta_m = \frac{QL^3}{8(48EI)} , \tag{68}$$

and the total deflection experienced by the beam is

$$\tilde{\delta}_m = 2\delta_m = \frac{QL^3}{4(48EI)} . \tag{69}$$

Thus, the new maximized load-point flexibility coefficient is

$$\frac{\tilde{\delta}_m}{Q} = \frac{L^3}{4(48EI)} . \tag{70}$$

The usual product becomes

$$P_{cr}\left(\frac{\tilde{\delta}_m}{Q}\right) = \frac{4\pi^2 EI}{L^2}\left(\frac{1}{4}\right)\left(\frac{L^3}{48EI}\right) = \frac{\pi^2 L}{48} . \tag{71}$$

which is exact.

This approach can also be extended to other cases in which higher modes are critical. The first example taken is that of a column which is encastre at both ends and pinned at a center support. In this case the buckle mode is again anti-symmetric, and the points of maximum flexibility can be determined from Roark (61) as $\lambda = .29$ and $.71$. If oppositely directed loads of equal magnitude Q are applied at these points, proceeding as before gives

$$\tilde{\delta}_m = 2\tilde{\delta}_m = 2(.00984)\,\frac{Q(L/2)^3}{EI}\,. \tag{72}$$

or

$$\frac{\tilde{\delta}_m}{Q} = .00246L^3/EI\,. \tag{73}$$

The critical compressive load is

$$P_{cr} = 2.05\pi^2EI/(L/2)^2 = 8.2\pi^2EI/L^2, \tag{74}$$

and the product of the critical load and the flexibility coefficient is

$$P_{cr}\left(\frac{\tilde{\delta}_m}{Q}\right) = .97\,\frac{\pi^2L}{48}\,, \tag{75}$$

giving an error of 3 per cent.

It is apparent that the foregoing techniques can be readily applied to all higher mode situations. The maximum flexibility coefficient must be determined for all contemplated modes by first applying a single concentrated lateral load and then adding additional loads of like magnitude in an alternating fashion, in each case adjusting the positions of the loads so that the deflection sum is a maximum. This defines the "maximum flexibility" configuration for that mode and the mode with the lowest value will then be preferred.

In showing that the preceeding analysis holds for all higher modes, let us assume that the strut is pin-ended. Having found the maximum flexibility configuration, we separately treat each segment between inflection points. The deflection of the segment is given by

$$\delta_m = \frac{Q(L_0)^3}{48EI} , \tag{76}$$

where L_0 is the length of the segment. If the supports are located such that the wave form is composed of only one harmonic, the segments are all of equal length, and

$$L_0 = \frac{L}{n_b} , \tag{77}$$

where n_b is the number of half-waves. Substitution of (77) into (76) gives

$$\delta_m = \frac{QL^3}{48n_b^3 EI} . \tag{78}$$

The total deflection $\tilde{\delta}_m$ is thus

$$\tilde{\delta}_m = n_b \delta_m = \frac{QL^3}{48(n_b)^2 EI} . \tag{79}$$

Furthermore, the buckling load is given by

$$P_{cr} = (n_b)^2 \frac{\pi^2 EI}{L^2} , \tag{80}$$

and the product of the critical load and the flexibility coefficient is given by

$$P_{cr}\left(\frac{\tilde{\delta}_m}{Q}\right) = \frac{L^3}{48(n_b)^2 EI} \left[\frac{(n_b)^2 \pi^2 EI}{L^2}\right] = \frac{\pi^2 L}{48} , \tag{81}$$

which is exact. It is thus clear that a crossover from one buckling mode to the next is always recognized by the higher-mode approach, and the need for arbitrary upper bounds is eliminated.

It should finally be noted that even if the strut is not pin-ended, the interior portion of the column deforms into sinusoidal

waves, and it can thus be concluded that the error for these cases diminishes with increasing buckle mode.

Non-ideal End Support

In this section we consider the case of non-ideal end support and thus remove, or attempt to remove, the last of the four restrictions. We have taken the term "ideal support" to mean that the rotational and translational restraints at the ends of a strut are either zero or infinite. Obviously, these conditions are unobtainable in practice, and a more general procedure with respect to boundary conditions is to consider finite restraint.

The first example in this class is the configuration shown in Figure 28d, with $K_2 = K_3$; viz., a uniform strut having infinite lateral restraint but symmetric finite rotational restraint in the form of identical torsional springs at the ends. Due to symmetry, the maximum load-point deflection is at the beam mid-point, and it is shown in Appendix III that the flexibility coefficient there is given by

$$\delta = \frac{1}{48}\left[1 - \frac{3K_2}{4(K_2+2)}\right], \tag{82}$$

where K_2 is the relative spring stiffness defined by

$$K_2 = k_2 L/EI. \tag{83}$$

It is furthermore shown that the buckling load ratio R is the root of

the characteristic equation

$$1 - \frac{16K_2}{\pi^2} \sum_{\text{odd}}^{\infty} \frac{1}{R-4n^2} = 0. \tag{84}$$

The root-finding scheme is outlined in the computer program included in Appendix III. Buckling load prediction, using equations (31), (65), and (67), was also incorporated in the program, and the results of the computer calculations are shown in Figure 30. The error in buckling load prediction using a lateral load is plotted against the spring stiffness K_2, and it is apparent that the error in all cases is bracketed by zero and minus 7 per cent.

A non-symmetric case can be studied if we consider the above configuration minus the right-end torsional spring; i.e., $K_2 = 0$. Here, the problem of finding the maximum load-point flexibility coefficient is complicated somewhat because its location depends on the spring stiffness. Nonetheless, the analysis is carried out in Appendix III, where it is shown that the flexibility coefficient varies with the load location λ according to the relation

$$\bar{\delta} = \frac{1}{3}(\lambda^2 - 2\lambda^3 + \lambda^4) - \frac{K_3}{12(K_3+3)}(4\lambda^2 - 12\lambda^3 + 13\lambda^4 - 6\lambda^5 + \lambda^6). \tag{85}$$

It is furthermore shown that the buckling load ratio R is the root of the characteristic equation

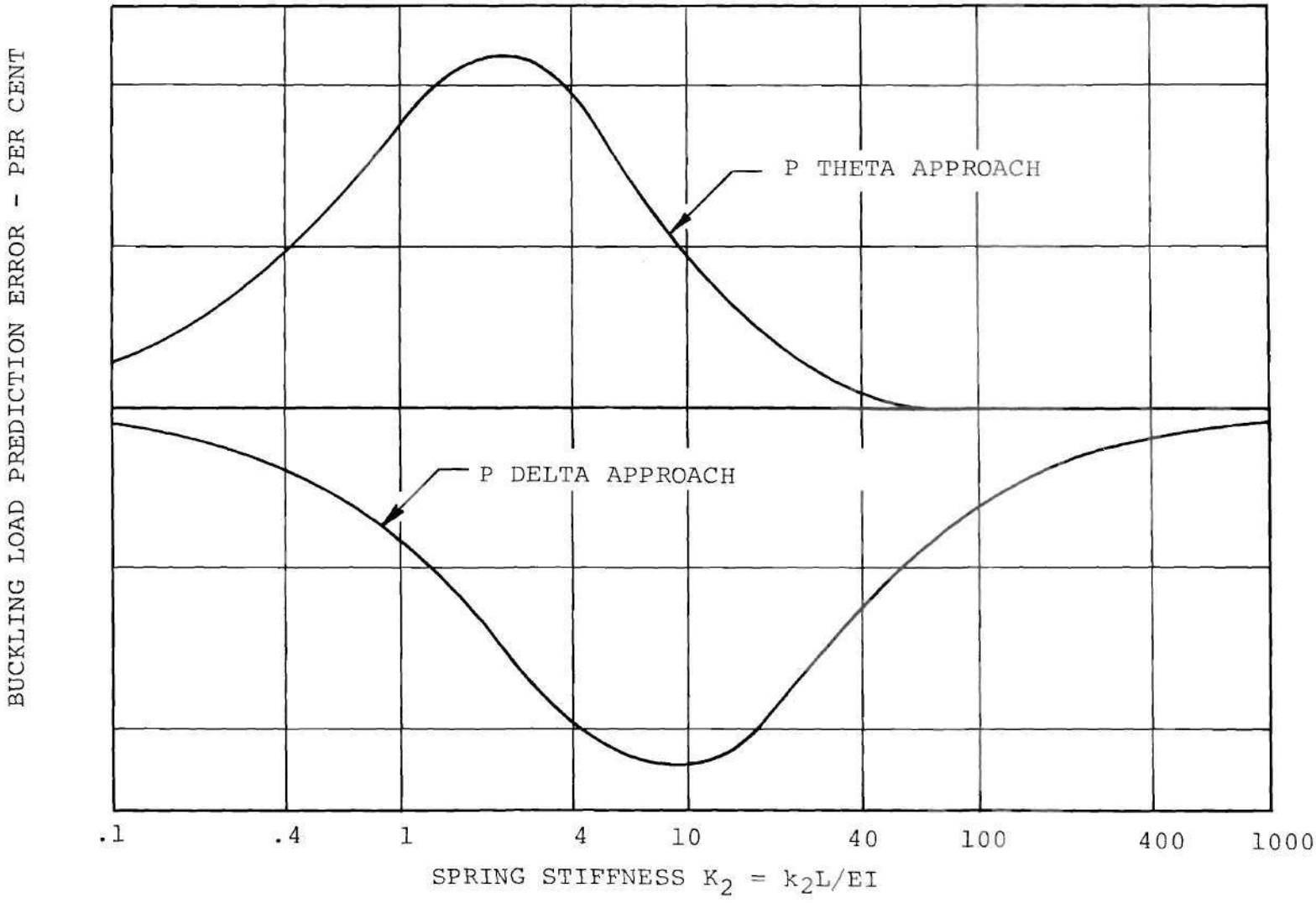

Figure 30. Variation of Buckling Load Prediction Error with Spring Stiffness K_2 for Configuration 28d, with $K_3 = K_2$

$$1 - \frac{8K_3}{\pi^2} \sum_{\text{all}}^{\infty} \frac{1}{R-4n^2} = 0, \qquad (86)$$

where the inclusion of the even terms reflects the lack of symmetry in the buckled shape.

It is clear that numerical techniques must be employed in finding the value of λ which maximizes expression (85), as well as the root of equation (86). Such techniques are incorporated in the program in Appendix III, and the results of the computer calculations are shown in Figures 31 and 32. The error in buckling load prediction using a lateral load is plotted against the spring stiffness K_3 in Figure 31, and it is clear that the error in all cases is bracketed by minus 2.0 per cent and plus 3.8 per cent. Figure 32 shows the variation of maximizing λ with spring stiffness, and it is important to note that while the location of the maximum flexibility coefficient varies with spring stiffness, at no point does it deviate from the column midpoint more than 10 per cent of the column length.

It finally remains to vary the lateral boundary restraint. As a first example, it is enlightening to consider the configuration in Figure 33a; viz., a strut clamped at one end and devoid of both lateral and rotational restraint at the other. Such boundary conditions are ideal, but they will still serve to illustrate some difficulties.

From Roark (61) it is seen that the critical load for such a system is

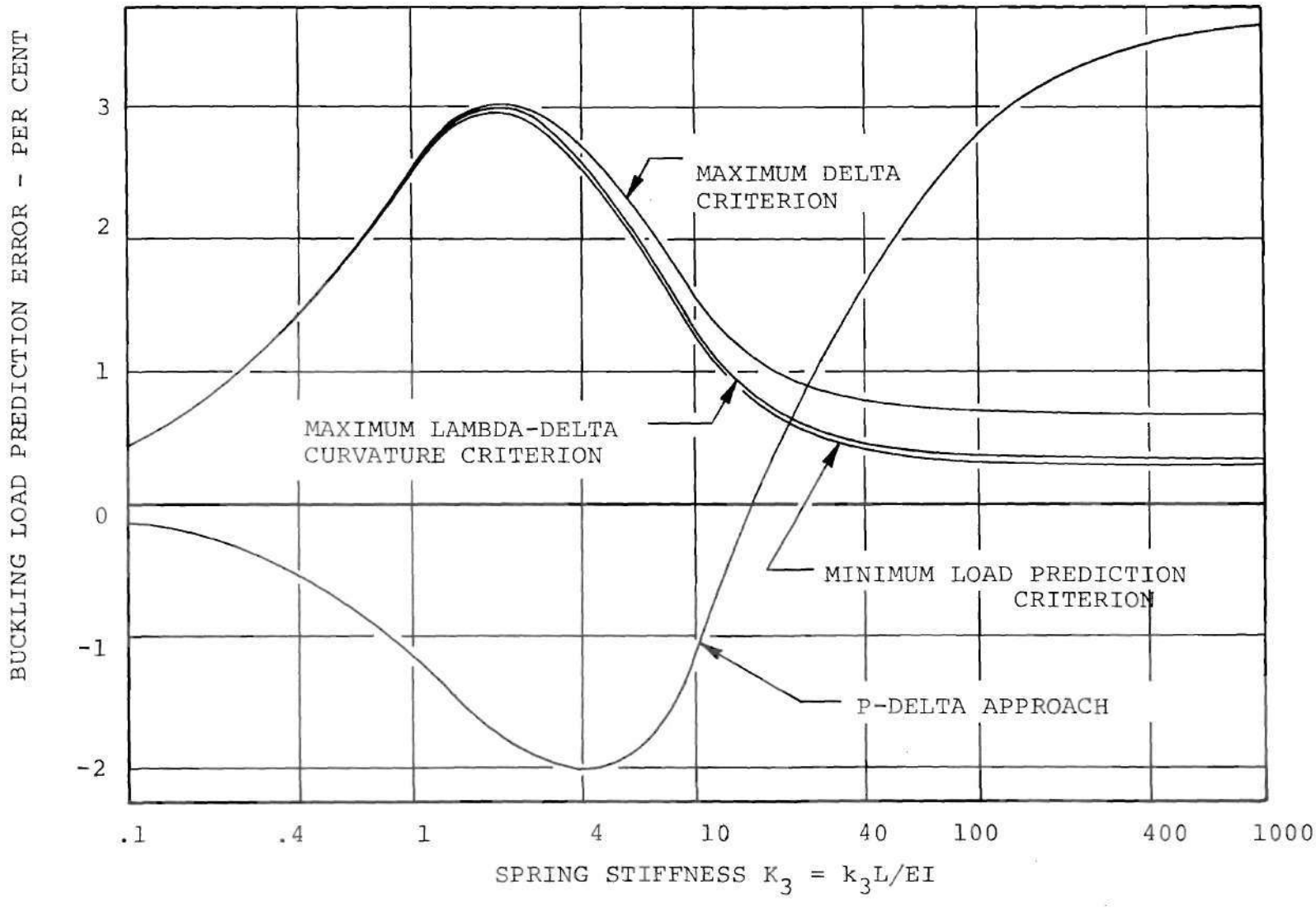

Figure 31. Variation of Buckling Load Prediction Error with Spring Stiffness K_3 for Configuration 28d, with $K_2 = 0$

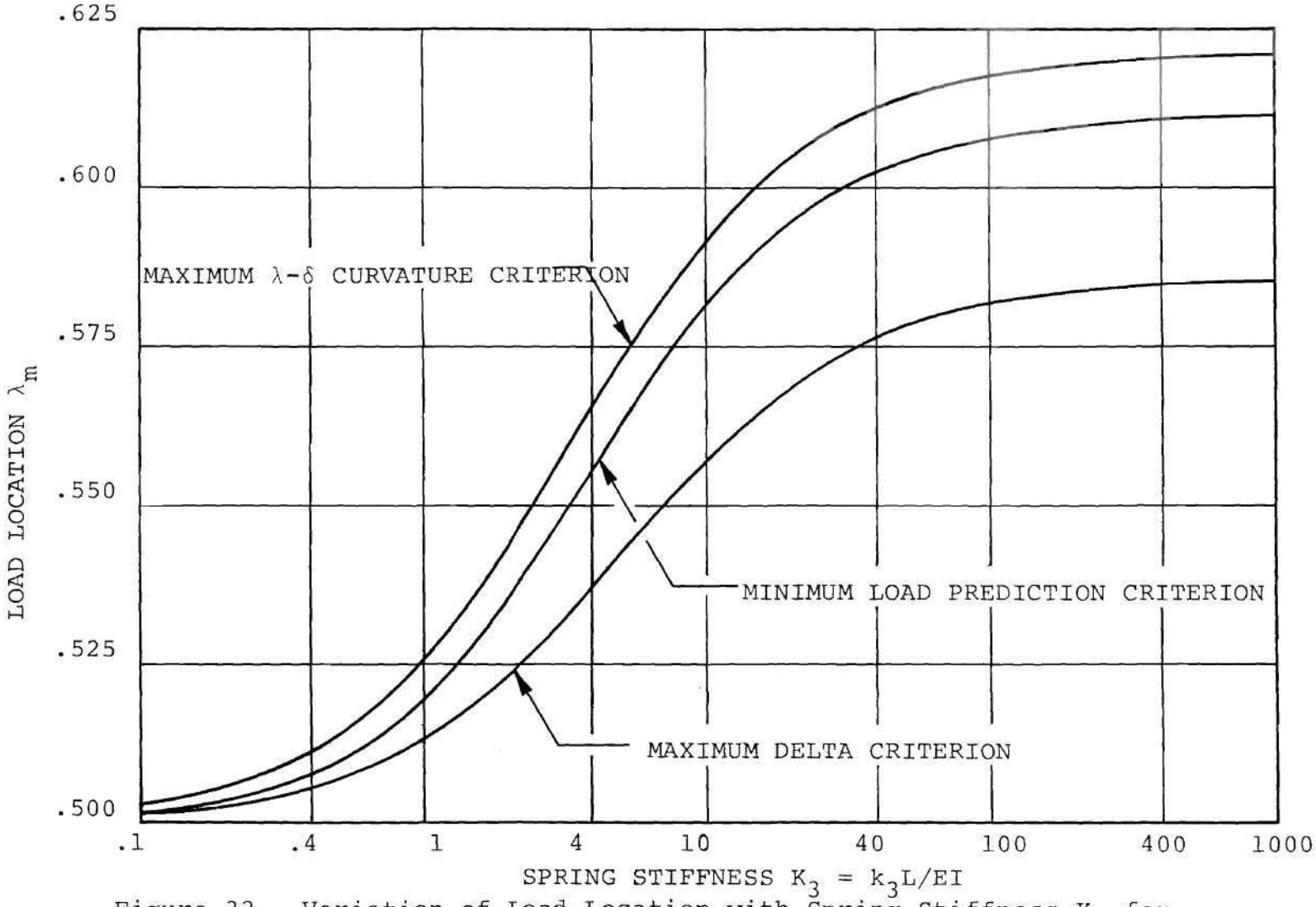

Figure 32. Variation of Load Location with Spring Stiffness K_3 for Configuration 28d, with $K_2 = 0$

$$P_{cr} = \frac{\pi^2 EI}{4L^2}, \tag{87}$$

while the maximum load-point flexibility coefficient is located at the end of the beam and is given by

$$\frac{\delta_m}{Q} = \frac{L^3}{3EI} . \tag{88}$$

Thus the familiar product becomes

$$P_{cr}\left(\frac{\delta_m}{Q}\right) = 4.0\ \frac{\pi^2 L}{48} . \tag{89}$$

a constant which is not so familiar and is, indeed, vastly in error. It is evident that we must finally set a condition for the validity of the basic relation shown in equation (31); viz., the relation appears to hold (at least to a good approximation) in all cases in which the lateral restraint at each end of the beam is infinite. It will be possible later to loosen that condition somewhat.

Meanwhile, a pertinent question is: what causes equation (31) to break down for the case of the cantilever beam? Perhaps the best clue can be obtained by considering this configuration, modified by changing the end lateral restraint from zero to infinity. This is the propped cantilever beam shown in Figure 28b and considered earlier. Here, the product of the maximum load-point flexibility coefficient

and the critical load was

$$P_{cr}\left(\frac{\delta_m}{Q}\right) = .968\,\frac{\pi^2 L}{48}\,, \tag{90}$$

with the maximizing load location λ_m being .586. Why such marked difference in the two cases?

The first phenomenon to note is the radical deviation of the location of the point of maximum flexibility in the cantilever beam case from the rest of the examples studied; it is the only case in which maximum deflection occurs outside the neighborhood of the mid-point. Indeed, if a cantilever is loaded at, say, the 60 per cent location, the load point flexibility coefficient is

$$\frac{\delta}{Q} = \frac{(.6L)^3}{3EI} = .072\,\frac{L^3}{EI}\,, \tag{91}$$

and the product becomes

$$P_{cr}\left(\frac{\delta}{Q}\right) = \frac{\pi^2 L}{55.6}, \tag{92}$$

which still displays noticeable error but that is of the correct order of magnitude.

The second, and perhaps most important, feature is that in all the configurations we have studied, excepting the cantilever case, the deflected shape under both destabilizing and non-destabilizing load

environments displays two inflection points, one or both of which may be located at the beam boundaries. The cantilever beam, of course, has only one. A point not to be overlooked is that the boundary conditions play a decisive role in the determination of the number of inflection points contained in the deflected shape. It is clear that the number of inflection points is intimately involved with the subject of wave shape, and it is equally obvious that there is a significant deviation of wave form in the cantilever case.

How do we resolve this difficulty? If we attempt to account directly for the number of inflection points, we can make some progress. Denoting the number of inflection points by n_p, we can write

$$P_{cr}\left(\frac{\delta_m}{Q}\right) = \frac{\pi^2 L}{12(n_p)^2}\,, \tag{93}$$

and this relationship now holds for all the cases we have considered, including the cantilever.

To proceed with the task of examining the influence of finite lateral restraint, it is instructive to consider the configuration shown in Figure 33b: a strut with rigid rotational and lateral support on the left end, and with linearly elastic rotational and translational restraint at the other. In so doing we can achieve the objectives of considering a fairly general set of boundary conditions, while investigating the single inflection point cases.

The first order of business is to find the critical load for

the system. Toward that end, the Rayleigh-Ritz procedure is used, with the assumed deflected shape taken as

$$w = \sum_{\text{odd}}^{\infty} a_n \left(1 - \cos \frac{n\pi x}{2L}\right), \tag{94}$$

where the notation "odd" indicates summation over odd values of the dummy index. Noting that we have energy stored in the springs, the total potential W may be written:

$$W = \frac{EI}{2} \int_0^L \left(\frac{d^2 w}{dx^2}\right)^2 dx + \frac{k_1}{2} (w)^2 \Bigg|_{X = L} \tag{95}$$

$$+ \frac{k_2}{2} \left(\frac{dw}{dx}\right)^2 \Bigg|_{X = L} - \frac{P}{2} \int_0^L \left(\frac{dw}{dx}\right)^2 dx.$$

Substitution of (94) into (95), integration, and noting the orthogonality of the functions in the deflection expansion gives

$$W = \frac{EI}{2} \sum_{\text{odd}}^{\infty} (a_n)^2 \left(\frac{n\pi}{2L}\right)^4 \left(\frac{L}{2}\right) + \frac{k_1}{2} \sum_{\text{odd } m}^{\infty} \sum_{\text{odd } n}^{\infty} a_m a_n \tag{96}$$

$$+ \frac{k_2}{2} \sum_{\text{odd } m}^{\infty} \sum_{\text{odd } n}^{\infty} a_m a_n \left(\frac{n\pi}{2L}\right)\left(\frac{m\pi}{2L}\right) \sin\frac{n\pi}{2} \sin\frac{m\pi}{2} - \frac{P}{2} \sum_{\text{odd}}^{\infty} (a_n)^2 \left(\frac{n\pi}{2L}\right)^2 \left(\frac{L}{2}\right).$$

Variation with respect to each arbitrary coefficient a_n yields the lateral equilibrium equations

$$a_n (EI) \left(\frac{n\pi}{2L}\right)^2 \left(\frac{L}{2}\right) + k_1 \sum_{\text{odd}}^{\infty} a_m \tag{97}$$

$$+ \frac{k_2}{2} \left(\frac{n\pi}{2L}\right)\left(\frac{\pi}{2L}\right) \sin\frac{n\pi}{2} \sum_{\text{odd}}^{\infty} a_m \, m \sin\frac{m\pi}{2} - P(a_n)\left(\frac{n\pi}{2L}\right)^2 \left(\frac{L}{2}\right) = 0, \quad n=1,3,5,\ldots,$$

due to the facts that

$$\delta_{a_n} \left[\left(\sum_{\text{odd}}^{\infty} a_n \right)^2 \right] = 2 \sum_{\text{odd}}^{\infty} a_m \tag{98}$$

and

$$\delta_{a_n}\left(\left[\sum_{\text{odd}}^{\infty} a_n\left(\frac{n\pi}{2L}\right)\sin\frac{n\pi}{2}\right]^2\right) \tag{99}$$

$$= 2\left(\frac{n\pi}{2L}\right)\sin\frac{n\pi}{2}\sum_{\text{odd}}^{\infty} a_m\left(\frac{m\pi}{2L}\right)\sin\frac{m\pi}{2}\,.$$

Solving for the coefficients a_n gives

$$a_n = \frac{-k_2\left(\frac{\pi}{2L}\right)^2 n\sin\frac{n\pi}{2}\sum_{\text{odd}}^{\infty} a_m\, m\sin\frac{m\pi}{2} - k_1\sum_{\text{odd}}^{\infty} a_m}{EI\left(\frac{n\pi}{2L}\right)^4\left(\frac{L}{2}\right) - P\left(\frac{n\pi}{2L}\right)^2\left(\frac{L}{2}\right)} \tag{100}$$

$$= \frac{-\frac{8}{\pi^2}K_2\, n\sin\frac{n\pi}{2}\sum_{\text{odd}}^{\infty} a_m m\sin\frac{m\pi}{2} - \frac{32}{\pi^4}K_1\sum_{\text{odd}}^{\infty} a_m}{n^2(n^2-R)}\,,$$

$$n = 1,\ 3,\ 5,\ \ldots,$$

where we have introduced the usual nondimensional quantities

$$K_1 = \frac{k_1}{EI/L^3}\,; \tag{101}$$

$$K_2 = \frac{k_2}{EI/L} \; ; \tag{102}$$

$$R = \frac{P}{\pi^2 EI/4L^2} \; . \tag{103}$$

It is to be noted that this is an infinite set of linear, but coupled, equations, and hence there is not as yet a workable expression for each of the a_n's. This difficulty may be overcome by summing in the following manner:

$$\sum_{\text{odd}}^{\infty} a_n = -\frac{8}{\pi^2} K_2 \sum_{\text{odd}}^{\infty} \frac{n \sin \frac{n\pi}{2}}{n^2(n^2-R)} \sum_{\text{odd}}^{\infty} a_m m \sin \frac{m\pi}{2} \tag{104}$$

$$-\frac{32}{\pi^4} K_1 \sum_{\text{odd}}^{\infty} \frac{1}{n^2(n^2-R)} \sum_{\text{odd}}^{\infty} a_m ;$$

$$\sum_{\text{odd}}^{\infty} a_n n \sin \frac{n\pi}{2} = -\frac{8}{\pi^2} K_2 \sum_{\text{odd}}^{\infty} \frac{n^2}{n^2(n^2-R)} \sum_{\text{odd}}^{\infty} a_m m \sin \frac{m\pi}{2} \tag{105}$$

$$-\frac{32}{\pi^4} K_1 \sum_{\text{odd}}^{\infty} \frac{n \sin \frac{n\pi}{2}}{n^2(n^2-R)} \sum_{\text{odd}}^{\infty} a_m .$$

We can write (104) and (105) in a simpler form:

$$\sum_{\text{odd}}^{\infty} a_n = -\frac{8}{\pi^2} K_2 T_2 \sum_{\text{odd}}^{\infty} a_n n \sin\frac{n\pi}{2} - \frac{32}{\pi^4} K_1 T_3 \sum_{\text{odd}}^{\infty} a_n, \tag{106}$$

$$\sum_{\text{odd}}^{\infty} a_n n \sin\frac{n\pi}{2} = -\frac{8}{\pi^2} K_2 T_1 \sum_{\text{odd}}^{\infty} a_n n \sin\frac{n\pi}{2} - \frac{32}{\pi^4} K_1 T_2 \sum_{\text{odd}}^{\infty} a_n, \tag{107}$$

where the functions T_1, T_2, and T_3 are functions defined by infinite series as follows:

$$T_1 = \sum_{\text{odd}}^{\infty} \frac{1}{n^2-R}\ ; \tag{108}$$

$$T_2 = \sum_{\text{odd}}^{\infty} \frac{\sin\frac{n\pi}{2}}{n(n^2-R)}\ ; \tag{109}$$

$$T_3 = \sum_{\text{odd}}^{\infty} \frac{1}{n^2(n^2-R)}\ . \tag{110}$$

Rearranging gives

$$\left(1 + \frac{32}{\pi^4} K_1 T_3\right) \sum_{\text{odd}}^{\infty} a_n + \frac{8}{\pi^2} K_2 T_2 \sum_{\text{odd}}^{\infty} a_n n \sin \frac{n\pi}{2} = 0; \tag{111}$$

$$\frac{32}{\pi^4} K_1 T_2 \sum_{\text{odd}}^{\infty} a_n + \left(1 + \frac{8}{\pi^2} K_2 T_1\right) \sum_{\text{odd}}^{\infty} a_n n \sin \frac{n\pi}{2} = 0. \tag{112}$$

It is clear that we have replaced the infinite set of equations by two equations in which both the variables and the coefficients are infinite series. The only nontrivial solution for the variables occurs when the determinant of the coefficients vanishes; i.e.,

$$\begin{vmatrix} \left(1 + \frac{32}{\pi^4} K_1 T_3\right) & \frac{8}{\pi^2} K_2 T_2 \\ \frac{32}{\pi^4} K_1 T_2 & \left(1 + \frac{8}{\pi^2} K_2 T_1\right) \end{vmatrix} = 0 . \tag{113}$$

Expansion of the buckling determinant yields the characteristic equation:

$$1 + \frac{32}{\pi^4} K_1 T_3 + \frac{8}{\pi^2} K_2 T_1 + \frac{256}{\pi^6} K_1 K_2 (T_3 T_1 - T_2^2) = 0 . \tag{114}$$

The solutions of this equation must be found by numerical means. Accordingly, a two-point iteration scheme was developed and incorporated into a BASIC computer program that is found in Appendix IV. Since for many values of K_1 and K_2 there existed more than one solution below the limiting first-mode value R = 16, care was taken to ensure that the lowest eigenvalue was obtained.

Having solved the eigenvalue problem it remains to perform the flexibility analysis. This is conveniently done in a manner paralleling the previous developments, using the dummy load method.

The first step in this process is to do the redundant analysis. Accordingly, the fact that the potential of applied displacements is zero for this problem means that the total complementary potential can be written as

$$W^* = \frac{Q^2L^3}{2EI}\int_0^1 \left[\frac{M(\xi)}{QL}\right]^2 d\xi + \frac{Q^2}{2k_1}\left(\frac{R_1}{Q}\right)^2 + \frac{Q^2L^2}{2k_2}\left(\frac{M_1}{QL}\right)^2 , \tag{115}$$

where the moment distribution $M(\xi)$ is a function of the two redundant quantities R_1/Q and M_1/QL. Specifically, we have

$$\frac{M(\xi)}{QL} = \begin{cases} (R_1/Q)(1-\xi) + M_1/QL + \xi-\lambda & 0 \le \xi \le \lambda \\ \\ (R_1/Q)(1-\xi) + M_1/QL & \lambda \le \xi \le 1 \end{cases} \tag{116}$$

Compatibility requires that the total complementary potential be minimized with respect to the independent parameters; the result is

$$\frac{\partial}{\partial\left(\frac{R_1}{Q}\right)}\left[\frac{W^*}{\frac{Q^2L^3}{2EI}}\right] = \int_0^1 2\left[\frac{M(\xi)}{QL}\right]\frac{\partial}{\partial\left(\frac{R_1}{Q}\right)}\left[\frac{M(\xi)}{QL}\right]d\xi + 2\,\frac{EI}{k_1L^3}\left(\frac{R_1}{Q}\right) = 0. \quad (117)$$

$$\frac{\partial}{\partial\left(\frac{M_1}{QL}\right)}\left[\frac{W^*}{\frac{Q^2L^3}{2EI}}\right] = \int_0^1 2\left[\frac{M(\xi)}{QL}\right]\frac{\partial}{\partial\left(\frac{M_1}{QL}\right)}\left[\frac{M(\xi)}{QL}\right]d\xi + 2\,\frac{EI}{k_2L}\left(\frac{M_1}{QL}\right) = 0. \quad (118)$$

Performing the indicated differentiation of equation (116), substitution into (117) and (118), and simplification give

$$\int_0^1\left[\left(\frac{R_1}{Q}\right)(1-\xi) + \left(\frac{M_1}{QL}\right)\right](1-\xi)d\xi - \int_0^\lambda(\lambda-\xi)(1-\xi)d\xi + \frac{R_1/Q}{K_1} = 0\ ; \quad (119)$$

$$\int_0^1\left[\left(\frac{R_1}{Q}\right)(1-\xi) + \left(\frac{M_1}{QL}\right)\right]d\xi - \int_0^\lambda(\lambda-\xi)d\xi + \frac{M_1/QL}{K_2} = 0\ . \quad (120)$$

Integration and simplification results in

$$\left(\frac{R_1}{Q}\right)\left(\frac{2+6}{K_1}\right) + \left(\frac{M_1}{QL}\right)(3) = 3\lambda^2 - \lambda^3\ ; \quad (121)$$

$$\frac{R_1}{Q} + \left(\frac{M_1}{QL}\right)\left(\frac{2+2}{K_2}\right) = \lambda^2 \ . \tag{122}$$

Solution of the above by Cramer's rule yields

$$\frac{R_1}{Q} = \lambda^2 K_1 \left[\frac{2(3-\lambda)(K_2+1) - 3K_2}{K_1K_2 + 12K_2 + 4K_1 + 12}\right] ; \tag{123}$$

$$\frac{M_1}{QL} = \lambda^2 K_2 \left[\frac{6 - (1-\lambda)\ K_1}{K_1K_2 + 12K_2 + 4K_1 + 12}\right] .$$

Knowing the redundants enables us to obtain the load-point flexibility coefficient. In using the dummy load method, a suitable equivalent structure is the cantilever beam shown in Figure 33a, with a unit load applied at $\xi = \lambda$. Again the basic relationship is

$$\delta = \frac{QL^3}{EI} \int_0^1 \left[\frac{M(\xi)}{QL}\right]\left[\frac{M_d(\xi)}{L}\right] d\xi, \tag{124}$$

where $M_d(\xi)$ is the moment distribution due to the dummy load. We have

$$\frac{M_d(\xi)}{L} = \begin{cases} \xi - \lambda & 0 \le \xi \le \lambda \\ 0 & \lambda \le \xi \le 1 \end{cases} \tag{125}$$

Substitution of (116) and (125) into (124) gives

$$\bar{\delta} = \int_0^{\lambda} \left[\left(\frac{R_1}{Q}\right)(1-\xi)(\xi-\lambda) + \left(\frac{M_1}{QL}\right)(\xi-\lambda) + (\xi-\lambda)^2\right] d\xi. \tag{126}$$

Integration is straightforward; the result is

$$\bar{\delta} = \frac{\lambda^3}{3} - \left(\frac{R_1}{Q}\right)\left(\frac{\lambda^2}{2} - \frac{\lambda^3}{6}\right) - \left(\frac{M_1}{QL}\right)\frac{\lambda^2}{2}. \tag{127}$$

The relation between $\bar{\delta}$ and λ is obtained by substitution of expressions (123) into (127), yielding

$$(K_1K_2+12K_2+4K_1+12)\,\bar{\delta} = \frac{\lambda^3}{3}(K_1K_2+12K_2+4K_1+12) \tag{128}$$

$$-\lambda^4(K_1K_2+3K_1+3K_2) + \lambda^5K_1(K_2+2) - \lambda^6\frac{K_1}{3}(K_2+1).$$

We now have at hand expressions for all the quantities needed in

the deflection analysis of the elastically-restrained beam. In evaluating the ability of equation (93) to predict buckling loads, it was of course necessary to maximize the expressions for $\bar{\delta}$. The general scheme for doing this was to systematically vary the load location, computing the load-point flexibility coefficient for each λ. The new value of $\bar{\delta}$ was compared to the previous value, with the process terminating when either a decrease in value, or a λ such that $\lambda > 1$, was encountered. Iteration was such that a maximum value of $\bar{\delta}$ was converged upon. The main reason for using this approach was the possible presence of absolute maxima, which would not correspond to a zero derivative.

The results of the buckling calculations are listed in Table 1 and illustrated in Figure 34. The buckling ratio, which, it must be noted, is four times the usual end fixity coefficient, is plotted against the relative rotational and lateral spring stiffnesses. The sharp crease near $K_1 = 40$ is due to a change in buckle mode there.

Figure 35 shows the variation of the quantity $R\bar{\delta}_m$ with the spring stiffnesses. The immediate observation is that the surface is far from flat, a conclusion that we should have anticipated in view of the cantilever beam result. Furthermore, our previous observations concerning inflection points account for the four-to-one change in elevation. Indeed, it would appear that equation (93) would provide a very good approximation to the true state of affairs for the extreme cases $K_1 = 0$ and $K_1 = \infty$. In point of fact the latter case was treated individually in Reference 59, where it was shown that the

Table 1. Buckling Loads for the Elastically-Restrained Beam of Figure 33b

SPRING STIFFNESS $K_2 = k_2 L/EI$

Spring Stiffness $K_1 = k_1 L^3/EI$

	0	.1	.4	1	2	4	5	10	40	50	100	400	1000	10^6
0	1.00000	1.07947	1.29966	1.66887	2.12489	2.68005	2.85664	3.32403	3.81062	3.84791	3.92436	3.98329	3.99525	4.00324
.1	1.03283	1.11248	1.33316	1.70309	2.15980	2.71534	2.89168	3.35877	3.84418	3.88134	3.95750	4.01621	4.02811	4.03607
.4	1.13112	1.21132	1.43347	1.80564	2.26447	2.82113	2.99739	3.46301	3.94480	3.98158	4.05689	4.11490	4.12666	4.13452
1	1.32670	1.40806	1.63327	2.01010	2.47336	3.03242	3.20853	3.67157	4.14580	4.18179	4.25541	4.31204	4.32351	4.33118
4	2.28197	2.36998	2.61310	3.01740	3.50754	4.08311	4.25952	4.70904	5.14614	5.17831	5.24370	5.29361	5.30367	5.31039
5	2.59665	2.68124	2.93134	3.34661	3.84799	4.43082	4.60757	5.05315	5.47772	5.50862	5.57128	5.61895	5.62855	5.63495
10	4.03525	4.14163	4.43580	4.92362	5.50372	6.14458	6.32730	6.75597	7.11875	7.14349	7.19287	7.22986	7.23726	7.24217
15	5.24864	5.37437	5.72539	6.31812	7.03258	7.79685	7.99892	8.42720	8.73350	8.75224	8.79022	8.81791	8.82312	8.82664
25	6.74547	6.89518	7.32471	8.09072	9.13645	10.4986	10.9097	11.6129	11.8352	11.8440	11.8601	11.8710	11.8731	11.8745
30	7.11608	7.26750	7.70038	8.47806	9.54850	11.0548	11.5868	12.9742	13.3238	13.3289	13.3373	13.3426	13.3435	13.3441
40	7.50761	7.65846	8.07556	8.83178	8.86635	11.3319	11.8563	13.4048	15.2454	15.3932	15.6976	15.9332	15.9810	16.0129
50	7.69728	7.84014	8.24814	8.99385	9.98268	11.4036	11.9132	13.4256	15.2462	15.3936	15.6977	15.9332	15.9810	16.0129
60	7.80578	7.94541	8.34425	9.06299	10.0409	11.4352	11.9369	13.4322	15.2463	15.3937	15.6977	15.9332	15.9810	16.0129
75	7.87531	8.01259	8.40483	9.11054	10.0755	11.4529	11.9542	13.4355	15.2464	15.3937	15.6977	15.9332	15.9810	16.0129
100	7.98552	8.11868	8.49947	9.18472	10.1268	11.4778	11.9675	13.4397	15.2464	15.3937	15.6977	15.9332	15.9810	16.0129
400	8.14020	8.26679	8.62956	9.28446	10.1925	11.5076	11.9882	13.4441	15.2465	15.3937	15.6977	15.9332	15.9810	16.0129
1000	8.16634	8.29173	8.65126	9.30085	10.2030	11.5122	11.9913	13.4448	15.2465	15.3937	15.6977	15.9332	15.9810	16.0129
10^6	8.18298	8.30761	8.66503	9.31117	10.2096	11.5150	11.9932	13.4451	15.2465	15.3937	15.6977	15.9332	15.9810	16.0129

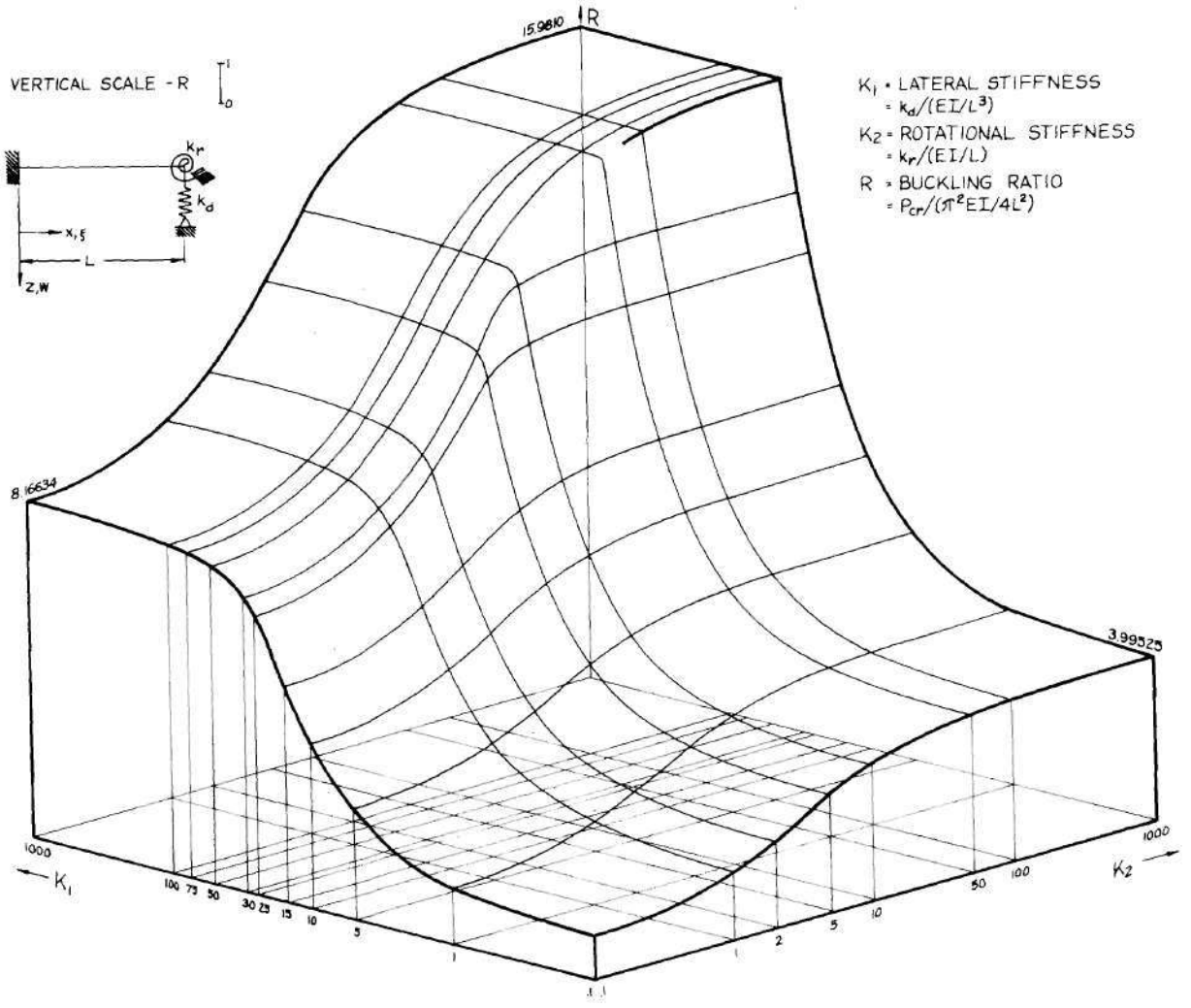

Figure 34. Variation of Buckling Load Ratio with End Restraint for Configuration 33b

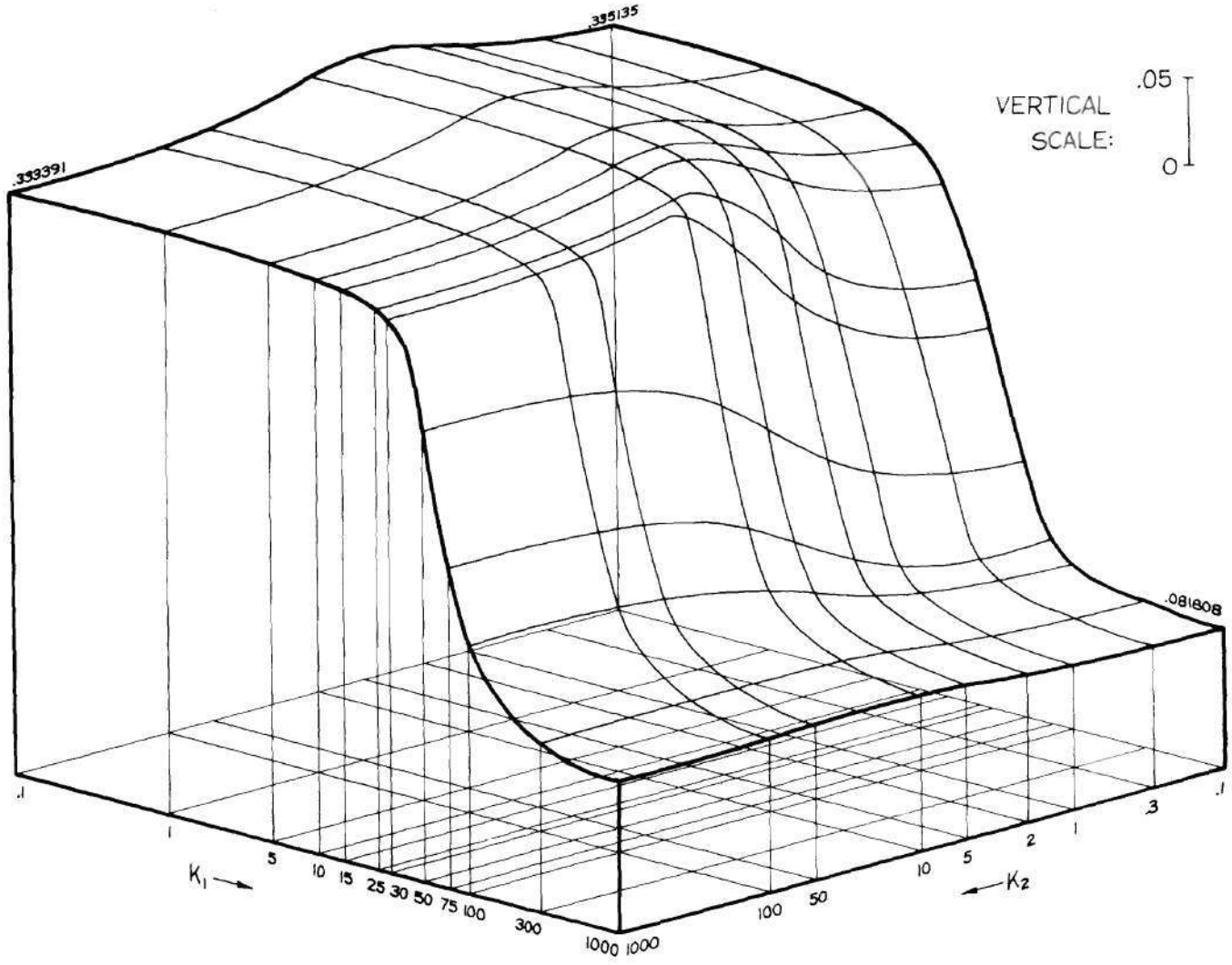

Figure 35. Variation of the Quantity $R\bar{\delta}_m$ with End Restraint for Configuration 33b

maximum deviation from equation (93) was less than 4 per cent. The maximum error in the former case is 7.1 per cent.

Concerning the validity of equation (93) for intermediate values of K_1, we might anticipate some difficulty. While the $R\bar{\delta}_m$ surface is certainly not flat, it is at least smooth. Yet somewhere between $K_1 = 0$ and $K_1 = \infty$ there is a change in the number of inflection points from one to two, a change which, by its integer nature, must be discontinuous. Hence, equation (93) must contain a discontinuity in buckling load prediction that does not reflect the actual state of affairs. A look at Figure 36, which shows the error incurred from using this equation as a buckling load prediction relation, confirms our worst fears. In the region of the discontinuity there is no way that the error, which is as high as 235 per cent, can be considered acceptable.

It is possible, however, to define regions in which the error is acceptable. The dotted lines show contours of 10 per cent error, and if that error is deemed acceptable, then the regions lying outside of those lines may be considered to constitute the domain of acceptability for equation (93). In short, that relation can be said to accurately predict the buckling load of the beam shown in Figure 33b for values of K_1 greater than 500 and less than 10.

It is important to consider what actually happens at the discontinuity. For $K_1 = 0$, the maximizing λ is unity (the load is at the end of the beam), and the flexibility coefficient there is an absolute maximum. By way of contrast, when K_1 is infinite, the maxi-

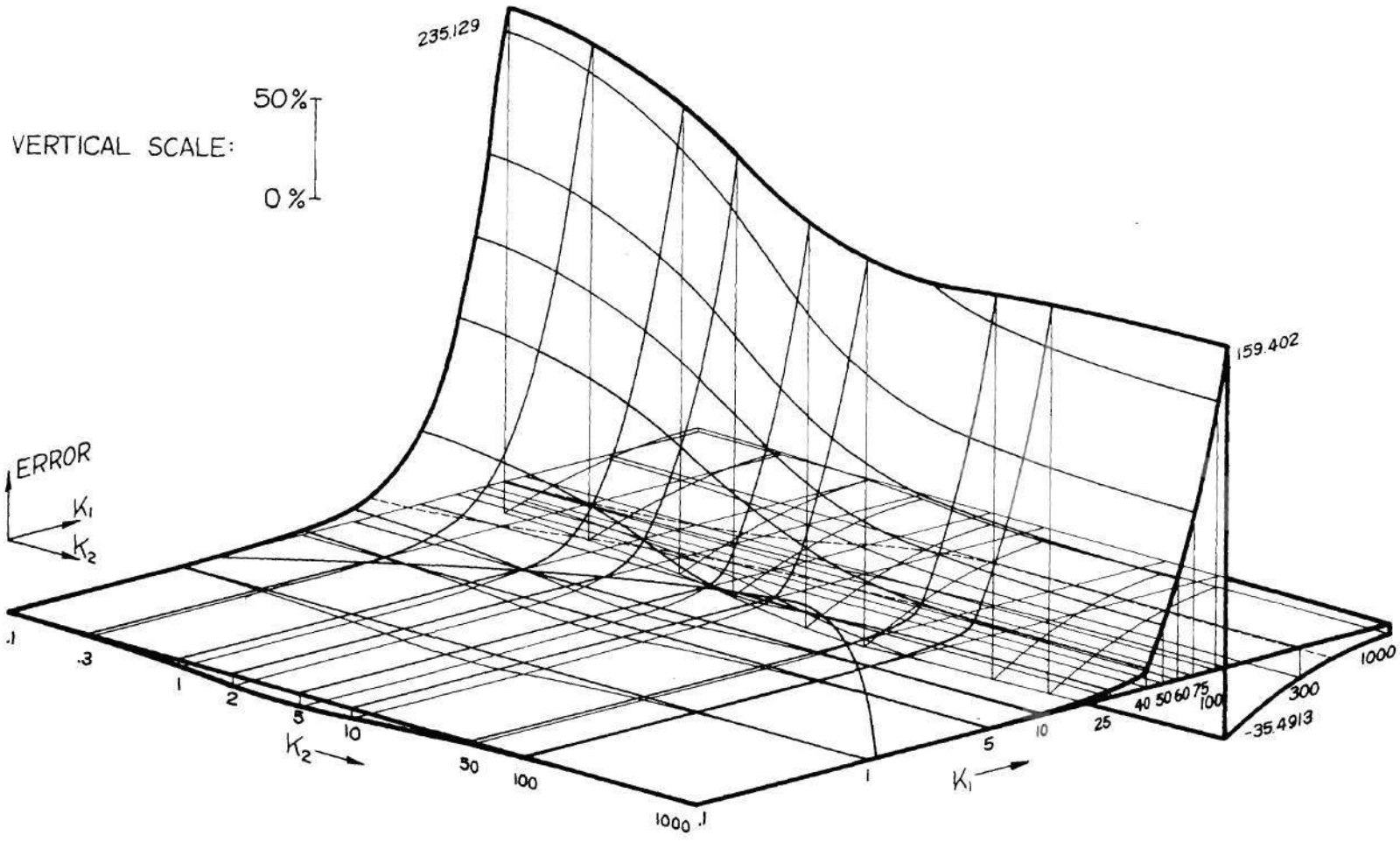

Figure 36. Error in Predicting the Buckling Load Using the P-Delta Approach for Configuration 33b.

mizing λ is in the neighborhood of the beam mid-point, and this flexibility coefficient is a relative maximum. For an intermediate range of K_1 values, both a relative and an absolute maximum exist; at the discontinuity, the maxima are equal, and there is an abrupt change in the λ corresponding to the greater of the two. The quantity $\bar{\delta}_m$ is of course continuous, and it is entirely due to the discontinuity in the buckling load prediction relation that there are huge, albeit rapidly decaying, errors in that region.

Obviously, it is not actually necessary to locate and count the inflection points in each case; it is sufficient to observe that $\lambda = 1$ implies one inflection point, and that any lesser λ implies the existence of two.

P-Theta Approach

Non-Ideal End Support

It is apparent that equation (93) is inadequate in predicting buckling loads when finite lateral restraint is present. Indeed, one may question whether any formula that involves merely the deflection under the load could ever be adequate, inasmuch as there is a strong hint that more than one measured quantity is needed.

We have thus far emphasized the importance of inflection points in beam behavior, indicating that there might be some sensitivity to wave form, as opposed to wave amplitude, that is lacking in the measurement of a single deflection only. It is noteworthy that an inflection point is also a point of extremal slope, and it is only natural to wonder if the measurement of maximum slopes might provide

a better estimation of the buckling load than using the deflection approach.

The first observation this new approach brings to mind is that a single load can produce more than one measurable slope. if, for example, we consider the case of the clamped-clamped beam, a load at the point of maximum flexibility (the mid-point) produces only one deflection under the load, but two extremal slopes - one positive and one negative. In this case, then, we would have two measurable parameters if we decided to consider all non-zero extremal slopes. This feature has two marked advantages: it may give us more flexibility in dealing with configurations having elastic restraint; and we may have as many different slopes to use as there are boundaries having unknown or non-ideal boundary support. This last point may have special significance in dealing with two-dimensional structures.

The second observation is that while the deflection of a beam under a concentrated lateral load is proportional to the cube of the length, the slope is proportional to the square of the length. Since the critical load is inversely proportional to the length squared, it is apparent that the product $P_{cr}(\theta/Q)$ is independent of specimen length. This is more than a slight convenience. It will be recalled from earlier discussions that the length quantity to be used in equation (93) is not necessarily the nominal strut length. In particular, when boundary configurations contain rigid carriers, attachments which move without participating in bending deformations, the question of effective strut length can be fairly involved; this issue is avoided in the proposed new approach.

In order to evaluate a "P-theta" procedure, we must obtain expressions for the slopes; this can be done in a fashion similar to that used in finding the deflections. For configuration 33b, the dummy load system is that shown in Figure 33c, where μ represents the "observation", as opposed to loading, point. The dummy load moment distribution is given by

$$\frac{M_d}{L} = \begin{cases} 1/L & 0 \le \xi \le \mu \\ \\ 0 & \mu \le \xi \le 1 \end{cases} \tag{129}$$

whereas the actual moment distribution is of course unchanged. The slope is given by

$$\theta = - \frac{QL^3}{EI} \int_0^1 \left[\frac{M(\xi)}{QL}\right] \left[\frac{M_d(\xi)}{L}\right] d\xi. \tag{130}$$

For

$$\mu \le \lambda, \tag{131}$$

substitution of (116) and (129) into (130) gives

$$\theta = -\frac{QL^3}{EI}\int_0^{\mu}\left[\left(\frac{R_1}{Q}\right)(1-\xi) + \frac{M_1}{QL} + \xi-\lambda\right]\left(\frac{1}{L}\right)d\xi \qquad (132)$$

$$-\frac{QL^3}{EI}\int_{\mu}^{\lambda}\left[\left(\frac{R_1}{Q}\right)(1-\xi)+\frac{M_1}{QL} + \xi-\lambda\right](0)d\xi - \frac{QL^3}{EI}\int_{\lambda}^{1}(0)d\xi,$$

or

$$\bar{\theta} = \frac{\theta/Q}{L^2/EI} = -\int_0^{\mu}\left[\left(\frac{R_1}{Q}\right)(1-\xi) + \frac{M_1}{QL} + \xi-\lambda\right]d\xi \qquad (133)$$

Integration yields

$$\bar{\theta} = \lambda\mu - \frac{\mu^2}{2} - \left(\frac{R_1}{Q}\right)\left(\mu - \frac{\mu^2}{Q}\right) - \left(\frac{M_1}{QL}\right)\mu. \qquad (134)$$

The location of extremal slope is found by differentiating equation (134) with respect to the measuring location μ, with λ fixed, of course. Forcing this derivative to vanish thus gives

$$\mu_m = \frac{\lambda - \left(\frac{R_1}{Q}\right) - \left(\frac{M_1}{QL}\right)}{1 - \left(\frac{R_1}{Q}\right)}, \qquad (135)$$

which is the location of the first inflection point encountered in

moving from the clamped toward the elastically-restrained end.

For the region to the right of the load, both the dummy and the actual moment distributions remain the same; the limits of integration change to reflect the fact that

$$\mu \geq \lambda. \tag{136}$$

Again, substitution of (116) and (129) into (130) gives

$$\theta = -\frac{QL^3}{EI}\int_0^{\lambda}\left\{\left[\left(\frac{R_1}{Q}\right)(1-\xi) + \frac{M_1}{QL}\right] + \xi-\lambda\right\}\left(\frac{1}{L}\right)d\xi \tag{137}$$

$$-\frac{QL^3}{EI}\int_{\lambda}^{\mu}\left[\left(\frac{R_1}{Q}\right)(1-\xi) + \frac{M_1}{QL}\right]\left(\frac{1}{L}\right)d\xi - \frac{QL^3}{EI}\int_{\mu}^{1}(0)d\xi,$$

or

$$\bar{\theta} = -\int_0^{\mu}\left[\left(\frac{R_1}{Q}\right)(1-\xi) + \left(\frac{M_1}{QL}\right)\right]d\xi + \int_0^{\lambda}(\lambda-\xi)d\xi. \tag{138}$$

Integration yields

$$\bar{\theta} = \frac{\lambda^2}{2} - \left(\frac{R_1}{Q}\right)\left(\mu - \frac{\mu^2}{2}\right) - \left(\frac{M_1}{QL}\right)\mu. \tag{139}$$

Again, by means of differentiation, the extremal slope location is found to be

$$\mu_m = 1 + \frac{(M_1/QL)}{(R_1/Q)} \tag{140}$$

Calculation of the extremal slope is now straightforward; the same computer program used to get the maximum deflection suffices. All that is required is to use the converged value of λ to calculate the location μ_m of the extremal slope and use that information to obtain the slope itself.

Physically, we can expect difficulties in maximizing the slope in equation (139) when $\lambda = 1$. Mathematically, the same is true. A look at equations (123) indicates that when $\lambda = 1$, the quantity (M_1/QL) is positive. Furthermore, we have

$$0 \leq (R_1/Q) \leq 1. \tag{141}$$

Therefore,

$$\mu_m = 1 + \frac{M_1/QL}{R_1/Q} \leq 1, \tag{142}$$

and μ_m is outside the range of consideration, due to the existence of

only one inflection point. Thus, to avoid the question of what to do when the second inflection point is not located on the beam (does not exist), only the first extremal slope, denoted as θ_m, will be considered at present.

The product $R\bar{\theta}_m$ is shown as a function of the rotational and lateral end restraint in Figure 37, and it is seen that the surface has only a two-to-one change in elevation, as opposed to the four-to-one change in the $R\bar{\delta}_m$ surface (Figure 35). Another difference is the discontinuity that occurs for values of K_1 in the neighborhood of 77 to 111. This phenomenon is a result of the abrupt change in maximizing λ that was discussed earlier. While the values of $\bar{\delta}_m$ are continuous at the discontinuity, the values of $\bar{\theta}_m$ are not, due to the fact that the abrupt change in λ_m results in marked changes in deflected shape, with corresponding abrupt changes in the maximum slope.

With regard to formulating a rule for predicting the buckling load on the basis of a lateral load test, it would be possible to handle the two-to-one drop-off in the $R\bar{\theta}_m$ surface in a fashion similar to that in which the four-to-one decrease in the $R\bar{\delta}_m$ surface was handled. In particular, a little reflection will indicate that a low of the form

$$R\bar{\theta}_m = \frac{1}{2n_p} \tag{143}$$

would work quite well for the flat areas of the surface. Substitution of the expressions for R and $\bar{\theta}_m$ enables us to formulate the rule equivalently:

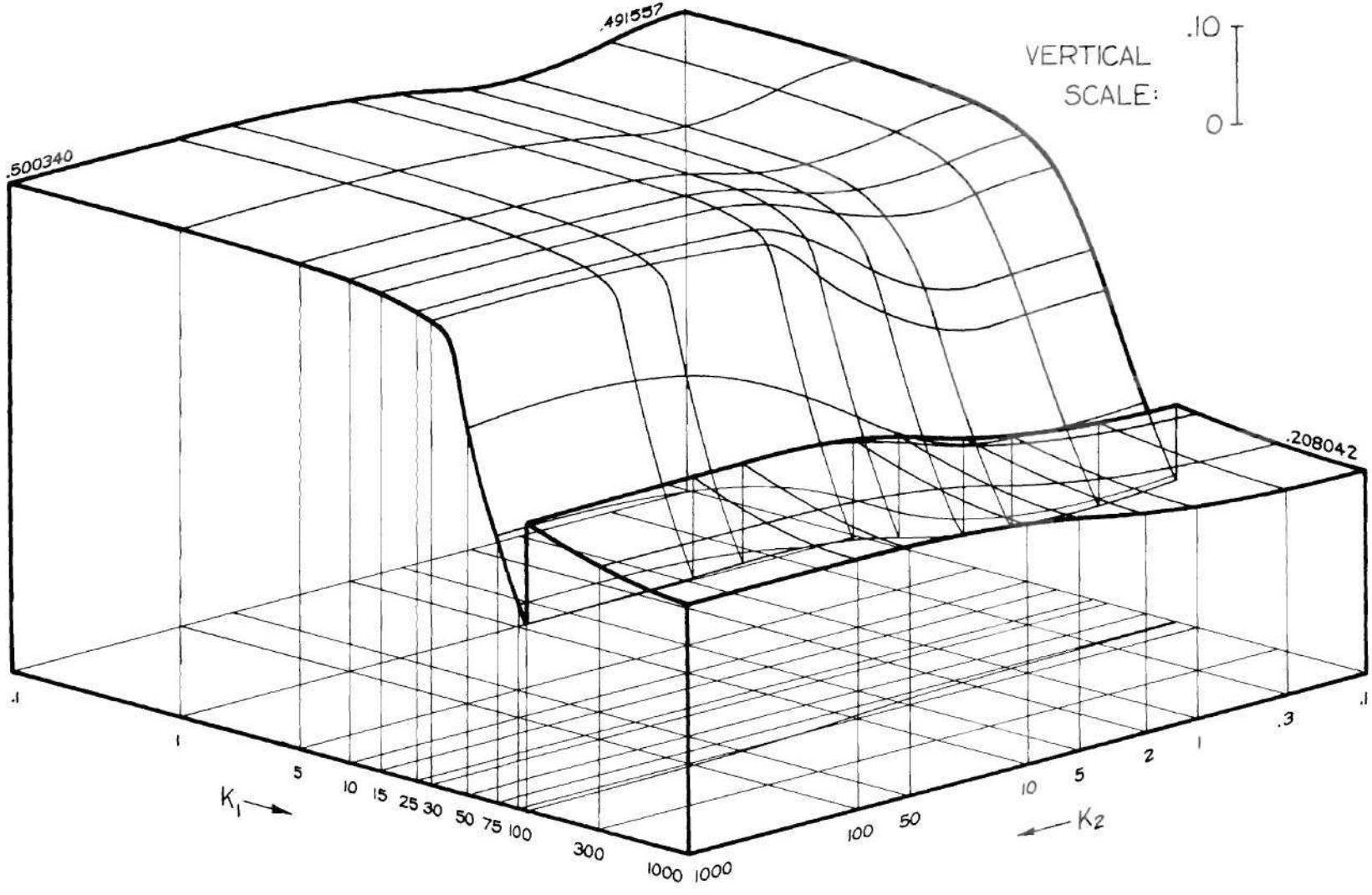

Figure 37. Variation of the Quantity $R\bar{0}_m$ with End Restraint for Configuration 33b

$$P_{cr}\left(\frac{\theta_m}{Q}\right) = \frac{\pi^2}{8n_p} \tag{144}$$

where n_p is again the number of inflection points.

It was previously noted that the number of inflection points was readily determined from the load location λ_m. Indeed, one might wonder if the quantity λ_m itself might be used in place of n_p, with the possible consequences that where small variations in λ_m exist, the prediction of the buckling load would be improved where the $R\bar{\theta}_m$ surface is not quite flat. Noting that n_p and λ_m form a roughly reciprocal relationship, we can readily formulate a slightly different rule:

$$R\bar{\theta}_m = \frac{\lambda_m}{2} . \tag{145}$$

or

$$P_{cr}\left(\frac{\theta_m}{Q}\right) = \pi^2 \frac{\lambda_m}{8} . \tag{146}$$

It is to be noted in this proposed rule that we have two discontinuous quantities, one on each side of (145) and (146), instead of just one. It is hoped, of course, that the discontinuities will neutralize one another in predicting the buckling load.

The evaluation of this buckling load prediction scheme was carried out, and Figure 38 shows the variation of the quantity

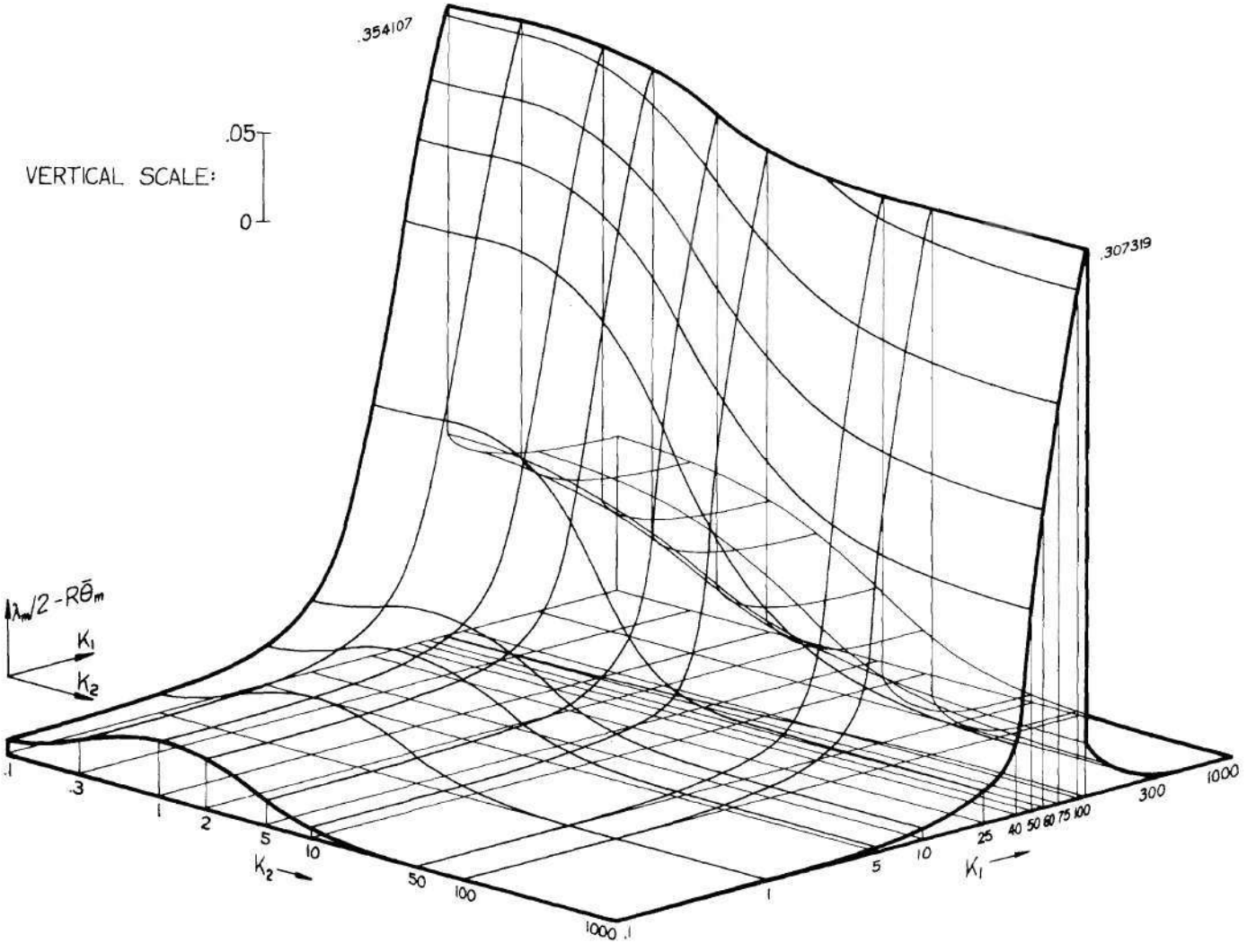

Figure 38. Error in the Relation $R\bar{\theta}_m=\lambda_m/2$ for Configuration 33b

$$R\bar{\theta}_m - \frac{\lambda_m}{2} = P_{cr}\left(\frac{\theta_m}{Q}\right) - \pi^2 \frac{\lambda_m}{8} \qquad (147)$$

with lateral and rotational spring stiffnesses. Unfortunately, it appears that the error in the rule along the discontinuity is still considerable; this fear is borne out in Figure 39, in which the error in the predicted buckling load is displayed. Obviously, the hoped-for neutralization did not occur. It is interesting, however, to compare these results with those in Figure 36. Along the lines $K_2 = 0$ and $K_2 = \infty$ the two surfaces are identical for values of K_1 less than the discontinuity values of 76.9255 and 111.310, respectively. In the remainder of the region to the left of the discontinuity, the differences in surface shape are quite small, and we can conclude that in this region, characterized by

$$\lambda_m = n_p = 1, \qquad (148)$$

the P-delta and P-theta approaches are nearly equivalent.

To the right of the discontinuity, variations in the load location λ_m occur, and we no longer have equivalence between the n and the λ_m rules. Hence, comparison between Figures 36 and 39 is no longer valid. It is interesting to note, however, that in the region where λ_m is less than unity, its influence has been harmful rather than helpful, as we had hoped. This buckling load prediction scheme is,

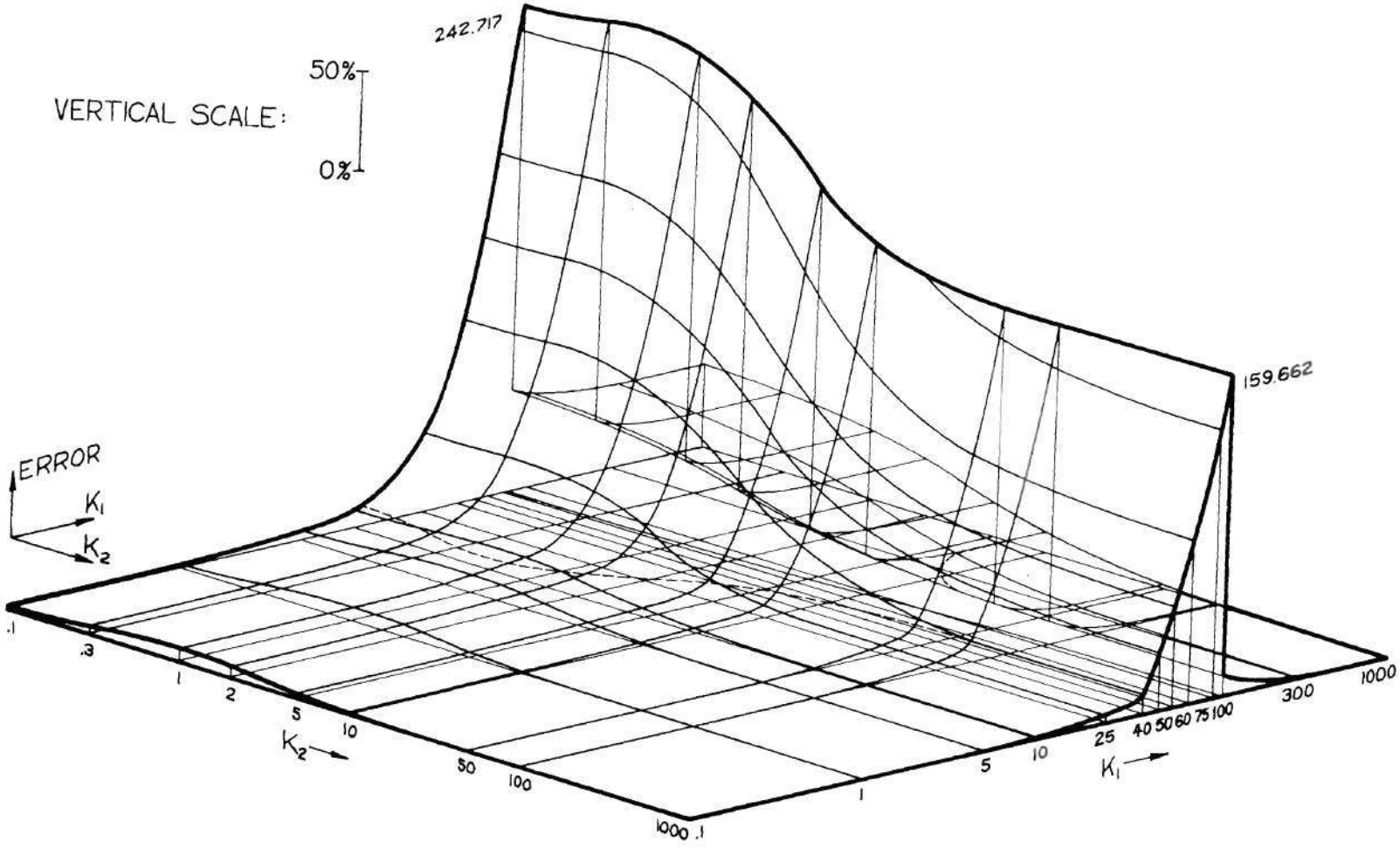

Figure 39. Error in Predicting the Buckling Load by the Relation $R\bar{\theta}_m = \lambda/2$ for Configuration 33b

nevertheless, valid in some regions; accordingly, the 10 per cent contours are again delineated by the dotted lines.

Where do we go from here? It is abundantly clear that our problems have occurred primarily at the discontinuity; hence, a non-destructive test to predict buckling loads should ideally be based on continuous quantities. It is also obvious that the use of the maximum load-point deflection is particularly bothersome in this regard. It does, however, possess many advantages, and a pertinent question is whether it would be possible to minimize the discontinuity while retaining the same basic scheme.

In taking this point of view, we may recall that in the neighborhood of the discontinuity, there are two extremal load-point flexibilities, one of which is relative and one of which is absolute. If a rule is formulated that uses slopes obtained from both load locations (and which works when the spring stiffnesses are zero or infinite), the resulting function, and hence load prediction, will be continuous where there is presently a discontinuity. We have, however, only delayed the day of reckoning. There will be one line along which the relative maximum ceases to exist, and another line along which the absolute maximum disappears. If we vary the spring stiffnesses such as to move outward from the original discontinuity across either of these lines, the number of extremal load locations will change abruptly from two to one; hence this approach would smooth the one discontinuity, but would introduce two new ones.

Another observation is that the maximum load-point deflection

and the maximum deflection do not necessarily coincide; i.e., the beam slope at the load point may not be zero, even though the load-point flexibility has been maximized. This is particularly true in the neighborhood of the discontinuity. Thus, a prediction rule that utilized maximum deflection instead of maximum load-point deflection would still result in an abrupt change in maximizing λ, but the change would occur for smaller values of K_1, with correspondingly smaller maximum errors. In other words, there would be end restraint configurations near the discontinuity for which we could write

$$(\text{max. load-point } \delta)\Big|_{\lambda_m \neq 1} < (\text{max. load-point } \delta)\Big|_{\lambda_m = 1} \quad (148)$$

$$< (\text{max. } \delta)\Big|_{\lambda_m \neq 1},$$

and the change from $\lambda_m = 1$ to λ_m in the neighborhood of the beam midpoint, while still abrupt, would occur before quite so much error had accrued. Of course the computational difficulty involved in evaluating this scheme, as well as the work involved in using it experimentally, is very much enhanced owing to the fact that for each value of load location, the entire length of the beam must be scanned to find the location of the maximum deflection. For this reason it was decided not to attempt to use this approach.

We must conclude, then, that any scheme in which the load location is dependent on beam deflection behavior is going to give us

a discontinuity in buckling load prediction, with resulting errors of considerable magnitude, whenever the prediction relation involves slopes. If these abrupt changes are to be avoided, another criterion governing load location must be used.

One can characterize all the tests thus far by (1) a simple buckling load prediction relation, and (2) a load location criterion sufficiently involved to make the test work. It is entirely possible to reverse our point of view and use a fixed load location, adjusting the prediction relation to minimize prediction errors. Working still with the elastically-restrained beam of Figure 33b, the load location that comes first to mind is $\lambda = .5$, and it now remains to verify whether this approach has any promise.

The first question to be settled is what relation to use in the buckling load prediction, assuming that we measure some maximum slope. The answer is most efficiently obtained by first considering the four limiting cases. We note that the $\lambda = .5$ coincides, for the clamped-clamped case, with the previous load criterion, and so we suspect that the relation

$$R\left|\bar{\theta}_m\right| = \frac{1}{4} \tag{149}$$

might work again. Indeed, we see that the error in using the above relation in the clamped-pinned case is only -2.2 per cent. However, the configuration having $K_1 = 0$ and $K_2 = \infty$ is considerably in error unless we restrict our consideration of maximum slopes to the region

between the load point ($\mu = .5$) and the weak end of the beam ($\mu = 1$). If we let θ_m be the greatest magnitude of the slope, this modification leaves the previous two limiting cases unaffected and makes the buckling load prediction in the last case exact.

In the case of the cantilever, however, we are not so fortunate. Here the error is exactly 100 per cent; for this case some correction is needed. One way of making such a correction is to use the relation

$$R\left|\bar{\theta}_m\right| = \frac{1}{4(1+c)} \cdot \tag{150}$$

where c is a correction factor that is unity for the cantilever and zero for the other three limiting cases. A number of formulas meeting this requirement are possible, but the most convenient and effective seems to be

$$c = \frac{384}{5}\ \bar{\delta}_1 \left|\ \bar{\theta}_1\right| \tag{151}$$

where the subscript 1 indicates slopes and deflections at the end ($\mu = 1$) due to a load at the middle. In trying equation (151) for finite elastic restraint, however, we observe that as either K_1 or K_2, or both, increase from zero, there is a decrease in c that is much too rapid. It turns out that a very simple way to correct this situation is to use the relation

$$R\left\{\bar{\theta}_m\right\} = \frac{1}{4(1+c^*)}, \tag{152}$$

where c^* is given by

$$c^* = c(2-c) , \tag{153}$$

and where c is determined as before from equation (151).

It is now judicious to observe that when $K_1 = \infty$, c and c^* are zero independently of K_2 (since $\bar{\delta}_1 = 0$); the same is true when $K_2 = \infty$, independently of K_1 (since $\bar{\theta}_1 = 0$). Along the first line, the buckling load prediction is quite well-behaved, the error being bracketed by -2.2 per cent and 6.3 per cent. Along the other line, the error increases from zero of $K_1 = 0$ to 8.2 per cent at $K_1 = 40$. Referring to Figure 34, we observe that this is the location of the crease, where the buckling load abruptly levels off. For this reason the error, as K_1 increases beyond 40, rises rapidly, to reach a peak of 70.7 per cent at $K_1 = 70$. In other words, the buckling load prediction continues to follow the precipitous slope seen in Figure 34 and drastically overshoots the actual buckling load when the crease is passed. It is interesting to observe that precisely at the peak of the error, the maximum and minimum slopes have the same magnitudes; this is the crossover point between the dominance of one to the dominance of the other in the calculation of $\bar{\theta}_m$. We would suspect, then, that the addition of some factor that distinguishes between positive and

negative slopes might be helpful. Indeed, consider the quantity

$$\frac{\bar{\theta}_{max} - \bar{\theta}_{min}}{|\bar{\theta}_m|} - 1 , \tag{154}$$

where $\bar{\theta}_{max}$ is the maximum slope, $\bar{\theta}_{min}$ is the minimum slope, and $|\bar{\theta}_m|$ is the greatest magnitude of the slope, and hence is the quantity used in the buckling load prediction relation (152). It is clear that expression (154), multiplied by the appropriate factor, has the proper qualities, and it might be noted that this is the first time we have made use of the fact, previously mentioned, that a single load can generate two extremal slopes. Since only half of the beam is being considered, only one of the slopes in the numerator of the quotient can be a relative extremum; the other extremum must be absolute. It is significant that the combination of relative and absolute extrema causes no problems. If the latter is zero, then quantity (154) is also zero. Thus, if the quantity is used in an additive fashion, the only limiting case affected is the clamped-pinned configuration, in which case expression (154) has a value of .25. In order to use the expression, we must either accept a considerable error for the clamped-pinned case or find a suitable multiplicative factor to force the expression to vanish, or nearly so. Choosing the latter alternative and trying various possibilities results in the relation

$$c^* = c(2-c) + 3.5\left(\frac{\bar{\theta}_{max} - \bar{\theta}_{min}}{\bar{\theta}_m} - 1\right)[1+(34\bar{\theta}_1)^3]\left(\frac{R_1}{Q}\right)^2, \quad (155)$$

where the various constants are selected to bring maximum correction at $K_1 = 70$, minimum correction at $K_1 = 40$, and proper correction for the clamped-pinned case.

It should be noted that equation (155) implies that its use as a practical test requires the measurement of the reaction at $\mu = 1$; this could be a severe difficulty. In this case the best course of action would be to use quantity (154) with a constant multiplicative factor, accepting the error in the clamped-pinned case as the cost of using the simpler test. Of course, if the test engineer knows a priori that his elastic restraint is considerably different than the clamped-pinned configuration, the cost may be negligible.

It remains to test equations (151), (152), and (155) along the line $K_2 = 0$. Doing so, we make the dismaying discovery that we have an error that is zero for the limiting case $K_1 = 0$ and -0.5 per cent for $K_1 = \infty$ but that peaks at a very nasty 75.68 per cent for $K_1 = 12$. The reason is simple. If we substitute the value $\lambda = .5$ into equations (123) we see that the moment at the end of the beam ($\mu = 1$) is given by

$$\frac{M_1}{QL} = \frac{K_2}{8}\left[\frac{12-K_1}{K_1K_2+12K_2+4K_1+12}\right]. \quad (156)$$

Hence, at $K_1 = 12$ the end moment is zero entirely independent of K_2; the rotational spring is unstrained. Thus, the end slope is also zero, and the beam deflected shapes for all values of K_2 exactly coincide. We may say, then that the test sees the zero slope condition at $\mu = 1$ and concludes that it is dealing with infinite rotational restraint, which in general is not true. The buckling load prediction is based on rotational fixity and in those cases where the actual buckling load is considerably less (for example, at $K_2 = 0$) the error is proportionately high.

The natural question to ask at this point is whether this difficulty might be avoided by the use of some other fixed λ. A look at equations (123) will show, however, that for any set λ there will be some value of K_1 for which M_1/QL is zero independent of K_2, except $\lambda = 1$. Since we know that a test using $\lambda = 1$ cannot yield any information for large values of K_1, we are forced to admit that the use of any fixed λ will result in some region of large error. Thus, the present test is inherently limited, as in any test using a fixed λ for a load location criterion, and dramatic improvement in the results is impossible.

The error associated with using equations (151), (152), and (155) is plotted in Figure 40; the trough is due to the presence of the quantity (154). While we do have a large maximum error, it must be remembered that it is still much smaller than the errors near the discontinuities in the earlier tests. Furthermore, we do have less than 10 per cent error along virtually the entire length of the line

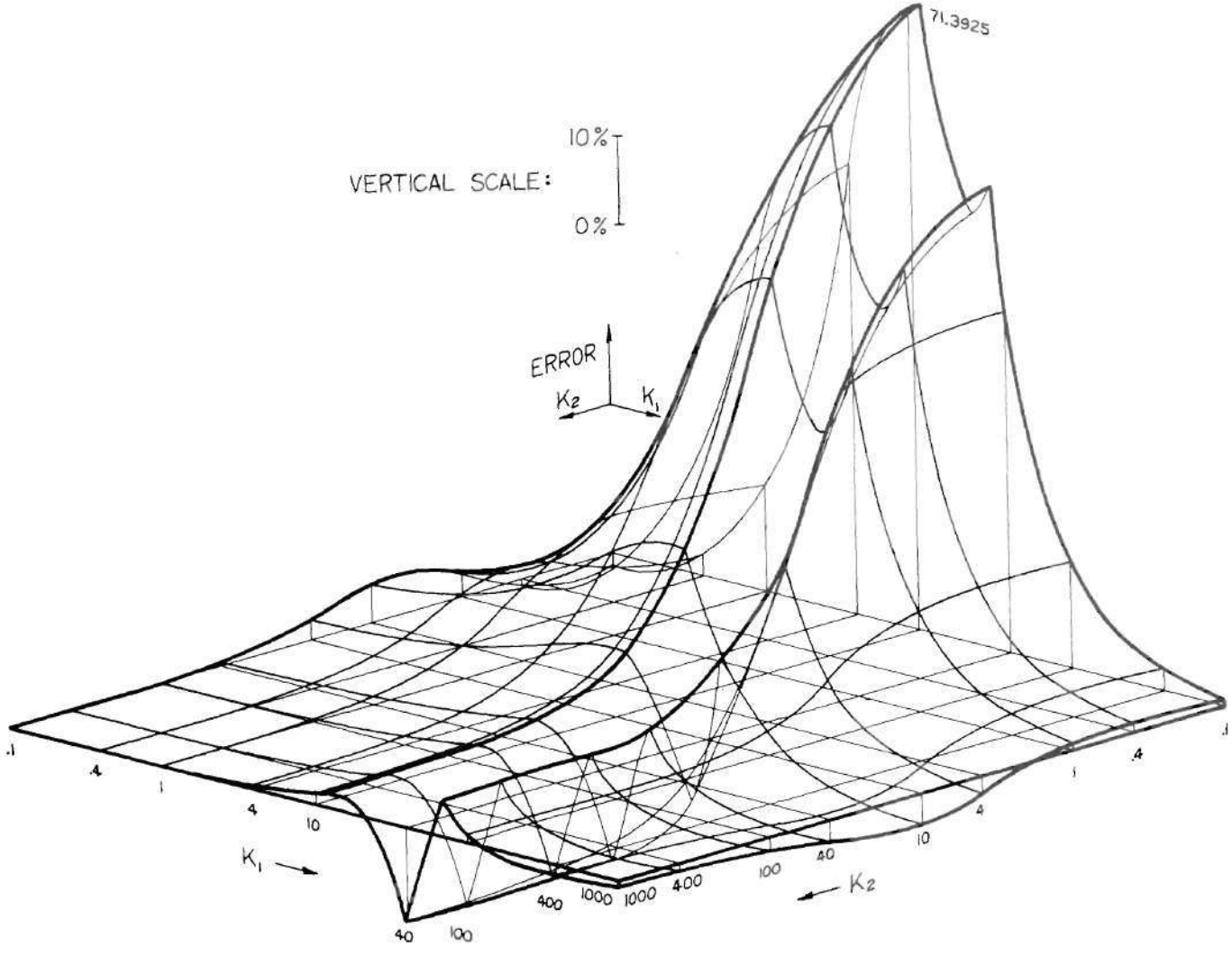

Figure 40. Error in Predicting the Buckling Load by the Mid-Point Lateral Load Test Only for Configuration 33b

$K_2 = \infty$, and this is a distinctly improved result. In fact, if the engineer has some reason to believe his beam restraint is not in the high-error region (and the engineer usually has some indication, from the design of the support structure, what sort of restraint he is dealing with), he has a test giving quite good accuracy, from a practical point of view.

If one still wishes to reduce the maximum error, there is always the possibility of using a different test having low positive error where the above test has high positive error. One could then perform both tests, estimate buckling with each, and choose as his final prediction the lower of the two. Looking at the $\lambda = 1$ region of Figure 39, an obvious second test is a lateral load at the end of the beam, even though it has the shortcoming mentioned earlier. The main difficulty in using it in conjunction with the mid-point test is that there is some overlapping of high-error regions due to the rapid rise in end-load test error with increasing K_1. It behooves us, then, to look for some attenuation factor we could attach to the buckling load prediction in the end-load test. Since we have already burdened ourselves with measuring the end reaction, an effective factor arrived at by trial and error is

$$\hat{c} = \frac{1 - \left(\frac{R_1}{Q}\right)^{175(\bar{\theta}_m + .065)}}{1.00001 - \left(\frac{R_1}{Q}\right)^{500(\bar{\theta}_m + .00001)}}, \qquad (157)$$

where the buckling load prediction relation is

$$R\bar{\theta}_m = \frac{\hat{c}}{2} , \tag{158}$$

which is really equation (149) in disguise. The results of the two-test combination are shown in Figure 41. For low values of K_1 the end load test gives the lower predicted buckling load, except in the immediate vicinity of the cantilever limiting case. For high values of K_1 the mid-point test has the better performance, and the cross-over boundary is the ridge of a cusp whose sharpness increases with decreasing K_2. In one area the demarcation line descends into the trough of Figure 40; it appears in Figure 41 as a heavy line tumbling off the tip of the cusp in the neighborhood of $K_2 = 3$.

While we have for the combined tests a maximum error of 27 per cent, which is still considerable, the error diminishes very rapidly in moving away from the crossover boundary. It may be said, then, that for all practical purposes the combined tests predict the buckling load for an elastically-restrained beam to within 10 per cent, and as a non-destructive test technique this is an enormous improvement over what the test engineer has had to work with previously.

Of course the empirical nature of the expressions (155) and (157) for the factors c^* and $\hat{c}$ introduces two considerable drawbacks into the test method: the expressions are impossible to memorize, and the measurement of several quantities is required to use them. We cannot escape the conclusion that the most desirable approach from a practical

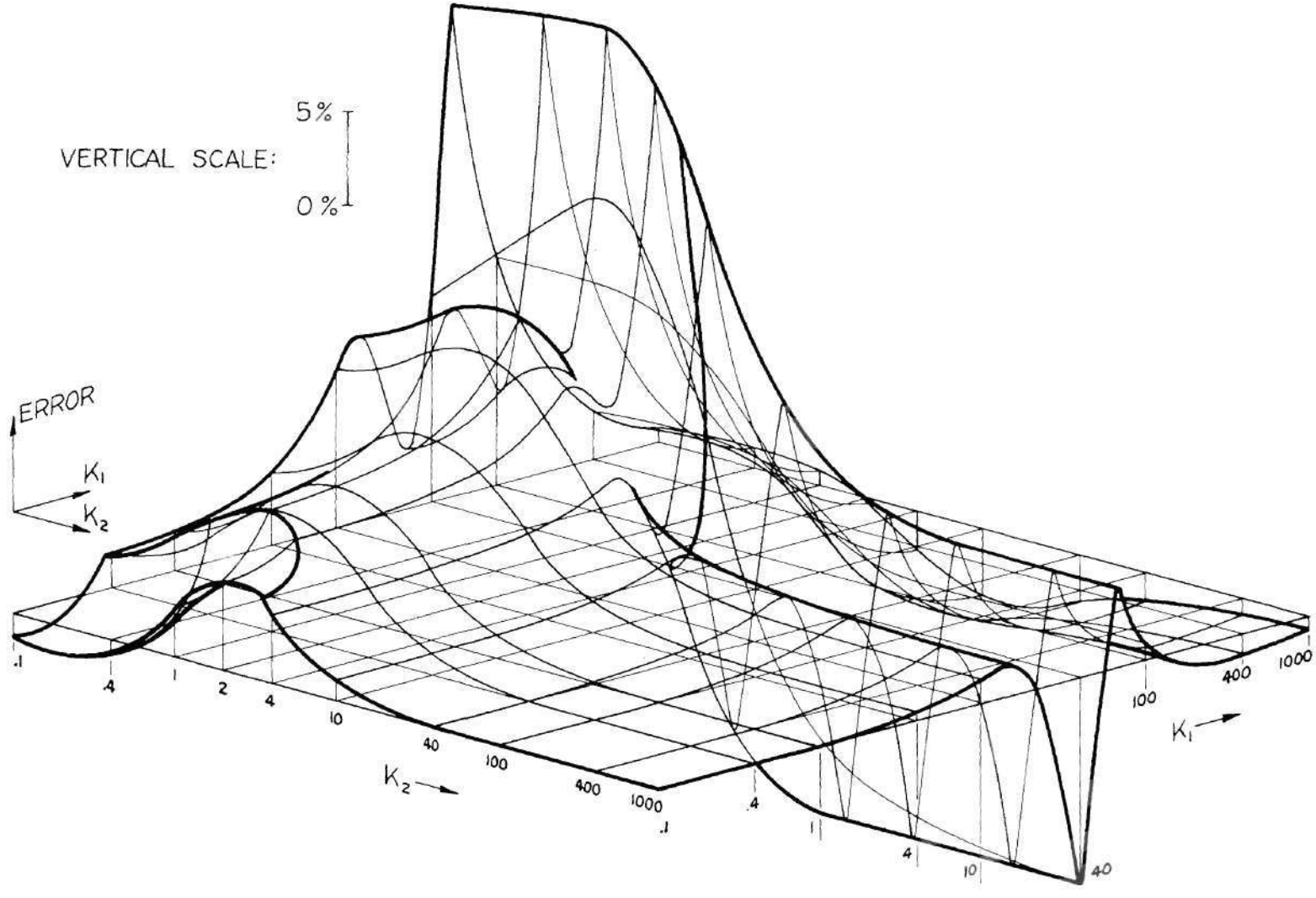

Figure 41. Error in Predicting the Buckling Load by End and Mid-Point Lateral Load Tests for Configuration 33b.

point of view is to use the original scheme with the simple buckling load prediction relation and the more involved load location criterion. Of course we must still deal with the discontinuity problem previously mentioned. In this regard, we may recall the success we enjoyed in using expression (154), where both positive and negative extrema were used, and it is interesting to speculate whether the same sort of trick might be useful in the original method. Consider, then the relation

$$\bar{\theta}_m = \frac{\bar{\theta}_{max} - \bar{\theta}_{min}}{2} \cdot \tag{159}$$

While this new expression for $\bar{\theta}_m$ has in common with expression (154) the property that it is not affected by the number or type of extrema encountered, it is clear that a discontinuity still exists where λ_m changes abruptly. Indeed, if we use the buckling load prediction relation

$$R\bar{\theta}_m = \frac{1}{4} , \tag{160}$$

we see that for $\lambda_m = 1$ there is no change in the predicted buckling load from the results of using the old relation (143). The really significant feature of using equations (159) and (160), however, is that the prediction relation itself is the same on each side of the discontinuity, even if the quantities used in the relation are not.

To see that this is a new result, one must only note the presence of λ_m or n in all the other relations based on a variable load location.

As for the discontinuity itself, we note that the change in predicted buckling load will tend to be somewhat less than before, due to the mitigating presence of the quantity $\bar{\theta}_{min}$ in equation (159) when λ_m is in the neighborhood of the beam mid-point. More importantly, we find that of the four limiting cases, the only one whose buckling load is not predicted exactly is the clamped-pinned beam, and its prediction is in error a miniscule .795 per cent. Thus, if some means of dealing with the abrupt change in λ_m can be found, the use of equations (159) and (160) shows great promise.

At this point it should be reiterated that the location of the lateral load was determined according to the value of λ which extremized the expression for $\bar{\delta}$, equation (128), and that the resulting extremum could either be relative or absolute. Moreover, most of the trouble in predicting the buckling load occurred when the extremum changed from one type to the other. A convenient way of skirting the discontinuity issue, then is to consider only those cases in which the relative maximum exists, which is to say that there will be a region of low K_1 values in which the test will not apply. Using this criterion, with equations (159) and (160) to predict the buckling load, results in the region of validity extending from $K_1 = \infty$ down to a line which, unfortunately, is only slightly beyond the original discontinuity. Thus, the size of the region is inadequate. Furthermore, the errors near the lower limits are horrendously large, all of which

means that this load location criterion must be thrown out.

It is possible, of course, to use other characteristics of the $\lambda - \bar{\delta}$ curve to arrive at other load location criteria, with the hope that equations (159) and (160) would still apply. In this regard, it is interesting to note that the set of cases in which a negative curvature exists contains as a subset all the cases displaying zero slope. Furthermore, the location of extremal negative curvature (zero third derivative with respect to λ of $\bar{\delta}$) closely approximates the location of zero first derivative, where both exist. Thus the results for $K_1 = \infty$ would not be greatly affected, while the region of validity might be extended considerably. We might then propose as a load location criterion that the load be applied at the location of extremal negative curvature, where it exists.

For the two limiting cases at $K_1 = 0$, we have already noted that equation (159) and (160) provide exact buckling prediction when $\lambda = 1$. It is only natural that we attempt to establish a completely general test that entails the following procedure:

(1) If the lateral restraint at the end is sufficiently small to permit measurable deflection when loaded at the end, $\lambda = 1$ is the one test position;

(2) If, and only if, the $\lambda - \bar{\delta}$ relation, equation (128), displays a region of negative curvature, a second test position exists and is located where that curvature is extremized;

(3) Where both test locations exist, the one leading to the larger θ_m, and hence smaller predicted buckling load, is used in the

prediction relation, equation (160).

Using this test result is a considerable improvement over the "maximum load-point flexibility" approach, as will be seen from a glance at Figure 42. The cusp that is prominent at low values of K_2 again denotes the crossover line from the dominance of the end load to that of the maximum curvature criterion. The error in the load prediction is generally well within 10 per cent, except for the small region in which the cusp rises to 42 or 43 per cent. It is of interest to note that the load location and the prediction error for the clamped-pinned beam are .621467 and .430716 per cent, respectively, whereas in the "maximum load-point flexibility" approach these figures were .585551 and .795 per cent.

It is interesting to wonder what further improvements might be obtained using equations (159) and (160). Noting that errors associated with the previous test and illustrated in Figure 42 are largely positive, we may investigate the maximum potential of the two equations by proposing a third load location criterion: the load should be applied in the location that maximizes the quantity $\bar{\theta}_m$ in equation (159) and hence minimizes the buckling load prediction of equation (160). The results of such a test are shown in Figure 43. The striking feature is the resemblance of this graph with that in Figure 42; they are indistinguishable save for the upper ridge of the trough near $K_1 = 30$. Here, the cusp indicates the crossover line between regions of relative and absolute maxima in $\bar{\theta}_m$, or between $\lambda_m = 1$ and λ_m near the mid-point. The results in the two cases are not precisely identical; the load

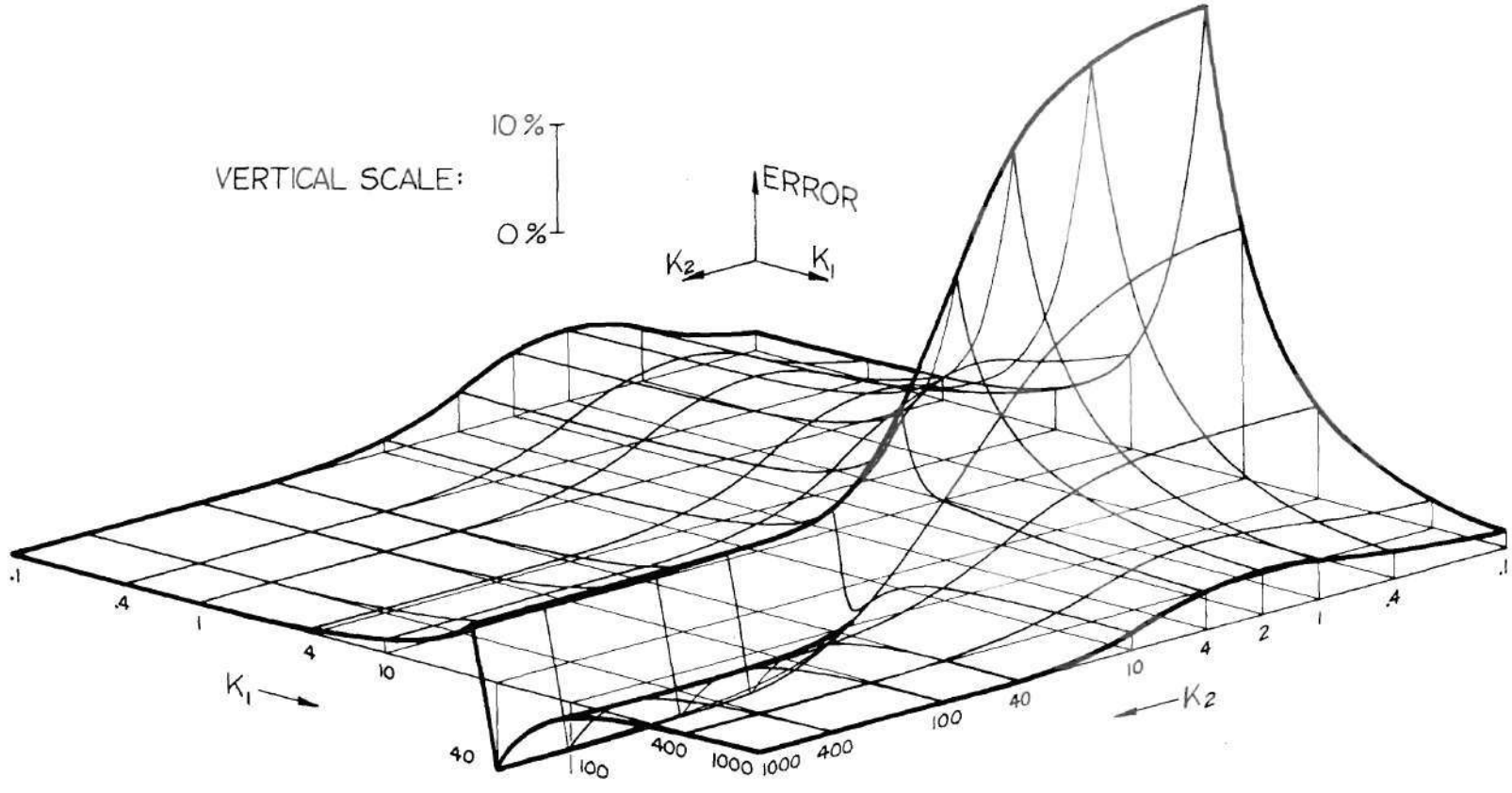

Figure 42. Error in Predicting Buckling Loads by the Maximum Lambda-Delta Curvature Criterion for Configuration 33b.

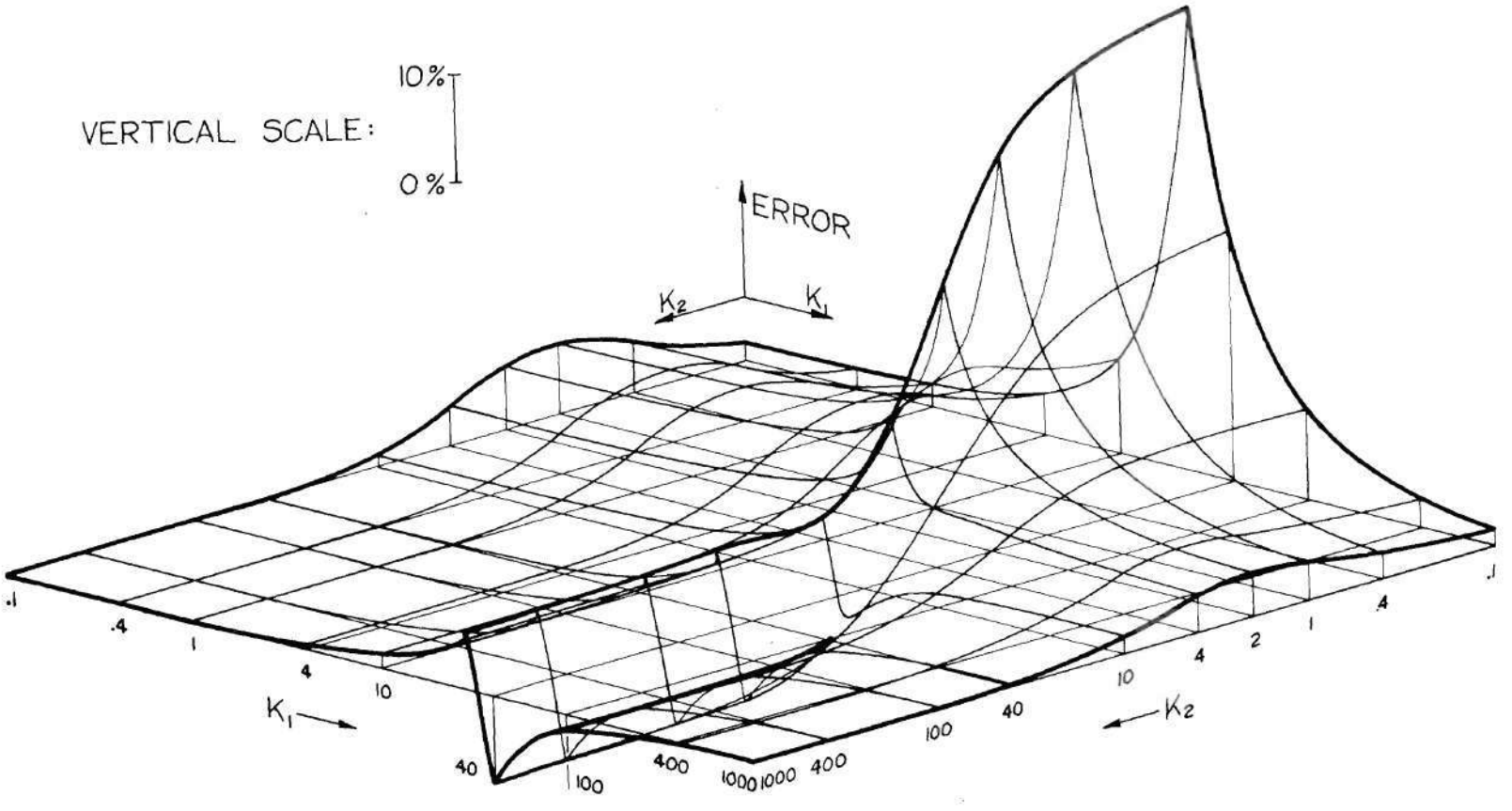

Figure 43. Error in Predicting Buckling Loads by the Minimum Load Prediction Criterion for Configuration 33b

locations were slightly different. For example, the load location and prediction error for the clamped-pinned case are now .611891 and .342265 per cent, respectively.

The implications of these observations are significant. The maximum-curvature criterion gives approximately the optimum load locations as far as equations (159) and (160) are concerned. That the equations are fairly insensitive to load location is indicated by the similarity of Figures 42 and 43; as an example, in the clamped-pinned case, a 1 per cent change in the load location produces a prediction error change of only .09 per cent.

Computer programs for obtaining the data graphed in Figures 42 and 43 are contained in Appendices IV and V, respectively.

It is appropriate at this point to further test the generality of the results of the P-theta approach by evaluating it, in conjunction with the three load location criteria, for the structures analyzed in the section dealing with the P-delta approach. In dealing with finite rotational end restraint, a more general procedure than that used previously is to consider the beam configuration in Figure 28d, with the difference being that both k_2 and k_3 are allowed to vary between zero and infinity. Of course this problem contains as special cases the two rotational restraint problems done earlier.

The analysis of this structure is carried out in Appendix III, and it is shown that the flexibility coefficient varies with the load location λ according to the relation

$$3(K_2K_3+4K_2+4K_3+12)\ \bar{\delta} = \lambda^2(3K_2+12) + \lambda^3(K_2K_3-8K_2+4K_3-24) \qquad (161)$$

$$+ \lambda^4(-3K_2K_3+6K_2-9K_3+12)$$

$$+ \lambda^5(3K_3)(K_2+2) + \lambda^6(-K_2K_3-K_2-K_3).$$

It is furthermore shown that for

$$\mu \leq \lambda, \qquad (162)$$

the slope, measured at $\xi = \mu$, and caused by a load at $\xi = \lambda$, is given by

$$\bar{\theta} = \left(\frac{M_1}{QL}\right)\left(\frac{1}{2} - \mu\right) + \left(\frac{R_1}{Q}\right)\left(\frac{1}{3} - \mu + \frac{\mu^2}{2}\right) \qquad (163)$$

$$+ \frac{\lambda^3}{6} - \frac{\lambda^2}{2} + \mu\lambda - \frac{\mu^2}{2},$$

where R_1/Q and M_1/QL are the right end vertical reaction and moment coefficients, respectively, and are given by

$$\frac{M_1}{QL} = \lambda K_2\left[\frac{\lambda K_3(\lambda-1) + 2(\lambda^2-1)}{K_2K_3+4K_2+4K_3+12}\right]; \qquad (164)$$

$$\frac{R_1}{Q} = \lambda \left\{ \frac{K_2[\lambda K_3(3-2\lambda) + 6-2\lambda^2] + 2\lambda K_3(3-\lambda) + 12}{K_2K_3+4K_2+4K_3+12} \right\} \quad (165)$$

This slope is extremized when

$$\mu_m = \frac{\lambda - \frac{M_1}{QL} - \frac{R_1}{Q}}{1 - \frac{R_1}{Q}} . \quad (166)$$

For

$$\mu \geq \lambda, \quad (167)$$

the slope in this interval is given by

$$\bar{\theta} = \left(\frac{M_1}{QL}\right)\left(\frac{1}{2} - \mu\right) + \left(\frac{R_1}{Q}\right)\left(\frac{1}{3} - \mu + \frac{\mu^2}{2}\right) + \frac{\lambda^3}{6} \quad (168)$$

and becomes an extremum for values of μ given by

$$\mu_m = \frac{\frac{M_1}{QL}}{\frac{R_1}{Q}} + 1. \quad (169)$$

For this problem, the buckling analysis is conveniently done in closed form; the characteristic equation is

$$m_b\,(K_2+K_3)(\sin m_b - m_b \cos m_b) + K_2K_3(2-2\cos m_b - m_b \sin m_b) \qquad (170)$$

$$+ (m_b)^3 \sin m_b = 0,$$

where

$$m_b = \pi \sqrt{\frac{R}{2}} \; . \qquad (171)$$

Again, numerical techniques must be employed in finding the maximizing λ, as well as the root of equation (170). Such techniques are outlined in the computer program included in Appendix III. A partial listing of results is shown in Table 2. For all three location criteria, the errors were non-negative for all values of K_2 and K_3. The maximum error for each case was 6.57 per cent and occurred when $K_2 = K_3 = 2$. In addition, the P-delta approach was tested for this configuration. The maximum error was 3.78 per cent, occurring when $K_2 = \infty$ and $K_3 = 0$; the minimum error was -6.56 per cent, occurring when $K_2 = K_3 = 10$.

For the special cases $K_2 = K_3$, the three load location criteria of the P-theta approach coincide, with $\lambda_m = .5$. Thus, the three curves of buckling load prediction are identical; they are plotted with the P-delta error curve in Figure 30.

Table 2. Some Results for the Beam with Unsymmetrical Rotational Restraint, As Shown in Figure 28d

SPRING STIFFNESS $K_2 = k_2L/EI$

Spring Stiffness $K_3 = k_3L/EI$

	0	.1	.4	1	4	10	40	100	400	1000	10^9
0	4.00000 0.00000 0.00000	4.07989 -.148034 .441227	4.30545 -.538321 1.45324	4.70052 -1.12347 2.53842	5.94162 -1.95652 2.61300	6.92077 -1.04602 1.35247	7.79932 1.70049 .458684	8.02351 2.83486 .362024	8.14226 3.53143 .343907	8.16676 3.68000 .340773	8.18308 3.78296 .340606
.1		4.16045 -.295630 .890673	4.38832 -.693449 1.91557	4.78773 -1.29524 3.01352	6.04275 -2.16856 3.09688	7.03331 -1.29019 1.80823	7.92070 1.44364 .888970	8.14668 2.57866 .768512	8.26672 3.27075 .764258	8.29124 3.42144 .761836	8.30769 3.52439 .762119
.4			4.62297 -1.11498 2.97139	5.03450 -1.75545 4.11672	6.33056 -2.75492 4.23505	7.35420 -1.96246 2.89525	8.26793 .728942 1.92331	8.50004 1.85530 1.80728	8.62261 2.55025 1.78111	8.64768 2.69878 1.77548	8.66471 2.80155 1.77399
1				5.46820 -2.46637 5.33621	6.84110 -3.70778 5.54639	7.92790 -3.08200 4.16955	8.89326 -.486828 3.15011	9.13661 .630076 3.02909	9.26521 1.31725 2.99592	9.29124 1.46935 2.99494	9.30900 1.56964 2.99109
4					8.49357 -5.81113 5.96248	9.82941 -5.86711 4.54356	11.0108 -3.71839 3.49765	11.3035 -2.66778 3.39717	11.4569 -2.00570 3.38101	11.4881 -1.86011 3.38141	11.5090 -1.76052 3.38284
10						11.4161 -6.56446 2.97007	12.8391 -4.89657 1.78119	13.1908 -3.92672 1.66744	13.3745 -3.29753 1.65031	13.4115 -3.15551 1.65376	13.4367 -3.06143 1.65288
40							14.5525 -3.59810 .385895	14.9421 -2.67542 .231173	15.1608 -2.05501 .201230	15.2051 -1.91580 .200141	15.2347 -1.81926 .200567
100		ACTUAL BUCKLING LOAD RATIO P-DELTA ERROR, PER CENT MIN. PREDICTION ERROR, PER CENT						15.3976 -1.74598 .070889	15.6076 -1.11629 .040022	15.6543 -.977245 .035761	15.6850 -.878426 .037709
400									15.8414 -.484056 .003985	15.8888 -.341477 .002065	15.9202 -.241112 .003295
1000										15.9364 -.198354 -.000215	15.9682 -.099821 -.000561
10^9											16.0000 0.0000 0.0000

For another set of special cases, characterized by $K_2 = 0$, the resulting error curves are plotted with that of the P-delta approach in Figure 31. Again, the striking feature is the similarity among all three curves in the P-theta approach, particularly between the maximum lambda-delta curvature criterion and the minimum load prediction rule. In Figure 32, the variation of λ_m with the spring stiffness K_3 is plotted for the three load location criteria. Here there is noticeably more dissimilarity in the curves than in the three P-theta error curves of Figure 31, and we have further evidence of the insensitivity of equations (159) and (160) to load location.

Intermediate Lateral Support and Higher Modes

To continue our evaluation of the P-theta approach, we will again consider the beam supported by a central lateral spring, as shown in Figure 28c. Due to symmetry, the three load location criteria coincide, with $\lambda_m = .5$. It is shown in Appendix II that maximum slope due to a central load Q occurs at the beam end point and is given by

$$\bar{\theta}_{max} = - \bar{\theta}_{min} = \frac{1 - \frac{R_5}{Q}}{16} , \qquad (172)$$

where the spring reaction coefficient R_5/Q is given by

$$\frac{R_5}{Q} = \frac{K_5}{K_5 + 48} \cdot \tag{173}$$

For spring stiffnesses less than $16\pi^2$, the buckling load occurs according to equation (67); for greater stiffnesses, the beam prefers to buckle in the second mode, where R = 16. Again using this value of R as an upper bound in the buckling load prediction analysis, the plot of prediction error against spring stiffness for the P-theta approach is identical with the results for the P-delta approach, shown in Figure 29.

The upper bound can again be eliminated if we account for higher modes, as before. In such cases, sets of equal alternating forces are applied such that the load-point deflection sum is maximized. The set used in buckling prediction is that having the highest sum.

The demonstration of the efficacy of this approach is most easily accomplished by assuming a pin-ended strut. Having found the maximum flexibility configuration, we may separately treat each segment between inflection points. The behavior is thus that of a simply-supported beam, and thus the maximum slope, occurring at the inflection point, has a magnitude given by

$$\theta_{max} = \frac{Q(L_0)^2}{16EI}, \tag{174}$$

where L_0 is the length of the segment. If the supports are such that the inflection points are equidistant, we have

$$L_0 = \frac{L}{n_b} , \tag{175}$$

where n_b is the number of half-waves. Substitution of (175) into (174) gives

$$\theta_m = \theta_{max} = \frac{QL^2}{16(n_b)^2 EI} . \tag{176}$$

Since the buckling load is expressible as

$$P_{cr} = \frac{(n_b)^2 \pi^2 EI}{L^2} , \tag{177}$$

the product of the critical load and the maximum slope becomes

$$P_{cr} \left(\frac{\theta_m}{Q}\right) = \frac{\pi^2}{16} , \tag{178}$$

or

$$R\bar{\theta}_m = \frac{1}{4} , \tag{179}$$

which is in exact agreement with equation (160). The buckling load prediction, being exact, is thus identical to that in the P-delta approach. Since in that technique the maximization of the deflection sum ensured the minimization of the buckling load prediction among all lateral load configurations (where the loads are equal in magnitude and alternating in direction), the same conclusion can be reached for the P-theta approach. Thus a crossover from one buckling mode to the next is always recognized by the higher-mode technique, and the need for arbitrary upper bounds is eliminated.

It is again to be noted the interior portion of a multi-bay column deforms into sinusoidal waves regardless of the restraint at the boundary, and hence the error for these cases diminishes with increasing buckle mode.

Nonuniform Columns

The generality of the results for the P-theta approach may be brought full cycle by examining its performance when dealing with a nonuniform section stiffness. In particular, it is enlightening to consider the parabolically-tapered beam dealt with earlier. Again using the dummy load method, with the equivalent structure of Figure 33c, the dummy load moment distribution is

$$M_d(\xi)/L = \begin{cases} 1/L & 0 \le \xi \le \mu \\ 0 & \mu \le \xi \le 1 \end{cases} . \qquad (180)$$

The actual moment distribution is given by equation (43), and the slope

is given by the usual expression

$$\theta = -QL^3 \int_0^1 \frac{[M(\xi)/QL][M_a(\xi)/L]}{EI(\xi)}\, d\xi. \tag{181}$$

For

$$\mu \leq \lambda, \tag{182}$$

substitution of (43) and (180) into (181) yields

$$\bar{\theta} = -\int_0^{\mu} \frac{[(R_1/Q)(1-\xi) + \xi-\lambda]}{1 - a^2\xi^2}\, d\xi. \tag{183}$$

As in previous developments, this expression may be readily integrated by expanding the integrand and using the logarithmic functions in equations (48). The result is

$$\bar{\theta} = \left(\lambda - \frac{R_1}{Q}\right)B_0(\mu) + \left(\frac{R_1}{Q} - 1\right)B_1(\mu). \tag{184}$$

The slope is easily extremized by using Leibnitz' rule, and we have

$$\mu_m = \frac{\frac{R_1}{Q} - \lambda}{\frac{R_1}{Q} - 1} \quad . \tag{185}$$

For the remainder of the beam, we have

$$\mu \geq \lambda, \tag{186}$$

and substitution of the moment distributions into equation (181) gives

$$\bar{\theta} = - \int_0^{\lambda} \frac{[(R_1/Q)(1-\xi) + \xi - \lambda]}{1-a^2\xi^2} \, d\xi - \int_{\lambda}^{\mu} \frac{[(R_1/Q)(1-\xi)]}{1 - a^2\xi^2} \, d\xi \quad . \tag{187}$$

It should be recalled that the integration formulae (48) used lower integration limits of zero. In order to use those relations, it is thus necessary to re-write the integrals in equation (187); lumping the integrands leads to

$$\bar{\theta} = - \int_0^{\mu} \frac{(R_1/Q)(1-\xi)}{1 - a^2\xi^2} \, d\xi - \int_0^{\lambda} \frac{(\xi-\lambda)}{1-a^2\xi^2} \, d\xi. \tag{188}$$

Now substitution of equations (48) into the above yields

$$\bar{\theta} = - (R_1/Q)B_0(\mu) + (R_1/Q)B_1(\mu) - B_1(\lambda) + \lambda B_0(\lambda) \quad . \tag{189}$$

Since the beam is pinned at $\mu = 1$, the slope is extremized there; hence, the extremal slope is given by

$$\bar{\theta}_{min} = - \left(\frac{R_1}{Q}\right) B_0(1) + \left(\frac{R_1}{Q}\right) B_1(1) - B_1(\lambda) + \lambda B_0(\lambda) \ . \qquad (190)$$

Of course, the value of λ used in these equations is a function of the particular load location criterion used. The three available criteria, the "maximum delta," the "maximum lambda-delta curvature," and the "minimum load prediction" rules, are such that the expressions (57), (61), and (159) respectively, must be extremized. It is apparent that we again require the use of numerical techniques, the particulars of which are contained in the computer program in Appendix I. The results are also displayed there, and we can see that the buckling load prediction errors for the three criteria are .534 per cent, .126 per cent, and -.006 per cent, respectively. Since the upper and lower bounds on the actual eigenvalue differed by .505 per cent, we can conclude for the maximum curvature and minimum prediction criteria that the results are more than excellent; they are exact.

In summary, equations (159) and (160) generally provide a good prediction of column buckling loads, using any of the load location criteria discussed. In the maximum delta approach, the experimentalist applies a single concentrated lateral load at varying locations λ, measures the deflection at the load point, and draws a graph of λ versus δ. He selects the value of λ for which the graph displays

maximum δ . He applies the lateral load to the structure at that point and measures the extremal slopes, calculating the buckling load according to (159) and (160).

In the maximum lambda-delta curvature approach, the technique is generally the same, except that λ_m is selected such that the negative curvature of the λ-δ plot is extremized. If the lateral restraint at one end of the beam is such that no negative curvature exists, or that an end load produces measurable deflections, or both, a load location λ_m at that end must also be considered. In any case, the extremal slopes are measured, and the buckling load is predicted according to (159) and (160). In cases where there are two possible values of λ_m, the one used is that leading to the lower load prediction.

In the minimum load prediction approach, the load location λ_m is such that $\bar{\theta}_m$ is maximized, thus minimizing the predicted buckling load.

The advantage of the first two techniques is that deflections, particularly when measured at specified locations (i.e., the load point), are more easily evaluated than a maximum slope whose location is unknown. The advantage of the third lies in the fact that for certain support configurations rigid-body displacements may inject uncertainties into deflection measurements, whereas in slope measurements one degree of freedom is dropped from consideration.

A final note is that the lateral load test provides a means of analytically estimating the buckling load of the elastically-restrained column. Since the calculation of the eigenvalue must require numerical techniques, since convergence is often very slow,

and since considerable care is sometimes required to be sure the eigenvalue obtained is the lowest, the test provides a quick analytical estimate of the buckling load to the person who does not have access to elaborate computing equipment, inasmuch as the lateral load analysis can all be done in closed form.

Page missing from thesis

CHAPTER V

CONCLUSIONS

The column is the logical starting point for research efforts, both past and present, in elastic stability; that it has received more attention than any other structural form is attested to by the number of papers published and by the space devoted to it here. One of the aims of the present research was to review, highlight, and evaluate the various experimental techniques that have been developed to study the effects of boundary restraint in column stability. An important result of the historical summary of end fixity experiments is that the engineer who intends to do column testing does not have to start from scratch in the design of end fixtures. He can read the review and critical comparison, decide on a general course of action, and obtain further details by consulting the papers referenced herein. If his interest is plates or shells, the bibliography serves as a starting point for a literature search.

Most of the effort in column end fixity work has been directed toward the development of devices to simulate a pin-end condition. It was demonstrated that fixtures which utilize sliding motions cannot work well in this regard. If, however, the sliding surfaces are separated by a film of oil under pressure, or by rollers or balls, such fixtures can perform quite satisfactorily. Other successful devices have utilized large bearing surfaces, at least one of which is curved,

that roll on one another. The main problem here is to keep the bearing stresses sufficiently small that the surfaces do not deform excessively or rupture under load. The best of these configurations has made use of a semi-cylinder rolling on a plane. The University of Washington device is an example of the successful treatment of the main design considerations; viz., the prevention of sideslip and the minimization of friction.

When both bearing surfaces are curved, and when both radii of curvature are small and have the same sign, we have a very well-known special case: the knife edge fixture. That this is a successful design is manifested by its wide use. Of course, the radii of curvature must be chosen such that bearing failure and slippage of the knife edge in the carrier do not occur.

It should be pointed out that in the knife edge device, as in many others, corrections must be made for effective length. Such an analysis was presented.

Whatever type of device the test engineer chooses to build, he does well to keep in mind the requirements for pin-end fixtures set forth so well by Templin:

1. There should be three degrees of freedom;

2. The device should possess as low a resistance to rotation as possible;

3. The method should be applicable to large total load systems;

4. Distortion should be minimal during use;

5. The device should apply either uniform axial loads or loads

with prescribed eccentricities;

6. It should be reasonable in cost, simple to install, and easy to maintain.

At this point it is useful to consider the relative purposes of analysis and experiment. Tests are carried out to discover what actually happens and to use that information to discover the fundamental laws governing the phenomenon. Analysis based on these laws is performed to predict future behavior in advance. If the predicted behavior is as yet unobserved, its occurrence must be regarded with some skepticism until it has been confirmed by tests. In short, experiment is the final arbiter of truth and fiction.

While it has been made quite clear that great ingenuity has been stimulated by the study of boundary effects, one can only conclude that much of the effort has been misdirected. That ideality is always held at arm's length by the laws of thermodynamics should be sufficient motivation to explore that which is, rather than attempting to verify that which cannot be. The necessity of dealing with the real world was emphasized by Salmon many years ago when he wrote: "The most pressing point for future research on the subject of columns is undoubtedly the degree of imperfection common in practical fixed ends; in short, what value of K should be assumed for such ends? A complete answer to this question is difficult, but at present the designer has no real data whatsoever regarding practical end conditions."

In order to study the behavior of columns of practical interest, it is evident that some type of non-destructive test is needed if the

test specimens are to have any destination other than the scrap heap. To date the only practical test method available has been the Southwell plot, but due to the danger of specimen destruction during sudden and unanticipated buckling, this approach does not meet all the requirements of a successful non-destructive test technique. Indeed, we may observe that any such test that predicts the behavior of a structure under destabilizing loads must use for a test environment some system of non-destabilizing forces.

The first class of non-destructive tests developed can be denoted by the term "P-delta approach." Here, the applicable prediction relation is

$$P_{cr}\left(\frac{\delta_m}{Q}\right) = \frac{\pi^2 L}{12(n_b)^2}\,, \tag{191}$$

where n_b is the number of inflection points in the deflected shape, L is the length of the beam, and (δ_m/Q) is the flexibility efficient associated with loads and deflections at the point of maximum lateral flexibility. If that point is at the end of the beam, n_b is unity; otherwise, $n_b = 2$. The relation gives a good approximation to the buckling load for lateral end restraint that is nearly ideal (zero or infinite restraint of lateral displacements at the end). The relation is not accurate for intermediate lateral end restraint, but the ease and simplicity of the test encourage its use whenever possible.

A second class of non-destructive tests is characterized by the term "P-theta approach" and the prediction relation

$$P_{cr}\left(\frac{\theta_m}{Q}\right) = \text{constant}, \tag{192}$$

where the load location, the measured slope, and the constant vary according to the specific test.

The first type of P-theta test uses the simplest possible load location criterion, with a prediction relation sufficiently involved to make the test work. This test was developed specifically for columns in which the lateral end restraint is non-ideal at one end; this is denoted the "weak" end and is characterized by $\mu = 1$. The procedure is as follows:

1. Load the beam at the mid-point, take the appropriate measurements, and compute the quanty

$$c^* = c(2-c) + 3.5\left(\frac{\bar{\theta}_{max}-\bar{\theta}_{min}}{|\bar{\theta}_m|} - 1\right)\left[1 + (34\bar{\theta}_1)^3\right]\left(\frac{R_1}{Q}\right)^2, \tag{193}$$

where

$$c = \frac{384}{5}\,\bar{\delta}_1\,|\,\bar{\theta}_1\,|, \tag{194}$$

and where

$\bar{\theta}_{max}$ = the greatest slope found between the load point and $\mu = 1$, taken positive

$\bar{\theta}_{min}$ = the least slope found in that interval, taken non-positive

$\bar{\theta}_{m}$ = the extremal slope having the greater magnitude

R_1/Q = the reaction at $\mu = 1$

$\bar{\theta}_{1}$ = the slope at $\mu = 1$

$\bar{\delta}_{1}$ = the deflection at $\mu = 1$,

all of the above quantities being non-dimensional ratios.

2. Calculate the first buckling load prediction by the relation

$$R\bar{\theta}_{m} = \frac{1}{4(1+c^*)} \tag{195}$$

3. With a concentrated load at $\lambda = 1$, measure the reaction at $\mu = 1$, in addition to the maximum slope, and compute the quantity

$$\hat{c} = \frac{1 - \left(\frac{R_1}{Q}\right)^{175(\bar{\theta}_m + .065)}}{1.00001 - \left(\frac{R_1}{Q}\right)^{500(\bar{\theta}_m + .00001)}} . \tag{196}$$

4. Calculate the second buckling load prediction by the relation

$$R\bar{\theta}_m = \frac{\hat{c}}{2} \ . \qquad (197)$$

The buckling load prediction is taken as the lesser of the two calculated loads.

The above procedure can be abbreviated in certain cases if the test engineer has some indication of how great the lateral restraint is. If at $\mu = 1$ the relative lateral support stiffness is less than 12, only the end load test (steps 3 and 4) is necessary. On the other hand, if the relative lateral stiffness is greater than 54, only the mid-point test suffices for all values of lateral restraint whenever the rotational restraint at $\mu = 1$ is greater than 10.

It is clear that the presence of the factor (R_1/Q) implies the measurement of a force in the support at $\mu = 1$. In a practical test this may not be possible, but the method can still be used if the test engineer is willing to accept as the price of added convenience the loss of some accuracy in the prediction of the buckling load. In this case, the factor $3.5(R_1/Q)^2$ in equation (193) must be replaced with come constant in the range .35 to .88, the lower part of the range being best for an end rotational restraint near zero and the upper part best for very high restraint. In the end load test, the quantity $\hat{c}$ is taken as a constant equal to unity.

If the reaction at $\mu = 1$ can be measured, this P-theta test is generally accurate to within 10 per cent. The only cases when this statement is not true occur when the end rotational restraint is near zero and the end relative lateral restraint is near 54; then the pre-

diction error can go as high as 27 per cent. However, the error falls off very rapidly as the boundary restraint varies from the maximum error-producing configuration.

The obvious disadvantage with this P-theta test is the complexity of the prediction relation factors (193) and (196), in addition to the problem of measuring the reaction at $\mu = 1$. In practice, this method would be used only when non-ideal lateral end restraint was present, and then only when all other tests broke down. In dealing with these non-ideal cases, however, this test does have the lowest maximum error.

The second type of P-theta test, by way of contrast, uses a simple prediction relation but somewhat more involved load location criteria. The prediction relation is

$$R\bar{\theta}_m = \frac{1}{4} , \tag{198}$$

where

$$\bar{\theta}_m = \frac{\bar{\theta}_{max} - \bar{\theta}_{min}}{2} , \tag{199}$$

and where the extremal slopes $\bar{\theta}_{max}$ and $\bar{\theta}_{min}$ can be located anywhere on the beam. The only distinguishing features of the members of this family of tests are the load location criteria.

The first of these criteria is known as the "maximum delta" rule, and the procedure is as follows:

1. Apply a single concentrated lateral load at some location λ and measure the deflection δ at the load point;

2. Vary the load location λ and repeat the above step until it is possible to draw a graph of λ versus δ;

3. λ_m is that λ for which the graph displays maximum δ;

4. Apply the lateral load at λ_m and measure the extremal slopes;

5. Calculate the buckling load according to equations (198) and (199).

The second of these criteria is the "maximum lambda-delta curvature" rule, and the procedure is identical to the above, except for step 3. When the end lateral restraint is high, λ_m is selected such that the negative curvature of the λ - δ is extremized. It is to be pointed out that the test is not particularly sensitive to errors in the choice of λ_m. For low values of end lateral restraint, the deflections due to an end load can be considerable, and in point of fact, the negative curvature region on the λ - δ plot can disappear altogether. In such cases, a load location λ_m at the weak end must also be considered. In situations in which there are two possible values of λ_m, the one used is that leading to the lower load prediction.

The third criterion is the "minimum load prediction" rule, and again the test procedure differs from that of the "maximum delta" criterion only in step 3. Here, the load location λ_m is such that $\bar{\theta}_m$ is maximized, thus minimizing the predicted buckling load.

The "maximum lambda-delta curvature" and "minimum load pre-

diction" criteria lead to results that are generally accurate to less than 10 per cent. The only difficulties to speak of arise when non-ideal lateral end restraint is encountered, and then only when the rotational restraint at the weak end is near zero and the lateral restraint there is in the neighborhood of 25 times the beam stiffness. In general, the performance of the "maximum delta" criterion is inferior to those of the other two rules.

It is important to note that in the second class of "P-theta" tests the extremal slopes are relative extrema and hence are located at inflection points, or points of zero moment. Since moment distributions for concentrated loads are piecewise linear, and since only one lateral load is applied at a time, a moment diagram is completely specified by moment measurements at four points. Thus, simple strain gage measurements may be used to determine extremal slope locations. Hence, the effort in comparing slopes for the "minimum load prediction" criterion is reduced to the same order of magnitude as the work in determining the location of maximum $\lambda - \delta$ curvature, particularly in situations where two possible values of λ_m exist for the "maximum lambda-delta curvature" criterion.

In the first class of "P-theta" tests, the slopes of interest may be absolute maxima due to the restriction of slope observation to one half of the beam. However, in this case it is only necessary to measure slopes at the load point and at $\mu = 1$, in addition to the above procedure, to obtain the maximum slopes.

It is also important to note that in all the "P-theta" load

prediction relations, the length L of the beam is not present. Quite often this merely means that there is one less measurement to make. However, in support configuration in which there are rigid carriers, we completely avoid the question of effective length, which as we have seen, can be fairly complicated. Furthermore, this feature may be of considerable importance in dealing with two-dimensional structures.

While primarily intended as practical non-destructive tests, the methods developed in this research can also be used by the analyst who needs a quick approximation to the buckling load of a column without resorting to numerical computation schemes. For his purposes, the "maximum lambda-dalta curvature" criterion is probably the most convenient due to the existence of a closed-form expression for $\bar{\delta}$ in terms of λ.

When a non-destructive test is needed for a structure of practical interest, probably the most straightforward and easily used is the "P-delta" approach if it applies; viz., if the lateral restraint is nearly ideal. Otherwise, the best procedure is likely the "maximum lambda-delta curvature" criterion or the "minimum load prediction" rule. If the beam support configuration is such that these tests could be suspected of unacceptable error, then the first class of "P-theta" test can be tried, and the lowest calculated buckling load used as a prediction. The combination of the two types of "P-theta" tests should produce good results since their high-error regions do not coincide.

A final observation is that in symmetric cases where the buckling load predictions from the "P-delta" and

load predictions from the "P-delta" and "P-theta" approaches are different, the corresponding errors are opposite in sign. Thus, in these cases it is possible to perform both tests and thereby obtain upper and lower bounds to the buckling load estimation.

That all these methods work so well is an indication that there is some general principle in solid mechanics that relates the eigenvalue problem to the behavior of structures under non-destabilizing load systems.

APPENDIX I

PARABOLICALLY-TAPERED BEAM

Computer Program

```
5  PRINT
10  PRINT "STRUBLE, 2/22/70, PARABOLICALLY-TAPERED
    BEAM"
20  PRINT
30  PRINT "LAMBDA","MU","DELTA","CALC D R","CALC
    T R"
40  PRINT "ABOVE FOR MAX DELTA.  SAME INFO THIS
    LINE FOR MAX CURVATURE"
45  PRINT "SAME INFO THIS LINE FOR MAX THETA CRITERION"
50  PRINT "ACTUAL R","   DELTA ERRORS FOR THE
    THREE CRITERIA"
55  PRINT "          THETA ERRORS FOR MAX DELTA,
    MAX CURV, MAX THETA"
60  PRINT
70  LET B=1/3
75  LET M1=0
80  LET Q=1
85  LET R=(17.79+17.88)*2/(3.14159↑2)
90  LET A=SQR(B)
100  DEF FNC(X)=.5*LOG((1+A*X)/(1-A*X))/A
110  DEF FND(X)=-LOG(SQR(1-(A*X)↑2))/(A↑2)
120  DEF FNE(X)=LOG((1+A*X)/SQR(1-(A*X)↑2))/A↑3-X/(A↑2)
130  LET R2=FNC(1)-2*FND(1)+FNE(1)
140  LET L=.55
150  GOSUB 700
160  LET D1=2*FNC(L)*(L-R1)+2*FND(L)*(R1-1)
190  LET L=L-D1/D2
200  IF ABS(D1/D2) <= 1.00000E-05 THEN 250
210  IF ABS(L-.5)<.5 THEN 150
220  IF M1=.7 THEN 570
230  LET M1=L=.7
240  GOTO 150
250  GOSUB 600
260  GOSUB 750
270  LET Q=2
280  LET A1=.55
290  LET B=.8
300  LET C=.1
310  LET G=0
320  FOR L=A1 TO B STEP C
```

```
330  LET G1=G
340  IF Q=2 THEN 380
350  GOSUB 600
360  LET G=T
370  GOTO 400
380  GOSUB 700
390  LET G=D2
400  IF ABS(G) <= ABS(G1) THEN 420
410  NEXT L
415  GOTO 570
420  IF C<1.00000E-05 THEN 470
430  LET A1=L-2*C
440  LET B=L
450  LET C=C/10
460  GOTO 310
470  LET L=L-C
480  GOSUB 600
490  GOSUB 750
500  IF Q=3 THEN 530
510  LET Q=3
520  GOTO 280
530  PRINT R,R[1],R[2],R[3]
540  PRINT " ",R[4],R[5],R[6]
550  PRINT
560  STOP
570  PRINT "NO SOLUTION"
580  STOP
600  REM THETA SUBROUTINE
610  LET R1=(L*FNC(L)-(L+1)*FND(L)+FNE(L))/R2
620  LET D=-R2*R1↑2+FNC(L)*L↑2-2*L*FND(L)+FNE(L)
630  LET U1=(R1-L)/(R1-1)
640  LET T1=(L-R1)*FNC(U1)+(R1-1)*FND(U1)
650  LET T2=-R1*FNC(1)+R1*FND(1)-FND(L)+L*FNC(L)
660  LET T=T1-T2
670  RETURN
700  REM D2 SUBROUTINE
710  LET R1=(L*FNC(L)-(L+1)*FND(L)+FNE(L))/R2
720  LET D2=2*R1*(L-1)/(1-(A*L)↑2)-2*(FNC(L)-FND(L))↑2/R2+2
     *FNC(L)
730  RETURN
750  REM PRINT SUBROUTINE
760  PRINT L,U1,D,1/(12*D),1/(2*T)
770  LET R[Q]=100*(1/(12*D)-R)/R
780  LET R[Q+3]=100*(1/(2*T)-R)/R
790  RETURN
999  END
```

APPENDIX II

PINNED-PINNED BEAM WITH INTERMEDIATE LATERAL SUPPORT

Analysis

Consider the pinned-pinned beam with intermediate lateral support shown in Figure 28c. The system is statically indeterminate; the unknown redundant R_5 can thus be found by the principle of the minimum of the total complementary potential. That potential is given by

$$\frac{W^*}{\frac{Q^2L^3}{EI}} = \frac{1}{2}\int_0^1 \left[\frac{M(\xi)}{QL}\right]^2 d\xi + \frac{\left(\frac{R_5}{Q}\right)^2 (EI)}{2k_5 L^3} \qquad \text{(II-1)}$$

$$= \int_0^{\frac{1}{2}} \left[\frac{M(\xi)}{QL}\right]^2 d\xi + \frac{\left(\frac{R_5}{Q}\right)^2}{2K_5},$$

since the structure is symmetric. The moment distribution $M(\xi)/QL$ is a function of the spring reaction coefficient R_5/Q and is given by

$$\frac{M(\xi)}{QL} = \begin{cases} \frac{1}{2}(1-R_5/Q)\xi & 0 \le \xi \le \frac{1}{2} \\ \frac{1}{2}(1-R_5/Q)(1-\xi) & \frac{1}{2} \le \xi \le 1 \end{cases} \qquad \text{(II-2)}$$

Substitution of (II-2) into (II-1) and integration gives

$$\frac{W^*}{\frac{Q^2L^3}{EI}} = \frac{1}{96}\left(1 - \frac{R_5}{Q}\right)^2 + \frac{\left(\frac{R_5}{Q}\right)^2}{2K_5} . \qquad \text{(II-3)}$$

The minimum principle is expressed by

$$\frac{\partial}{\partial\left(\frac{R_5}{Q}\right)}\left[\frac{W^*}{\frac{Q^2L^3}{EI}}\right] = 0. \qquad \text{(II-4)}$$

Carrying out the differentiation of (II-3) and solving for R_5/Q yields

$$\frac{R_5}{Q} = \frac{K_5}{K_5+48} , \qquad \text{(II-5)}$$

where K_5 is a relative spring stiffness defined by

$$K_5 = \frac{k_5L^3}{EI} . \qquad \text{(II-6)}$$

The load-point deflection is easily determined from the spring characteristic. We have

$$\bar{\delta} = \frac{\frac{\delta}{Q}}{\frac{L^3}{EI}} = \frac{\frac{\frac{R_5}{k_5}}{Q}}{\frac{L^3}{EI}} = \frac{\frac{R_5}{Q}}{\frac{k_5 L^3}{EI}} = \frac{\frac{R_5}{Q}}{K_5} = \frac{1}{K_5 + 48} \cdot \qquad \text{(II-7)}$$

The eigenvalue may be obtained from the differential equation, which is

$$EI \frac{d^4 w}{dx^4} + P \frac{d^2 w}{dx^2} = 0. \qquad \text{(II-8)}$$

A deflected shape that satisfies this equation is

$$w = L(B\xi + D \sin m_b \xi). \qquad \text{(II-9)}$$

Substitution of (II-9) into (II-8) gives

$$(m_b)^2 D \sin m_b \xi \left[(m_b)^2 \frac{EI}{L^3} - \frac{P}{L}\right] = 0, \qquad \text{(II-10)}$$

or

$$P = \frac{(m_b)^2 EI}{L^2} \cdot \qquad \text{(II-11)}$$

The value of m is of course obtained from the boundary conditions, which, in this case, are

$$w = \frac{d^2w}{dx^2} = 0 \qquad \xi = 0 \tag{II-12}$$

and

$$\left.\begin{aligned} &\frac{dw}{dx} = 0 \\ &\frac{k_5}{2} w = EI \frac{d^3w}{dx^3} \end{aligned}\right\} \quad \xi = \frac{1}{2} . \tag{II-13}$$

The conditions at $\xi = 0$ are automatically satisfied, and it remains to enforce the conditions at $\xi = 1/2$. The first of these requires that

$$B = - Dm_b \cos \frac{m_b}{2} . \tag{II-14}$$

The second mid-point condition results in the relation

$$D\left(\frac{K_5}{2}\right) \cos \frac{m_b}{2} \left\{ \tan \frac{m_b}{2} - \frac{m_b}{2} \left[1 - \frac{16}{K_5} \left(\frac{m_b}{2}\right)^2 \right] \right\} = 0 \tag{II-15}$$

A non-trivial solution exists when

$$\cos \frac{m_b}{2} = 0, \tag{II-16}$$

in which case we have $m = \pi$, or when

$$\tan \frac{m_b}{2} - \frac{m_b}{2}\left[1 - \frac{16}{K_5}\left(\frac{m_b}{2}\right)^2\right] = 0. \tag{II-17}$$

Since we are concerned with buckle shapes bounded by the first and second modes, it is clear that the limits on m are π and 2π, the latter corresponding to second mode (antisymmetric) buckling. In this range,

$$\tan \frac{m_b}{2} \leq 0 , \tag{II-18}$$

and thus (II-17) can be satisfied only when

$$1 - \frac{16}{K_5}\left(\frac{m_b}{2}\right)^2 \leq 0 , \tag{II-19}$$

or

$$K_5 \leq 16\pi^2. \tag{II-20}$$

It is apparent from the transcendental nature of equation (II-17) that numerical techniques must be employed to get the eigenvalue of the problem, and that singularities in the tangent function may lead to difficulties in this regard. An alternate approach is to use the Rayleigh-Ritz procedure from the outset. Accordingly, a suitable deflection assumption is

$$w = \sum_{\text{odd}}^{\infty} a_n \sin \frac{n\pi x}{L} , \qquad \text{(II-21)}$$

where the unknown coefficients are determined from the principle of the minimum of the total potential. That potential may be expressed as

$$W = \frac{EI}{2} \int_0^L \left(\frac{d^2w}{dx^2}\right)^2 dx + \frac{k_5}{2} (w)^2 \Big|_{x=L/2} - \frac{P}{2} \int_0^L \left(\frac{dw}{dx}\right)^2 dx. \qquad \text{(II-22)}$$

Substitution of (II-21) into (II-22) and performing the indicated operations results in

$$W = \frac{EI}{2} \sum_{\text{odd}}^{\infty} \left(\frac{n\pi}{L}\right)^4 a_n^2 \frac{L}{2} - \frac{P}{2} \sum_{\text{odd}}^{\infty} \left(\frac{n\pi}{L}\right)^2 a_n^2 \frac{L}{2} + \frac{k_5}{2} \sum_{\text{odd}}^{\infty} a_m \sin \frac{m\pi}{2} \sum_{\text{odd}}^{\infty} a_n \sin \frac{n\pi}{2},$$

where "odd" indicates summation over odd values only of the dummy index. The minimum principle may be written

$$\frac{\partial W}{\partial a_n} = 0, \quad n = 1,3,5, \ldots \tag{II-24}$$

Applied to equation (II-23), the result, after rearrangement, is

$$a_n = \frac{\frac{8}{4} K_5 \sin \frac{n\pi}{2}}{\frac{\pi}{n^2(R - 4n^2)}} \sum_{\text{odd}}^{\infty} a_m \sin \frac{m\pi}{2}, \quad n = 1,3,5, \ldots \tag{II-25}$$

where

$$R = \frac{P}{\frac{\pi^2 EI}{4L^2}} . \tag{II-26}$$

Multiplication of each side of (II-25) by $\sin \frac{n\pi}{2}$, summation over odd values of n, noting the interchangeability of dummy indices, and rearrangement, gives

$$\sum_{\text{odd } m}^{\infty} a_m \sin \frac{m\pi}{2} \left[1 - \frac{8}{\pi} K_5 \sum_{\text{odd } n}^{\infty} \frac{1}{n^2(R-4n^2)} \right] = 0. \tag{II-27}$$

Thus, for a non-trivial deflection function, we must require

$$1 - \frac{8}{\pi^4} K_5 \sum_{\text{odd } n}^{\infty} \frac{1}{n^2(R-4n^2)} = 0 \qquad \text{(II-28)}$$

and this is another characteristic equation.

Finally, the maximum slopes generated by the lateral mid-point load may be conveniently found by considering a pinned-pinned beam under a load equal to $R_5 - Q$, where R_5 is given by equation (II-5). It is thus clear than the extremal slopes are found at the beam ends, that the maximum and minimum slopes are equal in magnitude and opposite in sign, and that

$$\bar{\theta}_{max} = \frac{\frac{\theta_{max}}{Q}}{\frac{L^2}{EI}} = \frac{1 - \frac{R_5}{Q}}{16} . \qquad \text{(II-29)}$$

It is apparent from the nature of equation (II-28) that numerical techniques must be used in the computation of the buckling load, although it might be pointed out that very rapid convergence, on the order of $1/n^4$, would be expected. A two-point iteration technique for finding the root of (II-28) was developed, the details of which, along with the buckling load prediction, are contained in the following BASIC program.

Computer Program

```
10  PRINT
20  PRINT "STRUBLE, 10/16/69, BEAM WITH CENTRAL
    LATERAL SPRING"
30  PRINT
40  PRINT
50  PRINT "ACTUAL R","DELTA","THETA"
70  PRINT "D CALC R","T CALC R","D ERROR","T ERROR"
80  PRINT
90  PRINT
100  PRINT "K1 =";
110  INPUT K1
120  PRINT "FIRST GUESS =";
130  INPUT K
140  LET K=K-1.00000E-03
150  PRINT
160  LET P1=3.14159
170  LET R=D1=K
180  LET Q=1
190  LET S=0
200  FOR N=1 TO 1000 STEP 2
210  LET D=1/((R-4*N↑2)*N↑2)
220  LET S=S+D
230  IF ABS(D/S) <= 1.00000E-05 THEN 250
240  NEXT N
250  LET F=1-8*K1*S/P1↑4
260  IF Q#1 THEN 290
270  LET R=K+1.00000E-03
280  GOTO 420
290  LET H=K
300  LET K=R
310  LET R=(K-H*F/G)/(1-F/G)
320  IF ABS(R-10) <= 6 THEN 380
325  IF R<4 THEN 340
330  LET R=16
335  GOTO 380
340  PRINT "OVERFLOW"
345  LET D1=D1-1
350  LET K=D1
360  IF K<4 THEN 80
370  GOTO 170
380  IF ABS(R-K) <= 1.00000E-05 THEN 450
390  IF R#H THEN 420
400  PRINT "NON-CLOSING LOOP"
410  GOTO 345
420  LET G=F
430  LET Q=Q+1
440  GOTO 190
450  LET D=1/(K1+48)
```

```
460  LET T=1/16-K1/(16*(K1+48))
470  PRINT R,D,T
480  LET R8=1/(12*D)
490  IF R8 <= 16 THEN 510
500  LET R8=16
510  LET R9=1/(4*T)
520  IF R9 <= 16 THEN 540
530  LET R9=16
540  PRINT R8,R9,100*(R8-R)/R,100*(R9-R)/R
550  GOTO 80
999  END
```

APPENDIX III

BEAM WITH UNSYMMETRIC ROTATIONAL END RESTRAINT

General Analysis

Consider the uniform beam with unsymmetric rotational end restraint shown in Figure 28d. The system is statically indeterminate, but the unknown redundants can be found by the principle of the minimum of the total complementary potential. That potential is given by

$$W^* = \frac{Q^2L^3}{2EI}\int_0^1 \left[\frac{M(\xi)}{QL}\right]^2 d\xi + \frac{Q^2L^3}{2k_3}\left(\frac{M_o}{QL}\right)^2 + \frac{Q^2L^3}{2k_2}\left(\frac{M_1}{QL}\right)^2. \qquad \text{(III-1)}$$

Selecting for redundants the lateral reaction and the moment at the right end of the beam, the moment distribution due to a concentrated lateral load at $x = \lambda L$, or $\xi = \lambda$, is

$$\frac{M(\xi)}{QL} = \begin{cases} \dfrac{M_1}{QL} + \left(\dfrac{R_1}{Q}\right)(1-\xi) + \xi - \lambda & 0 \le \xi \le \lambda \\ \dfrac{M_1}{QL} + \left(\dfrac{R_1}{Q}\right)(1-\xi) & \lambda \le \xi \le 1 \end{cases} \qquad \text{(III-2)}$$

Static equilibrium considerations inply that

$$\frac{M_o}{QL} = \frac{M_1}{QL} + \frac{R_1}{Q} - \lambda . \qquad \text{(III-3)}$$

Substitution of (III-2) and (III-3) into (III-1) and integrating all terms in which a redundant appears gives

$$\frac{2EIW^*}{Q^2L^3} = \left(\frac{M_1}{QL}\right)^2 + \left(\frac{M_1}{QL}\right)\left(\frac{R_1}{Q}\right) + \frac{1}{3}\left(\frac{R_1}{Q}\right)^2 \qquad \text{(III-4)}$$

$$- \lambda^2 \left(\frac{M_1}{QL}\right) + 2\left(\frac{\lambda^3}{6} - \frac{\lambda^2}{2}\right)\left(\frac{R_1}{Q}\right) + \int_0^\lambda (\xi-\lambda)^2 d\xi$$

$$+ \frac{1}{K_3}\left(\frac{M_1}{QL} + \frac{R_1}{Q} - \lambda\right)^2 + \frac{1}{K_2}\left(\frac{M_1}{QL}\right)^2 ,$$

where

$$K_2 = \frac{k_2 L}{EI} \qquad \text{(III-5)}$$

and

$$K_3 = \frac{k_3 L}{EI} . \qquad \text{(III-6)}$$

The minimum principle is expressed by

$$\frac{\partial}{\partial\left(\frac{M_1}{QL}\right)}\left[\frac{2EIW^*}{Q^2L^3}\right] = 0 \qquad \text{(III-7)}$$

and

$$\frac{\partial}{\partial\left(\frac{R_1}{Q}\right)}\left[\frac{2EIW^*}{Q^2L^3}\right] = 0 \qquad \text{(III-8)}$$

Carrying out the differentiation of equation (III-4) results in

$$\left(\frac{M_1}{QL}\right)\left[2 + \frac{2}{K_3} + \frac{2}{K_2}\right] + \left(\frac{R_1}{Q}\right)\left[1 + \frac{2}{K_3}\right] = \lambda^2 + \frac{2\lambda}{K_3} \qquad \text{(III-9)}$$

and

$$\left(\frac{M_1}{QL}\right)\left[1 + \frac{2}{K_3}\right] + \left(\frac{R_1}{Q}\right)\left[\frac{2}{3} + \frac{2}{K_3}\right] = \lambda^2 - \frac{\lambda^3}{3} + \frac{2\lambda}{K_3} \qquad \text{(III-10)}$$

Solution of this system of equations by Cramer's rule, with simplification of the results, leads to

$$\frac{M_1}{QL} = \lambda K_2\left[\frac{\lambda K_3(\lambda-1) + 2(\lambda^2-1)}{K_2K_3 + 4K_2 + 4K_3 + 12}\right] \qquad \text{(III-11)}$$

and

$$\frac{R_1}{Q} = \lambda\left\{\frac{K_2[\lambda K_3(3-2\lambda) + 6 - 2\lambda^2] + 2\lambda K_3(3-\lambda) + 12}{K_2K_3 + 4K_2 + 4K_3 + 12}\right\}. \quad \text{(III-12)}$$

We are now in a position to obtain the load-point flexibility coefficient. In using the dummy load method, a suitable equivalent structure is a pinned-pinned beam laterally loaded with a unit force at $\xi = \lambda$. The deflection is given by the basis relationship

$$\delta = \frac{QL^3}{EI}\int_0^1\left[\frac{M(\xi)}{QL}\right]\left[\frac{M_d(\xi)}{L}\right]d\xi, \quad \text{(III-13)}$$

where $M_d(\xi)$ is the moment distribution due to the dummy load. We have

$$\frac{M_d(\xi)}{L} = \begin{cases} (1-\lambda)\xi & 0 \le \xi \le \lambda \\ \lambda(1-\xi) & \lambda \le \xi \le 1 \end{cases} \quad \text{(III-14)}$$

Substitution of (III-2) and (III-14) into (III-13) gives

$$\bar{\delta} = \frac{\frac{\delta}{Q}}{\frac{L^3}{EI}} = \int_0^\lambda\left\{\left[\frac{M_1}{QL} + \left(\frac{R_1}{Q}\right)(1-\xi)\right] + (\xi-\lambda)\right\}(\xi-\lambda\xi)d\xi + \quad \text{(III-15)}$$

$$+ \int_{\lambda}^{1} \left[\frac{M_1}{QL} + \left(\frac{R_1}{Q}\right)(1-\xi)\right](\lambda - \lambda\xi)d\xi .$$

The result, after considerable simplification, is

$$3(K_2K_3 + 4K_2 + 4K_3 + 12)\bar{\delta} = \lambda^2(3K_2 + 12) \qquad \text{(III-16)}$$

$$+ \lambda^3(K_2K_3 - 8K_2 + 4K_3 - 24)$$

$$+ \lambda^4(-3K_2K_3 + 6K_2 - 9K_3 + 12) + \lambda^5(3K_3)(K_2 + 2)$$

$$+ \lambda^6(-K_2K_3 - K_2 - K_3).$$

The slopes can be obtained in like fashion. In this case, the basic relationship is

$$\theta = -\frac{QL^3}{EI}\left[\frac{M(\xi)}{QL}\right]\left[\frac{M_a(\xi)}{L}\right]d\xi . \qquad \text{(III-17)}$$

A suitable equivalent structure is the same pinned-pinned beam, with the loading now a unit moment applied at the location $\xi = \mu$. The moment distribution due to the dummy load is given by

$$\frac{M_d(\xi)}{L} = \begin{cases} \frac{\xi}{L} & 0 \le \xi \le \mu \\ \frac{(\xi-1)}{L} & \mu \le \xi \le 1 \end{cases} . \qquad \text{(III-18)}$$

For $\mu \le \lambda$, substitution of (III-2) and (III-18) into (III-17) gives

$$\frac{\frac{\theta}{Q}}{\frac{L^2}{EI}} = \bar{\theta} = -\int_0^{\mu} \left[\frac{M_1}{QL} + \left(\frac{R_1}{Q}\right)(1-\xi) + \xi - \lambda\right]\xi d\xi \qquad \text{(III-19)}$$

$$-\int_{\mu}^{\lambda} \left[\frac{M_1}{QL} + \left(\frac{R_1}{Q}\right)(1-\xi) + \xi - \lambda\right](\xi-1)d\xi$$

$$-\int_{\lambda}^{1} \left[\frac{M_1}{QL} + \left(\frac{R_1}{Q}\right)(1-\xi)\right](\xi-1)d\xi .$$

Lumping together terms in the integrands enables us to write

$$\bar{\theta} = -\int_0^{1} \left[\frac{M_1}{QL} + \left(\frac{R_1}{Q}\right)(1-\xi)\right]\xi d\xi - \int_0^{\lambda} (\xi-\lambda)\xi d\xi \qquad \text{(III-20)}$$

$$+\int_{\mu}^{1} \left[\frac{M_1}{QL} + \left(\frac{R_1}{Q}\right)(1-\xi)\right]d\xi - \int_{\mu}^{\lambda} (\lambda-\xi)d\xi .$$

Integration leads to

$$\bar{\theta} = \left(\frac{M_1}{QL}\right)\left(\frac{1}{2} - \mu\right) + \left(\frac{R_1}{Q}\right)\left(\frac{1}{3} - \mu + \frac{\mu^2}{2}\right) + \frac{\lambda^3}{6} \qquad \text{(III-21)}$$

$$- \frac{\lambda^2}{2} + \mu\lambda - \frac{\mu^2}{2} .$$

The slope is extremized when its derivative with respect to μ vanishes; this occurs for

$$\mu_m = \frac{\lambda - \frac{M_1}{QL} - \frac{R_1}{Q}}{1 - \frac{R_1}{Q}} . \qquad \text{(III-22)}$$

For $\mu \leq \lambda$, the slope is given by

$$\bar{\theta} = - \int_0^{\lambda} \left[\frac{M_1}{QL} + \left(\frac{R_1}{Q}\right)(1-\xi) + \xi - \lambda\right]\xi d\xi \qquad \text{(III-23)}$$

$$- \int_{\lambda}^{\mu} \left[\frac{M_1}{QL} + \left(\frac{R_1}{Q}\right)(1-\xi)\right] \xi d\xi$$

$$- \int_{\mu}^{1} \left[\frac{M_1}{QL} + \left(\frac{R_1}{Q}\right)(1-\xi)\right](\xi-1)d\xi,$$

or

$$\bar{\theta} = -\int_0^1 \left[\frac{M_1}{QL} + \left(\frac{R_1}{Q}\right)(1-\xi)\right]\xi d\xi - \int_0^\lambda \xi(\xi-\lambda)d\xi \qquad \text{(III-24)}$$

$$+ \int_\mu^1 \left[\frac{M_1}{QL} + \left(\frac{R_1}{Q}\right)(1-\xi)\right]d\xi .$$

Integration gives

$$\bar{\theta} = \left(\frac{M_1}{QL}\right)\left(\frac{1}{2} - \mu\right) + \left(\frac{R_1}{Q}\right)\left(\frac{1}{3} - \mu + \frac{\mu^2}{2}\right) + \frac{\lambda^3}{6} . \qquad \text{(III-25)}$$

Extremization of the slope in this interval ($\mu \geq \lambda$) occurs when

$$\mu_m = \frac{\frac{M_1}{QL}}{\frac{R_1}{Q}} + 1 . \qquad \text{(III-26)}$$

The eigenvalue may be obtained from the differential equation, which is

$$EI \frac{d^4w}{dx^4} + P \frac{d^2w}{dx^2} = 0 \qquad \text{(III-27)}$$

A deflected shape that satisfies this equation is

$$w = A + B\xi + C \cos m_b \xi + D \sin m_b \xi. \qquad \text{(III-28)}$$

Substitution of (III-28) into (III-27) gives

$$\left(\frac{m_b}{L}\right)^2 \left[\left(\frac{m_b}{L}\right)^2 - \frac{P}{EI}\right] \left[C \cos m_b \xi + D \sin m_b \xi\right] = 0. \qquad \text{(III-29)}$$

For a non-trivial solution, we require

$$P = \frac{(m_b)^2 EI}{L^2} \quad . \qquad \text{(III-30)}$$

where the relationship between m_b and the boundary load ratio R is

$$(m_b)^2 = \frac{P}{\frac{EI}{L^2}} = \frac{\pi^2}{4} \frac{P}{\frac{\pi^2 EI}{4L^2}} = \frac{\pi^2}{4} R \; . \qquad \text{(III-31)}$$

The value of m is obtained from the boundary conditions, which are

$$\left.\begin{aligned} w &= 0 \\ \frac{EI}{L^2}\frac{d^2w}{d\xi^2} - \frac{k_3}{L}\frac{dw}{d\xi} &= 0 \end{aligned}\right\} \quad \xi = 0 \qquad \text{(III-32)}$$

$$\left.\begin{aligned} w &= 0 \\ \frac{EI}{L^2}\frac{d^2w}{d\xi^2} + \frac{k_2}{L}\frac{dw}{d\xi} &= 0 \end{aligned}\right\} \quad \xi = 1$$

Substitution of the deflection function (III-28) into the boundary conditions (III-32) yields four simultaneous linear homogeneous equations in A, B, C and D. For a non-trivial solution, we must require the determinant of the coefficients of A, B, C, and D to vanish, or

$$\begin{vmatrix} 1 & 0 & 1 & 0 \\ 0 & K_3 & (m_b)^2 & K_3 m_b \\ 1 & 1 & \cos m_b & \sin m_b \\ 0 & \frac{K_2}{m_b} - K_2 & \sin m_b - m_b \cos m_b & K_2 \cos m_b - m_b - m_b \sin m_b \end{vmatrix} = 0 \qquad \text{(III-33)}$$

Expansion of the determinant and simplification leads to the character-

istic equation:

$$m_b(K_2+K_3)(\sin m_b - m_b \cos m_b) + K_2K_3(2-2\cos m_b - m_b \sin m_b) + \qquad \text{(III-34)}$$

$$+ (m_b)^3 \sin m_b = 0$$

Although numerical techniques must be used to find the root of this equation, the terms are regular throughout the range of spring stiffnesses, making convergence fairly routine, particularly for the type of bisection scheme found in the computer program at the end of this appendix. At very high spring stiffnesses, some convergence difficulties can be encountered, but this is mitigated by slightly relaxing the convergence criterion, which leads to no detectable change in the calculated eigenvalue.

Symmetric Restraint

In the case of symmetric restraint, the spring stiffnesses K_2 and K_3 are equal, and thus we may obtain the results for this configuration by applying the conditions

$$K_2 = K_3 \qquad \text{(III-35)}$$

and

$$\lambda = \frac{1}{2} \qquad \text{(III-36)}$$

to the previous analysis. Substitution of (III-35) and (III-36) into (III-16) gives the expression for the flexibility coefficient:

$$\bar{\delta} = \frac{K_2 + 8}{192\ (K_2 + 2)}\ , \qquad \text{(III-37)}$$

or

$$\bar{\delta} = \frac{1}{48}\left[1 - \frac{3K_2}{4(K_2 + 2)}\right]. \qquad \text{(III-38)}$$

Expressions for the slopes can be obtained in like manner.

In calculating the buckling load, the appropriate characteristic equation could be obtained by substituting (III-35) into equation (III-34), and using the numerical techniques discussed previously; another approach, however, is the use of the Rayleigh-Ritz procedure. Accordingly, a suitable deflection assumption is

$$w = \sum_{\text{odd}}^{\infty} a_n \sin \frac{n\pi x}{L}\ , \qquad \text{(III-39)}$$

where the unknown coefficients a_n are determined from the principle of the minimum of the total potential. That potential may be expressed as

$$W = \frac{EI}{2}\int_0^L \left(\frac{d^2w}{dx^2}\right)^2 dx + 2\,\frac{k_2}{2}\left(\frac{dw}{dx}\right)^2\Bigg|_{x=0} - \frac{P}{2}\int_0^L \left(\frac{dw}{dx}\right)^2 dx \qquad \text{(III-40)}$$

Substitution of (III-39) into (III-40) and performing the indicated operations results in

$$W = \frac{EI}{2}\sum_{\text{odd}}^{\infty}\left(\frac{n\pi}{L}\right)^4 a_n^2\left(\frac{L}{2}\right) + k_2\sum_{\text{odd}}^{\infty}\left(\frac{m\pi}{L}\right) a_m \sum_{\text{odd}}^{\infty}\left(\frac{n\pi}{L}\right)a_n - \qquad \text{(III-41)}$$

$$- \frac{P}{2}\sum_{\text{odd}}^{\infty}\left(\frac{n\pi}{L}\right)^2 a_n^2\left(\frac{L}{2}\right) .$$

The minimum principle may be written

$$\frac{\partial W}{\partial a_n} = 0 , \quad n = 1,3,5, \ldots \qquad \text{(III-42)}$$

Applied to equation (III-41), the result, after rearrangement, is

$$a_n = \frac{16K_2L^2}{\pi^4}\,\frac{\left(\frac{n\pi}{L}\right)}{n^2(R-4n^2)}\sum_{\text{odd}}^{\infty}\left(\frac{m\pi}{L}\right) a_m , \quad n = 1,3,5, \ldots \qquad \text{(III-43)}$$

Multiplication of each side of (III-43) by $n\pi/L$, summation over odd values of n, noting the interchangeability of dummy indices, and rearrangement, gives

$$\sum_{\text{odd}}^{\infty} \left(\frac{m\pi}{L}\right) a_m \left[1 - \frac{16K_2}{\pi^2} \sum_{\text{odd}}^{\infty} \frac{1}{R-4n^2}\right] = 0 \ . \qquad \text{(III-44)}$$

Thus, for a non-trivial deflection function, we must require

$$1 - \frac{16K_2}{\pi^2} \sum_{\text{odd}}^{\infty} \frac{1}{R-4n^2} = 0 \ . \qquad \text{(III-45)}$$

an equation whose root is the buckling load ratio.

Zero Restraint at One End

Consider the beam of Figure 28d with the spring at the right end removed. This is another special case of the general configuration analyzed previously; it is mathematically characterized by the condition

$$K_2 = 0. \qquad \text{(III-46)}$$

Substitution of (III-46) into (III-16) gives the expression for the flexibility coefficient:

$$\bar{\delta} = \frac{\lambda^2}{K_3+3} + \frac{\lambda^3(K_3-6)}{3(K_3+3)} - \frac{\lambda^4(3K_3-4)}{4(K_3+3)} + \frac{\lambda^5 K_3}{2(K_3+3)} - \frac{\lambda^6 K_3}{12(K_3+3)}, \quad \text{(III-47)}$$

or

$$\bar{\delta} = \frac{1}{3}\left[1 - \frac{K_3}{K_3+3}\right]\lambda^2 + \left[\frac{K_3}{K_3+3} - \frac{2}{3}\right]\lambda^3 \quad \text{(III-48)}$$

$$+ \left[\frac{1}{3} - \frac{13K_3}{12(K_3+3)}\right]\lambda^4 + \frac{K_3}{2(K_3+3)}\lambda^5 - \frac{K_3}{12(K_3+3)}\lambda^6,$$

or

$$\bar{\delta} = \frac{1}{3}(\lambda^2 - 2\lambda^3 + \lambda^4) \quad \text{(III-49)}$$

$$- \frac{K_3}{12(K_3+3)}(4\lambda^2 - 12\lambda^3 + 13\lambda^4 - 6\lambda^5 + \lambda^6).$$

Again, slopes could be treated similarly.

With respect to calculation of the buckling load, we again have a choice of techniques. Again choosing the Rayleigh-Ritz procedure, a suitable deflection assumption is

$$w = \sum_{\text{all}}^{\infty} a_n \sin \frac{n\pi x}{L} , \qquad \text{(III-50)}$$

where the notation "all" indicates inclusion of even values of the dummy index in the summation, this being necessitated by the lack of symmetry in the problem. The total potential is given by

$$W = \frac{EI}{2} \int_0^L \left(\frac{d^2w}{dx^2}\right) dx + \frac{k_3}{2} \left(\frac{dw}{dx}\right)^2 \Bigg|_{x=0} - \frac{P}{2} \int_0^L \left(\frac{dw}{dx}\right)^2 dx . \qquad \text{(III-51)}$$

Substitution of (III-50) into (III-51) and performing the indicated operations results in

$$W = \frac{EI}{2} \sum_{\text{all}}^{\infty} \left(\frac{n\pi}{L}\right)^4 a_n^2 \left(\frac{L}{2}\right) + \frac{k_3}{2} \sum_{\text{all}}^{\infty} \left(\frac{m\pi}{L}\right) a_m \sum_{\text{all}}^{\infty} \left(\frac{n\pi}{L}\right) a_n - \frac{P}{2} \sum_{\text{all}}^{\infty} \left(\frac{n\pi}{L}\right)^2 a_n^2 \left(\frac{L}{2}\right) . \qquad \text{(III-52)}$$

The minimum principle,

$$\frac{\partial W}{\partial a_n} = 0, \quad n = 1,2,3,4, \ldots \qquad \text{(III-53)}$$

applied to equation (III-52) leads to

$$a_n = \frac{8K_3L^2}{\pi^4} \frac{\left(\frac{n\pi}{L}\right)}{n^2(R-4n^2)} \sum_{all}^{\infty} \left(\frac{m\pi}{L}\right) a_m , \qquad n = 1,2,3,4, \ . \ . \ \text{(III-53)}$$

Multiplication of each side of (III-53) by $n\pi/L$, summation over all values of n, noting the interchangeability of dummy indices, and rearrangement, gives

$$\sum_{all}^{\infty} \left(\frac{m\pi}{L}\right) a_m \left[1 - \frac{8K_3}{\pi^2} \sum_{all}^{\infty} \frac{1}{R-4n^2}\right] = 0. \qquad \text{(III-54)}$$

Thus, for a non-trivial deflection function, we require

$$1 - \frac{8K_3}{\pi^2} \sum_{all}^{\infty} \frac{1}{R-4n^2} = 0, \qquad \text{(III-55)}$$

and this is the equation whose root is the buckling load.

Computer Program

```
1   DIM D[15]
5   PRINT
10   PRINT "STRUBLE, 1/17/70, UNSYMMETRICAL ROTATIONAL
     RESTRAINT"
15   PRINT
20   PRINT
25   PRINT "LAMBDA","FIRST MU","SECOND MU","CALC
     D R","CALC T R"
30   PRINT "ABOVE FOR MAX DELTA.  SAME INFO THIS
     LINE FOR MAX CURVATURE"
35   PRINT "SAME INFO THIS LINE FOR MAX THETA APPROACH"
40   PRINT "ACTUAL R","    DELTA ERRORS FOR THE
     THREE APPROACHES"
45   PRINT "THETA ERRORS FOR MAX DELTA, MAX CURV,
     MAX THETA APPROACHES"
50   LET B[1]=1
55   LET B[2]=2
60   LET B[3]=4
65   LET D[1]=0
70   FOR Y=1 TO 4
75   FOR X=1 TO 3
80   LET D[X+1+3*(Y-1)]=B[X]*10↑(Y-2)
85   NEXT X
90   NEXT Y
92   LET D[14]=1000
94   LET D[15]=1.00000E+09
96   FOR X=1 TO 15
98   FOR Y=1 TO 15
100   LET K2=D[X]
101   LET K3=D[Y]
102   IF K2+K3=0 THEN 485
103   IF K3>K2 THEN 485
104   PRINT
105   PRINT
106   PRINT "K2, K3 =    ";K2;K3
110   LET C1=K2*K3+4*K2+4*K3+12
115   LET A[1]=3*K2+12
120   LET A[2]=K2*K3-8*K2+4*K3-24
125   LET A[3]=-3*K2*K3+6*K2-9*K3+12
130   LET A[4]=3*K3*(K2+2)
135   LET A[5]=-K2*K3-K2-K3
140   LET L=.5
145   LET Q1=0
150   GOSUB 500
155   LET L[1]=L
160   LET Q1=2
165   GOSUB 500
170   LET L[2]=L
```

```
175  LET A=.3
180  LET B=.7
185  LET C=.1
190  LET T=0
195  FOR L=A TO B STEP C
200  LET G1=T
205  GOSUB 625
210  IF T<G1 THEN 220
215  NEXT L
220  IF C<1.00000E-05 THEN 245
225  LET A=L-2*C
230  LET B=L
235  LET C=C/10
240  GOTO 190
245  LET L[3]=L-C
250  FOR Z=1 TO 3
255  LET L=L[Z]
260  LET Q=0
265  GOSUB 550
270  GOSUB 625
275  LET R[Z]=3*C1/(12*S)
280  LET R[Z+3]=1/(4*T)
285  PRINT L[Z],U1,U2,R[Z],R[Z+3]
290  NEXT Z
295  LET Q=0
300  LET C=.1*R[6]
305  LET A=(.8+Q/10)*R[6]
310  LET B=(1.22-Q/10)*R[6]
315  LET F=0
317  LET Q1=0
320  FOR R=A TO B STEP C
325  LET G=F
330  GOSUB 700
335  IF Q1=0 THEN 348
340  IF F=0 THEN 470
345  IF SGN(G)#SGN(F) THEN 365
348  LET Q1=Q1+1
350  NEXT R
351  IF Q=1 THEN 355
352  LET Q=1
353  LET C=C/10
355  GOTO 305
356  PRINT "NO SOLUTION"
360  GOTO 485
365  LET R=(F*(R-C)-G*R)/(F-G)
367  IF ABS(R-10)>6.5 THEN 355
370  IF ABS(C) <= 1.60100E-04 THEN 470
375  LET G=F
380  GOSUB 700
385  IF F=0 THEN 470
```

```
390  LET C=C*(-1)↑(1.5-.5*SGN(F/G))*10↑(Q-2)
395  LET A=R-(Q+1)*C
400  LET B=R+(Q+1)*C
405  GOTO 315
470  LET R=4*(M/3.14159)↑2
475  PRINT R,100*(R[1]-R)/R,100*(R[2]-R)/R,100*(R[3]-R)/R
480  PRINT " ",100*(R[4]-R)/R,100*(R[5]-R)/R,100*(R[6]-R)/R
485  NEXT Y
490  NEXT X
500  REM MAXIMIZING SUBROUTINE
505  LET Q=Q1+1
510  GOSUB 550
515  LET S0=S
520  LET Q=Q1+2
525  GOSUB 550
530  LET L=L-S0/S
535  IF ABS(S0/S)<1.00000E-05 THEN 545
540  GOTO 505
545  RETURN
550  REM EVALUATING SUBROUTINE
555  LET S=0
560  FOR I=1 TO 5
565  LET C[I]=1
570  FOR J=1 TO Q
575  LET C[I]=C[I]*(I-J+2)
580  NEXT J
585  LET S=S+C[I]*A[I]*L↑(I+1-Q)
590  NEXT I
595  RETURN
625  REM THETA SUBROUTINE
630  LET R1=L*(K2*(L*K3*(3-2*L)+6-2*L↑2)+2*L*K3*(3-L)+12)/C
     1
635  LET M1=L*K2*(L*K3*(L-1)+2*(L↑2-1))/C1
640  LET U1=(L-M1-R1)/(1-R1)
645  LET T1=M1*(.5-U1)+R1*(1/3-U1+.5*U1↑2)+(L↑3)/6-.5*L↑2+U
     1*L-.5*U1↑2
650  LET U2=1+M1/R1
655  LET T2=M1*(.5-U2)+R1*(1/3-U2+.5*U2↑2)+(L↑3)/6
660  LET T=(T1-T2)/2
665  RETURN
700  REM CHARACTERISTIC EQUATION
705  LET M=.5*3.14159*SQR(R)
710  LET F=M*(K2+K3)*(SIN(M)-M*COS(M))+SIN(M)*M↑3
715  LET F=F+K2*K3*(2-2*COS(M)-M*SIN(M))
720  RETURN
999  END
```

APPENDIX IV

COMPUTER PROGRAM FOR EVALUATING THE MAXIMUM LAMBDA-DELTA CURVATURE CRITERION

```
 10  REM PGM PREDICTS BUCK. LOAD WITH MAX. DELTA-LAMBDA
     CURVATURE
 15  PRINT
 20  PRINT "STRUBLE, 10/6/69, ELASTICALLY-RESTRAINED
     BEAM, MAX. CURV."
 30  PRINT
 40  PRINT
 45  PRINT "REMARKS"
 50  PRINT "LAMBDA","REACTION","MOMENT","POS. MU","NEG.
     MU"
 60  PRINT "MAX THETA","MIN THETA","ACTUAL R","CURV
     CALC R","ERROR"
 70  PRINT "END THETA","END CALC R","ERROR","MIN
     ERROR"
 80  PRINT
 90  PRINT
100   PRINT "K1,K2 =";
110   INPUT K1,K2
120   PRINT "FIRST GUESS =";
130   INPUT K
135   LET K=K-1.00000E-03
140   GOTO 600
150   PRINT
155   LET Q2=0
160   LET A[1]=(K1*K2+12*K2+4*K1+12)/3
165   LET A[2]=-(K1*K2+3*K1+3*K2)
170   LET A[3]=K1*(K2+2)
175   LET A[4]=-K1*(K2+1)/3
180   LET Q=2
185   GOSUB 425
190   LET Q=3
195   GOSUB 425
200   LET L=(L+L1)/2
202   LET Q1=0
205   GOSUB 550
210   LET S1=S
215   LET Q=4
220   GOSUB 550
225   LET L=L-S1/S
230   LET Q=3
235   IF ABS(L-.5) <= .5 THEN 270
```

```
240  IF Q1#0 THEN 260
245  LET Q1=1
250  LET L=L+.5*S1/S
255  GOTO 205
260  PRINT "OUT OF BOUNDS"
265  GOTO 80
270  IF ABS(S1/S) >= 1.00000E-05 THEN 202
275  LET R1=(L↑2)*K1*((3-2*L)*K2+6-2*L)/(3*A[1])
280  LET M=(L↑2)*K2*(6-(1-L)*K1)/(3*A[1])
282  IF Q2=1 THEN 305
285  IF Q=2 THEN 300
287  LET Q=2
290  GOSUB 550
292  IF S <= 0 THEN 315
295  PRINT "POS. MAX. CURVATURE, L =";L
300  LET L=Q2=1
302  GOTO 275
305  LET U2=T2=0
310  GOTO 330
315  PRINT "NEG. MAX. CURVATURE"
320  LET U2=1+M/R1
322  IF U2>1.00001 THEN 305
325  LET T2=.5*L↑2-R1*(U2-.5*U2↑2)-M*U2
330  LET U1=(L-R1-M)/(1-R1)
335  LET T1=L*U1-.5*U1↑2-R1*(U1-.5*U1↑2)-M*U1
340  IF Q1=2 THEN 370
345  LET R3=.5/(T1-T2)
350  PRINT L,R1,M,U1,U2
355  PRINT T1,T2,K,R3,100*(R3-K)/K
360  LET Q=Q1=2
365  GOTO 275
370  LET R5=.5/(T1-T2)
375  PRINT T1,R5,100*(R5-K)/K,
380  IF R3 <= R5 THEN 390
385  LET R3=R5
390  PRINT 100*(R3-K)/K
400  GOTO 80
425  LET A=.45
427  LET B=1
430  LET Q1=0
435  LET C=.1
437  LET L=A
440  GOSUB 550
445  FOR L=A+C TO B STEP C
450  LET S1=S
455  LET L1=L
460  GOSUB 550
465  IF SGN(S1)#SGN(S) THEN 545
470  NEXT L
475  IF Q1=1 THEN 495
480  LET Q1=1
```

```
465  LET C=C/10
490  GOTO 437
495  IF A=5.000000E-02 THEN 510
500  LET A=5.000000E-02
502  LET B=.55
505  GOTO 430
510  IF Q=2 THEN 530
515  PRINT "NO ZERO THIRD DERIVATIVE"
520  LET Q=2
525  GOTO 535
530  PRINT "NO INFLECTION POINTS"
535  LET L=1
540  GOTO 275
545  RETURN
550  LET S=0
555  FOR I=1 TO 4
560  LET C[I]=1
565  FOR J=1 TO Q
570  LET C[I]=C[I]*(I-J+3)
575  NEXT J
580  LET S=S+C[I]*A[I]*L↑(I+2-Q)
585  NEXT I
590  RETURN
600  LET A=32*K1/3.14159↑4
605  LET B=8*K2/3.14159↑2
610  LET C=256*K1*K2/3.14159↑6
615  LET R=D1=K
620  LET Q=1
625  LET Q1=1
630  GOSUB 850
635  LET S1=S
640  LET Q1=2
645  GOSUB 850
650  LET S2=S
655  LET Q1=3
660  GOSUB 850
670  LET F=1+A*S+B*S1+C*(S*S1-S2↑2)
680  IF Q#1 THEN 720
690  LET R=K+1.00000E-03
710  GOTO 760
720  LET H=K
730  LET K=R
740  LET R=(K-H*F/G)/(1-F/G)
742  IF ABS(R-9)<8 THEN 750
744  PRINT "OVERFLOW"
745  LET D1=D1-1
746  LET K=D1
747  IF K<1 THEN 80
748  GOTO 615
750  IF ABS(R-K) <= 1.00000E-04 THEN 790
752  IF ABS(R-H) >= 1.00000E-05 THEN 760
```

```
754  PRINT "NON-CLOSING LOOP"
756  GOTO 745
760  LET G=F
770  LET Q=Q+1
780  GOTO 625
790  LET K=R
800  GOTO 150
850  LET S=0
860  FOR I=1 TO 1000 STEP 2
920  LET D=(((-1)↑(I/2+3/2))↑(Q1-1))/((I↑2-R)*I↑(Q1-1))
930  LET S=S+D
940  IF ABS(D/S) <= 1.00000E-05 THEN 960
950  NEXT I
960  RETURN
999  END
```

APPENDIX V

COMPUTER PROGRAM FOR EVALUATING THE MINIMUM LOAD PREDICTION CRITERION

```
10  REM PGM PREDICTS BUCK. LOAD WITH LOAD AT MIN
    PREDICTION LOCATION
20  PRINT
30  PRINT "STRUBLE, 9/30/69, ELASTICALLY-RESTRAINED
    BEAM"
40  PRINT
50  PRINT
60  PRINT "REMARKS"
70  PRINT "LAMBDA","REACTION","MOMENT","1 MU 1","1
    MU 2"
80  PRINT "1 THETA MAX","1 THETA MIN","1 CALC
    R","ERROR"
90  PRINT "REACTION","MOMENT","2 THETA MAX","ERROR","MIN
    ERROR"
100  PRINT
110  PRINT
120  PRINT "K1, K2 =";
130  INPUT K1,K2
140  PRINT "BUCK. LOAD =";
150  INPUT K
170  PRINT
175  LET D=K1*K2+12*K2+4*K1+12
180  LET A=Q1=0
185  LET C=.1
190  LET B=1
195  LET G=0
200  FOR L=A TO B STEP C
205  LET G1=G
210  GOSUB 450
215  IF G<G1 THEN 230
220  NEXT L
225  GOTO 260
230  IF Q1=1 THEN 250
235  LET L=L-C
240  GOSUB 450
245  GOTO 260
250  PRINT "1 REL MAX"
255  GOTO 100
260  IF Q1=1 THEN 425
265  IF C<1.00000E-05 THEN 330
```

```
270  IF L <= 1.00000E-03 THEN 295
275  IF L >= .999 THEN 310
280  LET A=L-C
285  LET B=L+C
290  GOTO 320
295  LET A=0
300  LET B=C
305  GOTO 320
310  LET A=1-.9*C
315  LET B=1
320  LET C=C/10
325  GOTO 195
330  LET G2=G
335  IF Q#0 THEN 350
340  PRINT "REL MAX"
345  GOTO 385
350  IF Q#1 THEN 365
355  PRINT "ABS MAX"
360  GOTO 390
365  IF Q#2 THEN 380
370  PRINT "U2 > 1"
375  GOTO 385
380  PRINT "POS. T2"
385  LET Q1=1
390  PRINT L,R1,M,U1,U2,T1,T2,1/G2,100*(1/G2-K)/K
395  IF Q1=0 THEN 415
400  LET A=.99
405  LET C=1.00000E-02
410  GOTO 190
415  PRINT "1 ABS MAX"
420  GOTO 100
425  IF G2>G THEN 435
430  LET G2=G
435  PRINT R1,M,1/G,100*(1/G-K)/K,100*(1/G2-K)/K
440  GOTO 100
450  LET R1=(L↑2)*K1*((3-2*L)*K2+6-2*L)/D
455  LET M=(L↑2)*K2*(6-(1-L)*K1)/D
460  LET U1=(L-R1-M)/(1-R1)
465  LET T1=L*U1-.5*U1↑2-R1*(U1-.5*U1↑2)-M*U1
470  IF L >= .999 THEN 505
472  IF R1<1.00000E-06 THEN 515
475  LET U2=1+M/R1
480  IF U2>1.00001 THEN 515
485  LET T2=.5*L↑2-R1*(U2-.5*U2↑2)-M*U2
490  IF T2>0 THEN 525
495  LET Q=0
500  GOTO 535
505  LET Q=1
510  GOTO 530
515  LET Q=2
520  GOTO 530
```

```
525   LET Q=3
530   LET U2=T2=0
535   LET G=2*(T1-T2)
540   RETURN
999   END
```

BIBLIOGRAPHY

1. Salmon, E. H., A Treatise on the Strength and Design of Compressive Members, Henry Frowde and Hodder and Stoughton, London, 1921.

2. Euler, Leonard, "Sur la Force Des Colonnes," Memoria de l' Academia de Berlin, annee 1757, t. xiii, p. 242.

3. Young, T., A Course of Lectures on Natural Philosophy and the Mechanical Arts, 1st. ed., Vol. II, Sect. IX, London, 1807.

4. Ayrton, W. E., and Perry, John, "On Struts," The Engineer, 62, 1886, pp. 464-465, and 513-515.

5. Southwell, R. V., "On the Analysis of Experimental Observations in Problems of Elastic Stability," Proceedings of the Royal Society, London, Series A, 135, 1932, pp. 601-616.

6. Hodgkinson, Eaton, "Experimental Observations on the Strength of Pillars of Cast Iron and Other Materials," Philosophical Transactions of the Royal Society, Pt. II, 1840, p. 385.

7. Watertown Arsenal, "Reports on the Tests of Metals," 188-1885.

8. Christie, James, "Experiments on Wrought Iron Struts," Transactions of the American Society of Civil Engineers, Vol. XIII, 1884, p. 85.

9. Bauschinger, "Zerknickungs-Versuche," Mitteilung an das Mechanische-Technologie Laboratorium, Munchen, Heft 15, Mitteilung XVII, 1887, p. 11.

10. Tetmajer, "Die Gesetze der Knickungs und der Zusammeng-Esetzten Druckfestigkeit der Technisch Wichtigsten Baustoffe," Mitteilung der Material Anstalt auf Schweizer Polytechnikum in Zurich, Heft 4, 1890, Heft 8, 1896.

11. Lilly, "The Strength of Solid, Cylindrical, Round-Ended Columns," Report of the British Association, 1908, see Engineering, Sept. 18, 1908.

12. Lilly, "Eccentrically Loaded Columns, Proceedings of the Institute of Civil Engineers, Vol. CIXXXI, 1910, p. 460.

13. von Kármán, "Untersuchungen Über Knickfestigkeit," Mitteilung

und Forschungsareiten, Vol. d, 1, 1910, Heft 81.

14. "Steel Column Research," Second Progress Report of the Special Committee, Transactions of the American Society of Civil Engineers, Vol. 95, Paper No. 1789, 1931, pp. 1152-1172.

15. Osgood, William R., "Column Strengths of Tubes Elastically Restrained Against Rotation at the Ends," National Advisory Committee for Aeronautics Technical Report 615, 1938.

16. Barlow, Peter, "A Fixture for Obtaining Pin-Ended Conditions in Column Testing," Journal of the Aeronautical Sciences, Vol. 7, No. 2, Dec., 1939, pp. 72-74.

17. Barlow, Peter, "The Column Strength of Closed Thin-Walled Sections of 18-8 Stainless Steel," Journal of the Aeronautical Sicences, 1941, pp. 151-161.

18. Templin, R. L., "Hydraulically Supported Spherically Seated Compression Testing Machine Platen," Proceedings of the American Society for Testing and Materials, Vol. 42, 1942, pp. 968-976.

19. Goldberg, J. E., and Lenzen, K. H., "Roller Fixtures for Pin-Ended Columns," Proceedings of the Society for Experimental Stress Analysis, Vol. XVI, No. 1, 1959.

20. Timoshenko, S., Theory of Elasticity, McGraw-Hill Book Company, New York, 1934.

21. Estuar, F. R., and Tall, Lambert, "Testing of Pinned-End Steel Columns," Test Methods for Compression Members, American Society for Testing and Materials Special Technical Publication 419, 1967, p. 80.

22. Huber, A. W., "Fixtures for Testing Pin-Ended Columns," American Society for Testing and Materials Bulletin No. 234, Dec., 1958.

23. Adams, and Galambos, T. V., "Testing Techniques to Study the Inelastic Behavior of Steel Members," Test Methods for Compression Members, ASTM STP 419, 1967, p. 149.

24. Beedle, L. S., Ready, J. A., and Johnston, B. G., "Tests on Columns Under Combined Thrust and Moment," Proceedings of the Society for Experimental Stress Analysis, Vol. 8, 1950, pp. 109-132.

25. Schuman, L., and Back, G., "Strength of Rectangular Flat Plates Under Edge Compression," National Advisory Committee for Aeronautics Technical Report 356, 1930.

26. Cox, H. L., "Buckling of Thin Plates in Compression," Aeronautical Research Council Reports and Memoranda, No. 1551, London, 1933.

27. Cox, H. L., and Clenshaw, W. J., "Compression Tests on Curved Plates of Thin Sheet Duralumin," Aero. Res. Council. Rep. and Mem., No. 1894, London, 1941.

28. Cox, H. L., Thurston, F. R., and Coleman, E. P., "Compressive Tests on Seven Panels of Monocoque Construction," Aero. Res. Coun. Rep. and Mem., No. 2042, London, 1945.

29. Welter, G., "Curved Aluminum Alloy Sheets in Compression for Monocoque Constructions," Journal of the Aeronautical Sciences, July, 1945.

30. Hoff, N. J., and Mautner, S. E., "The Buckling of Sandwich-Type Panels," Journal of the Aeronautical Sciences, July, 1945.

31. Schuette, E. H., "Buckling of Curved Sheets in Compression and its Relation to the Secant Modulus," Journal of the Aeronautical Sciences, January, 1948.

32. Hoff, N. J., Boley, B. A., and Coan, J. M., "The Development of a Technique for Testing Stiff Panels in Edgewise Compression," Proceedings of the Society for Experimental Stress Analysis, Vol. V., No. 2, 1948.

33. Farrar, D. J., "Investigation of Skin Buckling," Aero. Res. Coun. Rep. and Mem., No. 2652, London, 1953.

34. Yamaki, N., "Experiments on the Postbuckling Behavior of Square Plates Loaded in Edge Compression," American Society of Mechanical Engineer, Transactions, Journal of Applied Mechanics, 83, June,

35. Chang, C. C., and Timmons, M. J., "Compression Tests of Sandwich Panels with Facings at Different Temperatures," Proceedings of the Society for Experimental Stress Analysis, Vol. XIX, No. 2, 1962.

36. Schlack, A. L., "Elastic Stability of Pierced Square Plates," Proceedings of the Society for Experimental Stress Analysis, Vol. XXI, No. 1, 1964.

37. Benson, A. S., and Mayers, J., "General Instability and Face Wrinkling of Sandwich Plates, Unified Theory and Applications," American Institute of Astronautics and Aeronautics Journal, Vol. 5, No. 4, pp. 729-739, April, 1967.

38. Nachbar, W., and Hoff, N. J., "On Edge Buckling of Axially Compressed Circular Cylindrical Shells," Quarterly of Applied

Mathematics, Vol. 20, p. 267, 1962.

39. Hoff, N. J., and Rehfield, L. W., "Buckling of Axially Compressed Circular Cylindrical Shells at Stresses Smaller than the Classical Critical Value," American Society of Mechanical Engineers, Transaction, Journal of Applied Mechanics, Vol. 32, p. 533, 1965.

40. Fischer, G.,"Über den Einfluss der Gelenkigen Lagerung auf die Stabilitat Dunnwandiger Kreiszylinderschalen Unter Axiallast und Innendruck," Zeitschrift fur Flugwissenschaft, Vol. 11, No. 3, p. 111, 1963.

41. Stein, M., "The Effect on the Buckling of Perfect Cylinders of Prebuckling Deformations and Stresses Induced by Edge Support," National Aeronautics and Space Administration Technical Note TN-D-2537, December 1964.

42. Babcock, C. D., and Sechler, E. E., "The Effect of End Slopes on the Buckling Stress of Cylindrical Shells,"NASA TN-D-2537, December 1964.

43. Love, A. E. H., The Mathematical Theory of Elasticity, 4th Edition, Dover Publications, New York, 1944, p. 605.

44. Southwell, R. V., "On the Collapse of Tubes by External Pressure," Philosophical Magazine, Series 6, Vol. 25, p. 687, 1913.

45. Wagner, Herbert, "Remarks on Airplane Struts and Girders Under Compressive and Bending Stresses," National Advisory Committee for Aeronautics Technical Memorandum No. 500, 1929.

46. Engesser, F.,"Über die Knickfestigkeit von Stäben Veränderlichen Trägheitsmomentes," Zeitschrift des Österreich, Ingenieur-und Architectur-Vereines, Vol. 61, p. 544, 1909.

47. Nater, H., "Knickung Elastisch Eingespannter Stäbe," Schweizerische Bauzeitung, Bd. 71, p. 215, May,1918.

48. Usinger, P., "Beitrage zur Knicktheorie," Der Eisenbau, Bd. 9, p. 169, August, 1918 .

49. Leduc, S., "Contribution A L'Étude des Poutres Prismatiques," Services Techniques de l'Aeronautique, Bulletin Technique No. 60, p. 43, June, 1929.

50. Bleich, F., "Theorie und Berechnung der Eisernen Brucken," Julius Springer, Berlin, 1924, and "Die Knickfestigkeit Elasticher Stabverbindungen," Der Eisenbau, Bd. 10, p. 27, February, 1919.

51. Zimmermann, H., Knickfestigkeit der Stabverbindungen, Wilhelm

Ernst und Sohn, Berlin, 1925.

52. Prager, W., "The Buckling of an Elastically Encastred Strut," Journal of the Royal Aeronautical Society, Vol. 49, No. 311, pp. 833-834, November, 1936.

53. Osgood, W. R., "Contribution to the Design of Compression Members in Aircraft," National Bureau of Standards Journal of Research, Vol. 13, No. 1, pp. 157-160, July, 1934.

54. Rein, W., Versuche zur Ermittlung der Knickspannungen fur Verschiendene Baustrahle, Julius Springer, Berlin, 1934.

55. Tuckerman, L. B., "Heterostatic Loading and Critical Astatic Loads," National Bureau of Standards Research Paper RP-1163, 1939.

56. Horton, W. H., Cundari, F. L., and Johnson, R. W., "The Analysis of Experimental Data Obtained from Stability Studies on Elastic Column and Plate Structures," Israel Journal of Technology, Vol. 5 No. 1-2, pp. 104-113, 1967.

57. Horton, W. H., and Cundari, F. L., "Applicability of the Southwell Plot to the Interpretation of Test Data from Instability Studies of Shell Bodies," United States Army Aviation Materiel Laboratories Report 68-77, March, 1969.

58. Horton, W. H., and Craig, J. I., "Experimental Observations on the Instability of Circular Cylindrical Shells," Israel Journal of Technology, Vol. 6, No. 1-2, pp. 101-115, 1968.

59. Horton, W. H., Craig, J. I., and Struble, D. E., "A Simple, Practical Method for the Experimental Determination of the End Fixity of a Column," Report on Contract DAA02J-68-C-0035, United States Army Aviation Materiel Laboratories, Fort Eustis, Virginia, May, 1969.

60. Pippard, A. J. S., and Pritchard, J. L., Aerospace Structures, Longman's Green and Company, London, 1936, p. 103.

61. Roark, R. J., Formulas for Stress and Strain, Third Edition, McGraw-Hill, New York, 1954.

62. Wang, C. T., Applied Elasticity, McGraw-Hill, New York, 1953, p. 274.

VITA

Donald E. Struble was born on October 10, 1942 in Oakland, California. He attended grammar school in Gridley, California and graduated from Gridley High School in 1960.

Mr. Struble attended California State Polytechnic College from September 1960 to June 1964, and graduated with honors. Subsequently, Mr. Struble accepted a fellowship to study at Stanford University, where he earned the Master of Science degree in Aeronautics and Astronautics in June of 1965. Mr. Struble continued as a research assistant at Stanford until September, 1967, at which time he transferred to the Georgia Institute of Technology. He was a research assistant there until March 1970.

He is married to the former Allison Florence Dietrick of La Habra, California. They have two children and presently reside in San Luis Obispo, California.